Byun, D. et al. (2003) *Eulerian Dispersion Models*. Chapter 10 of *AIR QUALITY MODELING - Theories, Methodologies, Computational Techniques, and Available Databases and Software. Vol. I - Fundamentals* (P. Zannetti, Editor). Published by The EnviroComp Institute (http://www.envirocomp.org/) and the Air & Waste Management Association (http://www.awma.org/).

# Chapter 10

# Eulerian Dispersion Models

Daewon W. Byun [(1)*], Avraham Lacser [(2)*], Robert Yamartino [(3)], and Paolo Zannetti[(4)]

[(1)] *Department of Geosciences, University of Houston, 4800 Calhoun, Houston, TX 77204, USA*
*dwbyun@math.uh.edu*
[(2)] *Israel Institute for Biological Research, POB 19 Ness Ziona 74100, Israel*
*lacser@iibr.gov.il*
[(3)] *191 East Grand Ave. #206, Old Orchard Beach, ME, USA*
*rjy@maine.rr.com*
[(4)] *EnviroComp Consulting Inc., 2298 Ocaso Camino, Fremont, CA, USA*
*zannetti@envirocomp.com*

[*] *Work performed while serving at the National Oceanic and Atmospheric Administration, on assignment to National Exposure Research Laboratory, EPA, Research Triangle Park, NC, USA*

**Abstract:** The main objectives of this chapter are to introduce the state-of-the-art numerical algorithms for the advection and diffusion used in Eulerian models and to discuss their theoretical and numerical characteristics. The Eulerian approach allows incorporation of different physical and chemical processes involved with the gaseous and particulate constituents in the atmosphere. The governing conservation equation for tracer species dispersion is derived. Approximations in the atmospheric dynamics and fundamental concepts used in the description of turbulence are explained. Some analytical solutions are provided for simplified dispersion conditions to illustrate basic processes in the atmospheric dispersion models. In the Eulerian approach, governing equations can be solved with a fractional time step or an explicit-implicit method to take advantage of numerical efficiency and knowledge of physical parameterizations of atmospheric surface flux exchange, advection, and diffusion processes. This chapter describes numerical solution methods for each physical process component in the Eulerian dispersion model. We provide fundamental steps used in the derivation of numerical advection algorithms, horizontal and vertical eddy diffusivity formulations, and local and non-local vertical diffusion methods. In the Appendix we have compiled vertical eddy diffusivity formulations in the literature, numerical

 

solution methods of the local and non-local vertical diffusion algorithms, and Numerical algorithms with two-level time differencing for constant grid spacing.

**Key Words:** Air quality modeling, advection, diffusion, numerical algorithms, Eulerian modeling, local and non-local closure, eddy diffusivity.

Air pollution diffusion can be numerically simulated by several techniques that are generally divided into two categories based on the frame of references: Eulerian models and Lagrangian models. Figure 1 shows that the Eulerian reference system is fixed with respect to earth while the Lagrangian reference system follows the atmospheric motion. Russell and Dennis (2000), in their recent critical review of photochemical models, state that Eulerian models are becoming dominant. This chapter describes the Eulerian formulations for the atmospheric advection and diffusion processes used in comprehensive air quality models. The basic governing conservation equation for tracer species is derived. To help reader's understanding of the physical processes involved, analytical solutions for simplified dispersion models are provided and discussed. For realistic atmospheric conditions where simple assumptions on the wind field or the diffusion parameters are not available, highly accurate numerical solutions are applied to solve the governing dispersion equation. The Eulerian approach allows incorporation of different physical and chemical processes involved with the atmospheric gaseous and particulate constituents. The governing equations can be solved with a fractional time step or explicit-implicit method to take advantage of numerical efficiency and knowledge of physical parameterizations of atmospheric surface flux exchange, advection, and diffusion processes. The main objectives of this chapter are to introduce the state-of-the-art numerical algorithms for the advection and diffusion used in Eulerian models and to discuss their theoretical and numerical characteristics.

## 1 Air Quality Modeling Methods

Many different numerical techniques can be used for studying the behavior of the atmosphere. Lewis F. Richardson around 1910 made first attempt of numerical weather prediction with mechanical calculators and complex computing forms. In the mid-1940s, John von Neumann of the Institute of Advanced Studies at Princeton began to redesign the first electronic computer ENIAC (developed by J. Mauchly and P. Eckert) primarily for the purpose of weather prediction with the stored - program technique, which is now known as the von Neumann's design. Since, the development of modern digital computers has followed closely to the von Neumann's design and new computational capabilities have been regularly tested with "grand challenge" problems of other computational science fields. Very often, weather prediction models have been among the initial testing programs for newer, faster, and larger computer architectures.

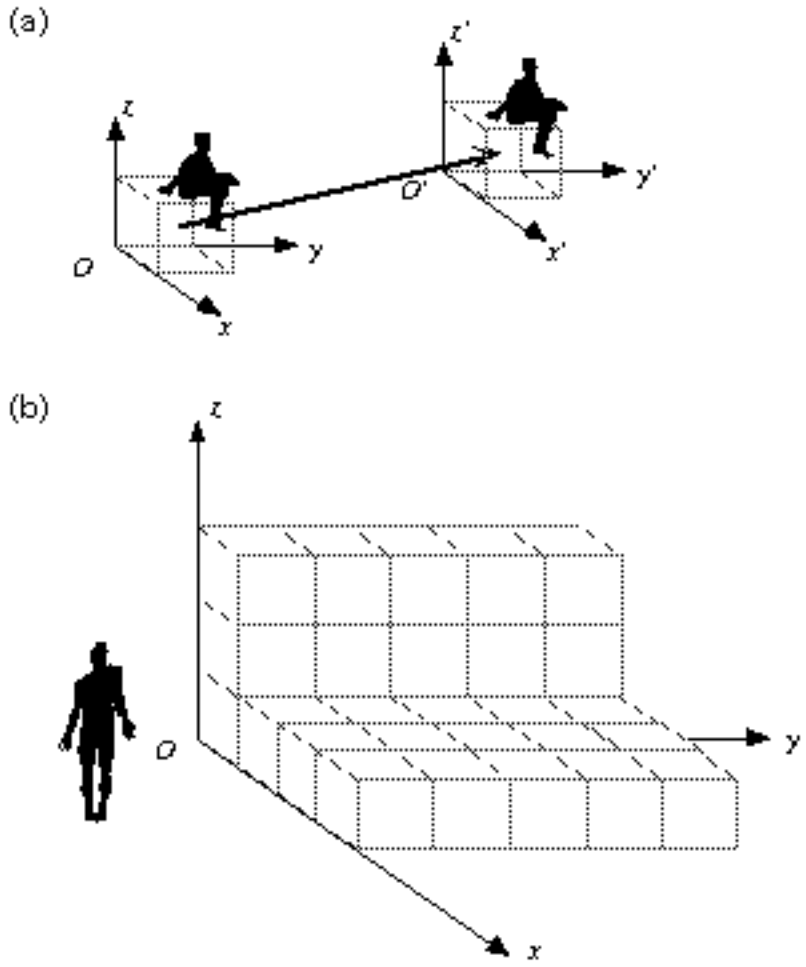


**Figure 1. (a) In the Lagrangian system, the observer follows movement of air parcel, and (b) in the Eulerian system, the observer studies atmospheric motion at a fixed reference point.**

As digital computer memory capacity has become larger, and CPU speed has become faster, the complexity of weather prediction models has increased tremendously. As a part of atmospheric processes, techniques used for solving atmospheric diffusion have been slowly but surely benefiting from the developments in atmospheric science and computer hardware development. For example, simple approaches such as Gaussian and box modeling techniques were popular initially and then use of Lagrangian modeling paradigm followed. Starting in the mid-1970s, the Eulerian or hybrid air quality models have been available for air pollution assessment studies and the acceptance has been strengthened by the need to include complex atmospheric processes under one system. In the following, we briefly introduce different modeling techniques.

## 1.1 Gaussian Models

Gaussian models have been used for last forty years as the most common air pollution models for regulatory applications as they are based on analytical solutions that require less computational power than numerical models. They employ Gaussian statistical distribution formulas to describe the three-dimensional concentration field generated by the diffusion of emissions of inert species under static meteorological and emission conditions. Because that the Gaussian formulation is based on the uniformity of the eddy diffusivity, the validity deteriorates severely in vertical wind shear, diurnal variations of wind and atmospheric stability, and topography and land use variations. Furthermore, their applicability is affected by certain temporal and spatial scale considerations for which the averaged conditions can be estimated to satisfy the limiting assumptions. Because of this, various types of special Gaussian models have been built to address specific environmental conditions. EPA distributed many of these models as a part of UNAMAP models starting in the late 1960s. EPA has advertised most UNAMAP (User's Network for Applied Modeling of Air Pollution; see Zannetti, 1990) models to be just guideline models and stressed that the models may be used only if the situations are suitable for the particular model. For the details, readers should refer to Chapter 7 for the Gaussian plume models and Chapter 8 for Gaussian puff models.

## 1.2 Box Models

Box models are zero-dimensional models that assume pollutants in an imaginary box or column are bounded by the ground and the potential temperature inversion base and spatially homogeneous, instantaneously well mixed. Using a continuity equation, the rates of pollutant concentration changes in the box (caused by horizontal advection, emission, entrainment of background pollutants due to mixing layer growth, and chemical reactions) can be simulated. The box model can then predict the temporal variations of the spatially averaged concentrations, and can estimate mass balances of multiple pollutants over the limited domain represented in the box. Because of the simplifications used in the development of these box models, they are incapable of predicting air quality for regions with significant spatially inhomogeneous emissions, or where the characteristic turbulent mixing time scale is larger than the chemical reaction time scales. Refer to Chapter 2 for additional description of box models.

## 1.3 Lagrangian Models

Lagrangian (or Trajectory) models are based on species conservation equations describing atmospheric diffusion and chemical reactions stated in terms of moving coordinates. The observer adopts moving coordinates that follow sets of hypothetical columns of air similar to the ones described in the photochemical box models. The air columns move along with the prevailing winds, so there are no advection terms in the set of governing equations. Primary pollutant emissions

are injected into the columns when they pass over source regions. Similar to box models, trajectory models simulate chemical reactions in each column. While Lagrangian models are one step beyond box models in logical development, the assumptions they carry are not appropriate when topographical features cause complex wind fields or vertical wind shear within the columns. Uncertainty in the trajectory of column of air under large wind shear, and difficulties in describing source and sink processes are almost insurmountable because of the inherent assumption that the integrity of air parcels must be maintained with the Lagrangin approach. Trajectory modeling is good when simple back-trajectory transport can be used to adequately describe the motion of pollutants. Lagrangian models require a factor of one to two orders of magnitude more computational resources than box models depending on the number of atmospheric columns followed. Lagrangian models, however, are not as computationally expensive as Eulerian models. Consult Chapter 11 for an in-depth description of the Lagrangian models.

## 1.4 Eulerian Models

In the Eulerian approach, the observer adopts a fixed frame of reference, usually the surface of the earth. This enables easy representation of the pollutant production and transformation processes. Most Eulerian models use a grid system defined in an orthogonal set of coordinates to describe atmospheric dynamics (advection and diffusion), emissions sources, and chemical production and destruction. Most numerical weather prediction models and comprehensive air quality models rely on this paradigm. Eulerian models generate four-dimensional (space and time) trace species concentration fields for each of the species modeled. Eulerian models generally use fewer simplifying assumptions in the simulation of atmospheric transport compared to other modeling techniques. By the nature of the grid discretization, Eulerian models cannot resolve trace species concentration features at sub-grid scales because emissions are instantly mixed into the grid. Although one can attempt to use very small grid size to resolve the detailed emissions distributions, there is a practical limit at which atmospheric turbulence statistics cannot be described with parameterizations in terms of the mean state variables (such as wind and temperature) as well as the inhibiting high computational cost. To compensate for this deficiency, some Eulerian models include either trajectory submodels or Gaussian dispersion submodels to treat initial transport and chemical transformations of pollutants coming from large point source emissions within the grid. These hybrid (e.g., "plume-in-grid") grid models attempt to minimize the effect of instantaneous dilution of pollutants over the entire grid box assumed by pure Eulerian models. Once the point source plumes reach a certain size, they are added to the existing concentrations in the appropriate grid cells, and subsequently go through transformation and transport processes within the grid model. Numerical diffusion in the advection process and difficulties in representing atmospheric mixing processes are some of the drawbacks of Eulerian models (see section 5).

# 2 Eulerian Formulations

Here we introduce the governing equations for Eulerian dispersion modeling. We discuss assumptions used for the description of atmospheric dynamics, turbulence, and averaging techniques that allow deterministic formulations of the stochastic atmospheric dispersion phenomena.

## 2.1 Conservation Equations for Air Pollutants

First, we assume that pollutant concentrations are sufficiently small, such that their presence would not affect the meteorology to any detectable extent. Hence, the species conservation equations can be solved independently of the Navier-Stokes and energy equations. In a Cartesian coordinate system, the continuity equation for air and the governing conservation equation for a pollutant are given

$$\frac{\partial \rho}{\partial t} + \frac{\partial \rho u}{\partial x} + \frac{\partial \rho v}{\partial y} + \frac{\partial \rho w}{\partial z} = 0 \tag{1}$$

$$\frac{\partial \varphi_i}{\partial t} + \frac{\partial \varphi_i u}{\partial x} + \frac{\partial \varphi_i v}{\partial y} + \frac{\partial \varphi_i w}{\partial z} = Q_{\varphi i} \tag{2}$$

where $x$ and $y$ are horizontal coordinates of the reference rotated earth-tangential coordinates and $z$ is the distance normal to the $x$-$y$ surface; $u$, $v$, and $w$ are corresponding wind components; $\rho$ is air density, $\varphi_i$ represents concentration of trace species $i$, and $Q_{\varphi i}$ is the source/sink of the pollutant through emissions, deposition, and reactions with other pollutants.

In this chapter, for simplicity we have adapted a Cartesian coordinate system. However, operational mesoscale meteorological models often use quasi-orthgonal terrain-following coordinates. Because the large-scale motions of the atmosphere are quasi-horizontal with respect to the earth's surface, motions in horizontal and vertical directions can be separated using the metric tensor components that define the coordinate transformation in the meteorological generalized coordinate system. Refer to Byun (1999a) for the corresponding governing set of equations.

Eqs. (1) and (2) can be combined to provide a conservation equation for the species mixing ratio, $q_i = \dfrac{\varphi_i}{\rho}$

$$\frac{dq_i}{dt} = \frac{\partial q_i}{\partial t} + u\frac{\partial q_i}{\partial x} + v\frac{\partial q_i}{\partial y} + w\frac{\partial q_i}{\partial z} = \frac{Q_{\varphi i}}{\rho} \tag{3}$$

Eq. (3) is the governing equation of the Lagrangian model, which is based on the principle that mixing ratio is conserved following the air parcel when there is no source term (i.e., $Q_{\varphi_i} = 0$). Eulerian models can also realize the same constraint. However, because the information must be discretized on the Eulerian grid, a numerical advection scheme based on Eq. (3) is sometimes called a Semi-Lagrangian Transport (SLT) method.

## 2.2 Assumptions on Atmospheric Dynamics

The temporal and spatial scales of atmospheric motion span many orders of magnitude (see Figure 2). Therefore, it is impossible to model the motion with a straightforward explicit method. To make atmospheric simulations manageable, scientists have applied several techniques to reduce the range of scales involved by applying simplification assumptions and averaging techniques. The spectral gap (low dynamic energy region which can vary from tens of minutes to a few hour time-scale) helps to separate weather from turbulence. Because of this gap, it is possible to consider these two entities (weather and turbulence) independently and to execute proper mathematical operations to determine the statistical properties. The nonlinear Navier-Stokes equations contain information about atmospheric motion and transport over a broad range of spatial and temporal scales, ranging from global scale eddies to the smallest eddies contributing to molecular dissipation.

Several important hypotheses, basic assumptions, limits of applications in air quality modeling, and examples of usage of atmospheric turbulence and dispersion theories, are briefly discussed below. More detailed information on atmospheric turbulence and diffusion can be found in Pasquill and Smith (1983), Panofsky and Dutton (1984), Stull (1988), and Arya (1988, 999).

### 2.2.1 Hydrostatic and Non-Hydrostatic Assumptions

The hydrostatic equilibrium assumption states that gravity and the vertical pressure gradient force are in balance. Under hydrostatic equilibrium, the atmospheric pressure at a given height is simply related to the weight of the air above. Since the atmosphere is constantly moving, the hydrostatic assumption considers not only the static components of pressure and density but also the dynamic perturbation pressure field (which is responsible for the horizontal velocity field) to the perturbation density field. The vertical acceleration due to gravity is smaller than the horizontal acceleration driven by the horizontal pressure difference. The result is that the vertical acceleration cannot be easily determined from the vertical momentum equation for large-scale atmospheric motions.

This hydrostatic approximation is invalid for small-scale motions such as convection where the vertical acceleration has a magnitude similar to gravity. For

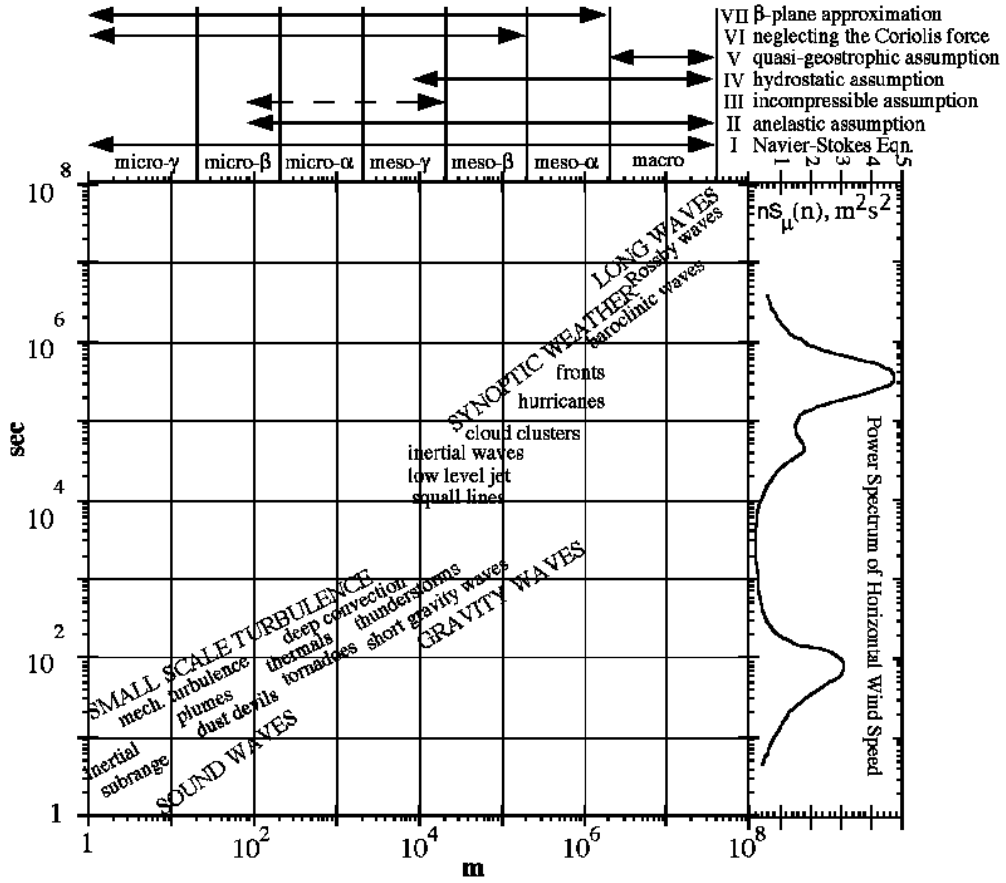


**Figure 2. Temporal and spatial scales for atmospheric dynamic systems. A spectral gap is apparent around the time scale of thousand seconds. (Dennis et al., 1996).**

mesoscale atmospheric models with small horizontal grid sizes (e.g., less than 2 km) where the influence of thermodynamics has direct impact on the atmospheric motions, the hydrostatic pressure calculation may result in less realistic predictions of the atmospheric flows. For this reason, the nonhydrostatic primitive set of equations has recently been applied to study small-scale atmospheric features. The primary difference between the nonhydrostatic model and its hydrostatic counterpart is that the nonhydrostatic model requires explicit integration of the vertical velocity component.

There are two methods for nonhydrostatic pressure calculation. One uses a fully compressible continuity equation. The other employs an elastic continuity equation. For the latter, a Poisson partial differential equation for pressure has to be solved at each time step. Furthermore, when terrain-following coordinate transformations are used solving the Poisson equation is very costly. Researchers

have found that the integration time step for an elastic nonhydrostatic model can be much larger than that for a hydrostatic model, especially when the acoustic waves are solved separately from other meteorological waves (e.g., Klemp and Wilhelmson, 1978).

### 2.2.2 Incompressible Atmosphere Assumption

The incompressible atmosphere assumption involves the thermodynamic characteristics of air. The equation of state describes how density is affected by the changes in pressure and temperature fields. The incompressibility of air can be assumed if the time rate of change of density variation is much smaller than the time scales of motion (Batchelor, 1967). This condition is satisfied mostly for the case when wind speed is substantially less than the speed of sound, and the speeds of gravity waves are much slower than the speed of sound, and limits the vertical extent of motion to be less than about one kilometer. The result is that the change of density due to pressure variation is negligible, and so the fluid behaves as if it were incompressible. Basically, the incompressible atmosphere assumption is a shallow-water approximation for an adiabatic atmosphere. With the incompressibility assumption, the distinction between the conservative form equation (Eq. 2) and its advective form (Eq. 3) becomes blurred. Consequently, concentrations in the form of either density or mixing ratio are often used indiscriminately in atmospheric diffusion equations. One might expect that as long as the wind field satisfies the nondivergent flow approximation, an air quality model would satisfy the pollutant species mass conservation. The implication of this assumption is that a nondivergent wind field does not guarantee the mass conservation of pollutant species if there is inconsistency in air density and wind fields. It is surprising that the lack of mass conservation under the nondivergent flow has not been addressed rigorously in air quality modeling studies.

### 2.2.3 Boussinesq Approximations

The set of Boussinesq approximations used in atmospheric boundary layer studies can be summarized as follows:

- Deviations of thermodynamic variables from reference values (denoted by subscript $o$) are small (hydrostatic atmosphere at rest):

$$\frac{p-p_o}{p_o} << 1\,,\ \frac{T-T_o}{T_o} << 1\,,\ \frac{\rho-\rho_o}{\rho_o} << 1 \tag{4}$$

- Molecular properties are essentially constant. Since deviation of temperature is small, most molecular properties such as viscosity ($\nu$), molecular diffusivity ($\gamma$), and molecular heat conductivity ($\kappa$) are constant at the given temperature $T_o$.

- Variations in temperature and density can be ignored except when they are associated with buoyancy forces. By carefully ordering the derivation steps from the more fundamental compressible equations to the Boussinesq equations, it can be shown that the fluctuations in density become only significant when multiplied by the acceleration due to gravity.

The Boussinesq approximations are often used in air quality modeling to simplify equations of motion and trace gas conservation. However, for small horizontal scales or for deep atmospheric layers, the assumptions in the Boussinesq approximations may not hold. Using Boussinesq approximations lead to the following simplification of the equations of motions in the planetary boundary layer (PBL):

- Flows can be treated as incompressible.
- The equation of state for fluctuating components is simplified so the ratio of fluctuating density to total density can be approximated by the ratio of temperature fluctuation to the reference temperature.

Many Eulerian dispersion models use such limiting assumptions on atmospheric dynamics as described above. Often an incompressible atmosphere assumption is used with the Bousinesq approximations. These assumptions are acceptable only for certain limited situations such as studying atmospheric dispersion in the shallow boundary layer with little topographic features and nondivergent wind field. Recently, air quality models with nonhydrostatic assumptions have been developed (e.g., Chang et al., 1997; Byun and Ching, 1999), and the effects of air density variations on pollutant transport are considered in such models.

## 2.3 Assumptions on Atmospheric Turbulence

We cannot explicitly solve the instantaneous species conservation equation for the smallest scales due to computer limitations and uncertainties in the input data. We must then transform Eqs. (1) and (2) to form a deterministic relation. We assume that there is a natural separation of atmospheric motions between a homogeneous fine scale and the inhomogeneous mesoscale that is affected by the topography, surface conditions, and large-scale weather. Then we introduce the concept of turbulence and mean components for studying stochastic atmospheric flows. We expect that as long as the turbulent components can be parameterized we can obtain deterministic governing equations for the mean flow. Basic concepts of atmospheric turbulence are reviewed below and more detailed information can be found in Stull (1988) and Arya (1999).

### 2.3.1 Isotropic Turbulence

Isotropy implies that fluid motions are invariant with respect to rotation and reflection of the coordinates. True isotropy occurs only when homogeneity is present in all directions. In isotropic turbulence, the variances of the three

velocity components are the same because they are invariant with the rotation of the coordinate axis. Another consequence of isotropy is that the velocity components are not correlated with each other. However, in the PBL, the variances of the velocity components are not equal, and the horizontal and vertical velocity components are correlated near the ground. Thus the atmospheric turbulence in the PBL is not strictly isotropic. However, the smallest fluctuations imbedded in the larger scales of motions can be isotropic. The invariant characteristic of the smallest scales of turbulence is termed local isotropic turbulence. Measurements of boundary-layer turbulence show that these predictions are indeed satisfied, provided that the size of the turbulent eddies involved is small compared to the distance to the surface. Such eddies are far enough from the surface that they are independent of boundary influences. In the case of isotropy, or local isotropy, the nine components of Reynolds stress (momentum fluxes) can be reduced to just functions of the longitudinal (along the wind) and lateral (across the wind) covariances. By rotation of coordinates, any longitudinal spectrum can be transformed into any other longitudinal spectrum. However, rotation of coordinates cannot transform longitudinal functions into lateral functions. Since all longitudinal functions are the same and all lateral functions are the same under coordinate rotations, these two functions describe spectral properties of isotropic or locally isotropic turbulence.

### 2.3.2 Taylor's Hypothesis

When the mean velocity of a flow which carries eddies is much greater than the turbulent fluctuations, one may assume that the sequence of change in turbulent components at a fixed point is simply due to the passage of an unchanging pattern of turbulent motion over that point. The field of turbulence is translated by the mean velocity and the spatial turbulence pattern can be depicted exactly with the temporal turbulence pattern by the transformation $x = U\ t$, where $x$ is the longitudinal distance, $U$ is the transport mean wind speed, and t is the travel time. This is called the Taylor's hypothesis or the frozen-wave hypothesis. The Taylor's hypothesis is significant as it enables to infer spatial structure of turbulence from measurements at one point. For the Taylor's hypothesis to be valid, the turbulence must be temporally stationary and spatially homogeneous at least along the direction of mean wind. These conditions are often satisfied in wind tunnels, and are often approximately valid in the atmosphere provided the measurement location and period are chosen carefully. Strong wind shears in the vertical will generally distort eddies as they move (tearing them apart, in effect) so that the Taylor's frozen-wave hypothesis cannot be sustained. In spectral terms, the hypothesis fails at frequencies $f$ smaller than vertical wind shear. Taylor's hypothesis can hardly be valid when standing waves (such as those produced by hills and mountains) cause spatial variations but have little effect on temporal measurements at one location. In atmospheric dispersion modeling, a relationship between the Lagrangian and Eulerian spectra is often derived from the Taylor's frozen-wave hypothesis.

### 2.3.3 Homogeneity

A turbulent flow is homogeneous if its statistics do not vary in space. The presence of the earth's surface is important in two ways with respect to homogeneity. First, statistics will vary relative to distance from the ground so that it is unlikely that homogeneity could prevail, even approximately, except in the horizontal. Second, if the terrain and land use are inhomogeneous, with hills and valleys, or with cities, fields, and forests, then the flow near the ground can hardly be expected to be horizontally homogeneous because of the effects of the surface on the flow itself. Horizontal homogeneity of small-scale motions near the ground is usually not a good approximation over most continental areas. The terrain is neither flat enough nor sufficiently homogeneous, and in general, local statistics over large areas will not be the same. Perhaps, at higher levels in the boundary layer, horizontal homogeneity is more nearly approached. The assumption of vertical homogeneity is almost never valid because of the presence of wind shear and stratification. Mean wind speed and temperature vary rapidly with height near the terrain surface, and then somewhat less rapidly aloft. In a homogeneous turbulence, the spatial correlation is not a function of the spatial coordinate but instead is only a function of the separation vector.

### 2.3.4 Stationarity

A random variable is said to be stationary if its one-dimensional probability functions are independent of time and its joint (multi-dimensional) probability functions are invariant with respect to a fixed translation in time (i.e., dependent only on time difference rather than time itself). In reality we do not insist that the variable be exactly stationary. Instead we accept quasi-stationarity (a series of near-equilibrium states) if there is a significant separation between the time scales of turbulence and of large-scale weather phenomena. Usually this assumption is valid for small-scale flows under steady meteorological conditions where influence of synoptic scale disturbance is not present.

### 2.3.5 Ergodicity

The ergodicity hypothesis states that for stationary random fields time averages converge to ensemble (probability) averages as the averaging interval becomes very long. Similarly, for homogeneous random fields, spatial averages converge to ensemble averages (discussed in Section 2.4) as the spatial interval for averaging becomes very large. When temporal and ensemble averages coincide in a suitable sense, the stochastic process is referred to as ergodic. Ergodicity is a very important concept involving volume-preserving coordinate transformations. Ergodicity requires stationarity. To ensure ergodicity, one must establish or assume certain properties for ensemble-averaged quantities such as second- or fourth-order covariances. This assumption allows linkage of theoretical turbulence description to the experiment results where time averages in statistically stationary flows are used. Mean-square ergodicity is possible even

for nonstationary processes, and therefore is often applied in the study of atmospheric turbulence. It implies that the variance of the sample averages vanishes as time goes to infinite, even though they may not converge to an ensemble average.

### 2.3.6 Similarity and Dimensional Analysis

Before detailed causal relations can be identified in a system, a dimensional analysis can provide a simple but powerful method to establish relationships between the various quantities in the system based on their fundamental dimensions (Arya, 1988). If conditions surrounding two experiments are identical, the result should be similar. By dimensional analysis, a similarity relationship may be found. Similarity theory predicts universal functions, which may be determined experimentally and tested for reproducibility at other locations. The surface boundary layer theory used in describing atmospheric mixing characteristics is mostly derived from the similarity theory.

## 2.4 Averaging Techniques

Atmospheric motions consist of a vast spectrum of temporal and spatial scales. For convenience, the scales are separated to isolate properties of atmospheric motions to a limited portion of the spectrum. The set of primitive equations that represents the stochastic atmospheric system must be averaged to a set of deterministic equations before the equations can be solved numerically. The averaging process filters the total flow into mean and turbulent components. The spectral gap discussed above (see Figure 2), is not deep enough to provide a completely satisfactory solution, but it guides us on how to separate the mean and turbulent motions. For example, to characterize turbulence and mean flow in the surface layer, one-hour averages are often used to separate large-scale from micro-scale processes. In this averaging process we limit the descriptions of the atmospheric motions to terms of statistical characterization. However, the averaging processes in atmospheric numerical models are more complex than the simple distinction between instantaneous descriptions and statistical averages. Because we rely on a grid system to represent atmospheric motions and processes over a large domain, in effect we are applying spatial averaging over the grid size to represent atmospheric phenomena in a grid cell. The governing set of equations for the atmospheric motions and reactions are obtained by applying the ensemble averaging to transform the stochastic atmospheric system (described in 3.2.1) to a deterministic system and, by applying discrete volume averaging, to convert into the numerical solution space.

Cotton and Anthes (1989) summarized expected characteristics of averaging operators for use in atmospheric modeling as follows:

- The operators should provide formal mechanisms for distinguishing between resolvable and unresolvable eddies.

- The operators should provide sets of equations that are more amenable to integration (either analytically or numerically) than unaveraged systems of equations.
- The average set of atmospheric variables should be capable of being measured by current or anticipated atmospheric sensing systems.

The following averaging techniques fit the above characteristics.

### 2.4.1 Ensemble Averaging

Atmospheric motions are composed of a variety of eddies whose behavior is mostly stochastic and random. This makes a deterministic approach of solving the governing Navier-Stokes equations of motion for the entire spectrum of eddies in the atmosphere impossible; instead, one has to rely on statistical methods. Ensemble averaging is an ideal concept that completely removes randomness and filters out eddies of all sizes. Therefore, the ensemble-averaged equation must contain parameterization covering the entire spectral range of eddy motions including the largest energy-containing scales. The largest eddies in any turbulent flow are very sensitive to atmospheric and surface conditions. Therefore, such a parameterization cannot be uniformly valid in a wide range of flows. Turbulent flows differ from one another principally in their large-eddy structure. Small-scale eddies in turbulent flows seem to be statistically similar. The ensemble averaging process enables us to describe the stochastic atmospheric processes in a deterministic sense. The equation for ensemble averaging is:

$$\overline{f_e} = \lim_{N\to\infty} \frac{1}{N} \sum_{k=1}^{N} f_k \tag{5}$$

where $f_k$, $k$=1,$N$ are different realizations of $f$.

However, because atmosphere is neither stationary nor homogeneous, we need to find alternative average operators that are suitable for the understanding of field measurements as well as for the implementation in computational models. The ensemble averaging is often substituted by the temporal averaging, which will be described below.

### 2.4.2 Reynolds Decomposition and Averaging

Although behaviors of atmospheric motions are stochastic, only average statistics are important and their detailed fluctuation of individual eddies is little or no concern. Osborne Reynolds toward the end of nineteenth century suggested decomposition of atmospheric variables into mean (denoted with over bar) and turbulent components (denoted with prime), i.e., $f = \overline{f} + f'; g = \overline{g} + g'$ where $f$ and $g$ are two dependent variables or functions of random variables. The Reynolds averaging conditions are (Arya, 1999):

$$\overline{f+g} = \overline{f} + \overline{g} \tag{6a}$$

$$\overline{cf} = c\overline{f} \tag{6b}$$

$$\overline{gf} = \overline{g}\overline{f} \tag{6c}$$

$$\overline{\frac{\partial f}{\partial s}} = \frac{\partial \overline{f}}{\partial s} \tag{6d}$$

$$\overline{\int f ds} = \int \overline{f} ds \tag{6e}$$

where $c$ is a constant, $s = x, y, z$, or $t$. The only averaging operation that satisfies the Reynolds averaging conditions is ensemble averaging, defined above.

### 2.4.3 Temporal Averaging

Temporal averaging is the most popular averaging technique used because many instruments are available that are capable of measuring time series of atmospheric parameters at low cost. Other techniques (such as the ensemble averaging) are extremely difficult to obtain under varying atmospheric conditions. Temporal averaging has been used as a substitute for the ensemble averaging when atmospheric turbulence is assumed to satisfy the ergodicity condition described earlier. In order for temporal averaging to characterize atmospheric turbulence, the optimal selection of an averaging period is essential. The averaging period should be sufficiently long to ensure a stable averaging of signals from the energy containing eddies but not too long to the point that diurnal variations or synoptic changes in the atmospheric conditions are masked. In most studies of PBL, the optimum averaging time ranges between $10^3$ to $10^4$ seconds, depending on the height of observation, the stability condition, and the moment of the parameter under study (Arya, 1988). An atmospheric model that relies on PBL parameterizations should be considered as having corresponding inherent uncertainties in its predictions due to the temporal averaging technique applied. The equation for temporal averaging is:

$$\overline{f}_t = \lim_{T\to\infty} \frac{1}{2T} \int_{-T}^{T} f dt \tag{7}$$

where $T$ is one half of the period around the time at which the average is evaluated.

### 2.4.4 Grid-Volume Averaging

Using a grid-volume averaging method, eddies smaller than the spatial scale are removed, leaving a filtered field that is defined at every point continuously in the modeling domain. Grid-volume averaging is similar to applying a moving

average to a time series, Eq. (7). It is simply averaging over fixed volumes, so that the averaged field is defined only at the center of the (non-overlapping) averaged volumes. When the grid size is much smaller than the wavelength of the energy containing eddies of the system, the grid-volume average is a well-defined function. A volume-averaged model with a grid size much smaller than the energy containing eddies requires a very simple parameterization. This forms the basis of the large eddy simulation (LES). If the grid size is of comparable magnitude to the energy-containing scales, or greater than the turbulent integral scale, the Reynolds flux in the sub-grid scale must be parameterized. Therefore, if the same parameterization is used, the volume-averaged model with sufficiently large grid size becomes similar to the ensemble-averaged model where the turbulent transfer must always be parameterized. Because the grid-volume average is defined over a finite volume at an instant in time, it is not measurable and models based on grid-volume average cannot be conventionally tested against the measurement. A volume-averaged model cannot provide information on the variability across the model grid volume.

The running volume-averaging process results in another continuous function in space. For example, simple volume averaging over a rectangular cell is defined as:

$$\langle f(x,y,z)\rangle = \frac{1}{\Delta V}\int_{z-\Delta z/2}^{z+\Delta z/2}\int_{y-\Delta y/2}^{y+\Delta y/2}\int_{x-\Delta x/2}^{x+\Delta x/2} f(x',y',z')dx'dy'dz' \tag{8}$$

where $\Delta V = \Delta x \Delta y \Delta z$. A general volume averaging is defined with a filter function as:

$$\langle f_G(x,y,z)\rangle = \frac{1}{\Delta V}\int_{z-\Delta z/2}^{z+\Delta z/2}\int_{y-\Delta y/2}^{y+\Delta y/2}\int_{x-\Delta x/2}^{x+\Delta x/2} G(x-x',y-y',z-z')f(x',y',z')dx'dy'dz' \tag{9}$$

where $G$ is the appropriate weighting function whose modulus is one. In the Eulerian modeling, a discrete averaging is applied to a deterministic function (an ensemble averaged quantity here) over the fixed volume of the cell $(i,j,k)$ to provide a discrete formulation of the governing equation:

$$\langle \bar{f}_\ell(x_i,y_j,z_k)\rangle = \frac{1}{\Delta V}\int_{z-\Delta z/2}^{z+\Delta z/2}\int_{y-\Delta y/2}^{y+\Delta y/2}\int_{x-\Delta x/2}^{x+\Delta x/2} \overline{f_e}(x',y',z')dx'dy'dz' \tag{10}$$

## 2.5 Reynolds-Averaged Conservation Equations for Air Pollutants

To make the instantaneous species continuity equation useful for air quality simulation, we need to derive the governing diffusion equation. The first step is to decompose variables in Eq. 1 into mean and turbulent components. The velocities and concentrations of the various species in atmospheric flow are turbulent quantities and undergo turbulent diffusion. Because turbulent diffusion is much greater than molecular diffusion for most trace species, the latter can be ignored. Also we assume the ergodic hypothesis holds for the ensemble averaging process, which means the ensemble average of a property can be substituted with the time average of that property. The turbulence is assumed stationary for the averaging time period of interest (e.g., 30 minutes to one hour for atmospheric applications). The Reynolds decompositions of air density ($\rho$) and species concentration ($\varphi_i$) are expressed as:

$$\rho = \overline{\rho} + \rho' \tag{11}$$

$$\varphi_i = \overline{\varphi}_i + \varphi_i' \tag{12}$$

Some of the parameters in the conservation equations (1), (2) and (3) are nonlinearly related to each other and, therefore, direct application of Reynolds decomposition to these parameters will introduce covariance terms that complicates the turbulence equations. Instead, we define averaged mixing ratio and its fluctuation component based on Eqs. (11) and (12):

$$\overline{q}_i \equiv \overline{\varphi}_i / \overline{\rho} \tag{13a}$$

$$q_i' \equiv \varphi_i' / \overline{\rho} \tag{13b}$$

Similarly, the average contravariant wind components and their fluctuations are defined as

$$\overline{u} \equiv \overline{\rho u} / \overline{\rho};\ \ \overline{v} \equiv \overline{\rho v} / \overline{\rho};\ \ \overline{w} \equiv \overline{\rho w} / \overline{\rho} \tag{14a}$$

$$u' \equiv u - \overline{u}; v' \equiv v - \overline{v}; w' \equiv w - \overline{w} \tag{14b}$$

This definition allows the continuity equation for the Reynolds averaged variables to keep the original conservation form shown in Eq. (1) as

$$\frac{\partial \overline{\rho}}{\partial t} + \frac{\partial \overline{\rho u}}{\partial x} + \frac{\partial \overline{\rho v}}{\partial y} + \frac{\partial \overline{\rho w}}{\partial z} = 0 \tag{15}$$

Decomposing velocity components in Eq. (2) using Eqs. (14a) and (14b), the Reynolds averaged trace species conservation equation, neglecting the molecular diffusion, is:

$$\frac{\partial \overline{\varphi_i}}{\partial t} + \frac{\partial}{\partial x}\overline{(\overline{\varphi_i} + \varphi_i')(\overline{u} + u')} + \frac{\partial}{\partial y}\overline{(\overline{\varphi_i} + \varphi_i')(\overline{v} + v')} + \frac{\partial}{\partial z}\overline{(\overline{\varphi_i} + \varphi_i')(\overline{w} + w')} = \overline{Q}_{\varphi_i} \quad (16)$$

The source function (i.e., emissions of pollutants) is assumed to be deterministic for all practical purposes and there is no turbulent component. The Reynolds flux terms in Eq. (16) can be approximated in terms of the mixing ratio to give:

$$\frac{\partial \overline{\varphi_i}}{\partial t} + \frac{\partial \overline{\varphi_i}\overline{u}}{\partial x} + \frac{\partial \overline{\varphi_i}\overline{v}}{\partial y} + \frac{\partial \overline{\varphi_i}\overline{w}}{\partial z} + \frac{\partial}{\partial x}\left(\overline{\rho}\,\overline{q_i'u'}\right) + \frac{\partial}{\partial y}\left(\overline{\rho}\,\overline{q_i'v'}\right) + \frac{\partial}{\partial z}\left(\overline{\rho}\,\overline{q_i'w'}\right) = \overline{Q}_{\varphi_i} \quad (17)$$

Equation (17) has the "closure problem" that prevents direct solution. This problem occurs because of the nonlinearity of the conservation equations, which, upon averaging a random field, leads to unknown turbulence flux terms (Reynolds flux) involving the correlations of the random field components. Meteorological models only resolve the mean wind components (*u, v, w*) leaving an unresolved portion that is sometimes of the same magnitude as the mean wind. Therefore, the turbulent flux terms can be very large. Even a very fine scale meteorological model (e.g., grid resolution of 1 km) cannot provide detailed enough information about the turbulent fluctuations. The spatial and temporal scales of the smaller turbulent eddies are so small that a correct numerical integration of Eq. (17) would be practically impossible. Wyngaard (1982) suggested that it would probably require a grid size of about 1 mm in the entire computational domain, which is computationally impractical for air quality problems.

The recognition that the uncertainties brought by the turbulent component can be minimized but never eliminated is the key to understanding the significance of the ensemble averaging. This point can be clarified by noting that state variables such as wind components and concentrations are stochastic variables; i.e., there exists an infinite family of functions of these state variables that satisfy the equation of motion and atmospheric diffusion equation. The situation is described in Figure 3, where each possible member of wind of the family generates a different concentration. The average, at a certain point and time, of all possible concentrations generated by the different wind gives the theoretical ensemble mean concentration. Naturally, if we could measure wind and concentration continuously and in space and time, we could evaluate the exact member of the family that has occurred in reality. Lacking this information, we must assume that all theoretically acceptable wind fluctuations are equally possible, thus allowing, in the best of possible conditions, the computation of mean concentration ($\overline{\varphi}_i$) instead of the instantaneous (actual) $\varphi_i$. *An important conclusion that follows from the ensemble averaging process is that the concentration output provided by all Eulerian models is conceptually different from the air quality data gathered*

*from monitoring activities*. The monitoring data provide estimates of the actual concentration within the error limit of the monitoring technique while model outputs are estimates of the ensemble average. The monitoring data may have representativeness problem and model output has certain degree of error caused by the uncertainties in the input data and approximations in the numerical and/or analytical solutions.

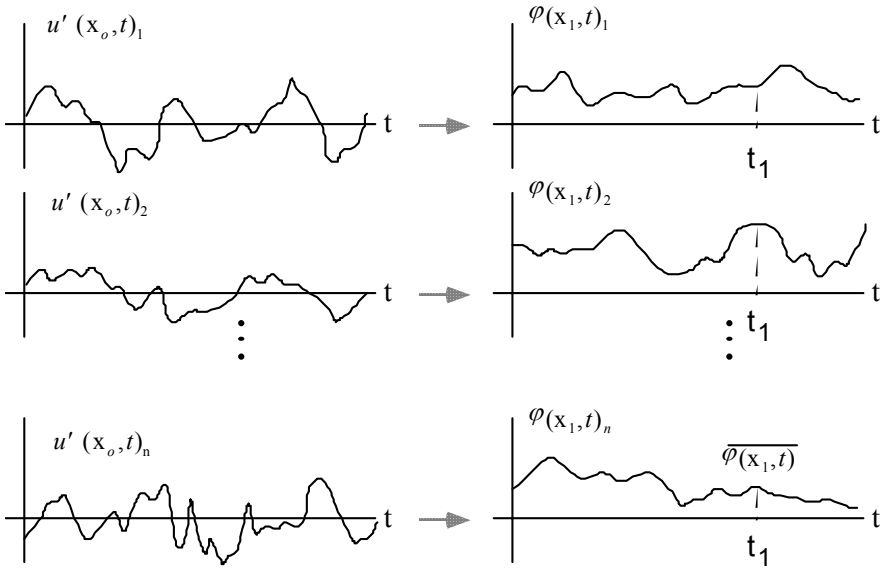


**Figure 3. The infinite family or ensemble of velocity functions (turbulent component) *u'* and the corresponding family of concentration distributions ($\varphi$) each portrayed at fixed points $x_o$ and $x_1$ as functions of time. The subscript n (n=1,2…) denotes the member of realization of the ensemble. The ensemble mean value $\overline{\varphi}$ at a given time $t_1$ is formed by averaging $\varphi(x_1,t)_n$ over the infinite ensemble, as indicated by the vertical dashed line (adapted from Lamb; in Longhetto, 1980).**

The turbulent flux terms can be parameterized using a simple closure scheme such as the eddy diffusion concept (K-theory):

$$\overline{q_i'u'} = -K^{1l}\frac{\partial \overline{q}_i}{\partial x^l};\ \overline{q_i'v'} = -K^{2l}\frac{\partial \overline{q}_i}{\partial x^l};\overline{q_i'w'} = -K^{3l}\frac{\partial \overline{q}_i}{\partial x^l} \qquad (18)$$

where $K^{jl}$ denotes the eddy diffusivity tensor over the index $l$ ($l$=1,2, or 3) and repeated index $l$ in the equation represents summation over the all three components. For convenience, we postulate that the diffusivity tensor in Cartesian coordinates is diagonal, i.e., all the off-diagonal components vanish such that $K^{11} = K_{xx}$, $K^{22} = K_{yy}$, $K^{33} = K_{zz}$, and $K^{ij} = 0$ for $i \neq j$. Then the governing atmospheric diffusion equation (when the turbulent flux terms are expressed with the eddy diffusion theory) is:

$$\frac{\partial \overline{\varphi}_i}{\partial t} + \frac{\partial \overline{\varphi}_i \overline{u}}{\partial x} + \frac{\partial \overline{\varphi}_i \overline{v}}{\partial y} + \frac{\partial \overline{\varphi}_i \overline{w}}{\partial z} - \frac{\partial}{\partial x}(\overline{\rho} K_{xx} \frac{\partial \overline{q}_i}{\partial x}) - \frac{\partial}{\partial y}(\overline{\rho} K_{yy} \frac{\partial \overline{q}_i}{\partial y}) - \frac{\partial}{\partial z}(\overline{\rho} K_{zz} \frac{\partial \overline{q}_i}{\partial z}) = \overline{Q}_{\varphi_i} \tag{19}$$

(a) (b) (c) (d) (e) (f)

The terms in Equation (19) are summarized as follows:

(a) time rate of change of pollutant concentration;
(b) horizontal advection;
(c) vertical advection;
(d) horizontal eddy diffusion (diagonal term);
(e) vertical eddy diffusion (diagonal term);
(f) emissions, loss of pollutant at boundaries, and effects of chemical reactions.

## 3 Analytical Solutions for Ideal Atmospheric Conditions

The governing atmospheric diffusion equation, Eq. (19), can only be solved with a numerical technique. Analytical solutions are available under special simplifying assumptions. In the natural Cartesian coordinate where the wind is assumed to blow towards the positive $x$-axis (i.e., $\overline{u} = U$, $\overline{v} = 0$) and the vertical velocity is negligible ($\overline{w} = 0$), the governing equation for a trace species is simplified as:

$$\frac{\partial \overline{\varphi}}{\partial t} + U \frac{\partial \overline{\varphi}}{\partial x} = \frac{\partial}{\partial x}\left( K_{xx} \frac{\partial \overline{\varphi}}{\partial x} \right) + \frac{\partial}{\partial y}\left( K_{yy} \frac{\partial \overline{\varphi}}{\partial y} \right) + \frac{\partial}{\partial z}\left( K_{zz} \frac{\partial \overline{\varphi}}{\partial z} \right) + \overline{Q}_{\varphi} \tag{20}$$

in which Boussinesq approximation and incompressible flow assumptions were applied. Analytical solutions to Eq. (20) and its simplified form are discussed in Hanna et al (1982), Pasquill and Smith (1983), Seinfeld (1986), Tirabassi et al. (1986), and Arya (1999). One common method for obtaining an analytical solution is reducing the dimensionality of the problem. A two-dimensional solution for ground-level sources and a solution valid for linear profiles of $K_{zz}$ can be found, for example, in Calder (1949) and Rounds (1955). Smith (1957) found a solution for elevated sources with $U$ and $K_{zz}$ profiles following Schmidt's conjugate power law:

$$U = U_r (z / z_r)^{\alpha} \tag{21}$$

$$K_{zz} = K_{zr} (z / z_r)^{\beta} \tag{22}$$

in which the powers of momentum profile and eddy diffusivity strictly satisfy the conjugate relationship $\alpha + \beta = 1$. $U_r$ and $K_{zr}$ are wind speed and eddy diffusivity, respectively, at the reference height $z_r$. Yeh and Huang (1975) and

Demuth (1978) obtained more general analytical solutions. They considered a steady state condition with accompanying boundary conditions

$$\overline{\varphi} = \frac{\overline{Q}_{\varphi}}{U(h_e)}\delta(z-h_e)\delta(y) \qquad \text{at } x = 0 \tag{23a}$$

and

$$K_{zz}\frac{\partial\overline{\varphi}}{\partial z} = 0 \qquad \text{at } z = 0 \text{ and } h \tag{23b}$$

where $h_e$ is the final effective height of the emissions (i.e., height of pollutant after plume rise), and $h$ is the depth of the PBL, and $Q_{\varphi}$ is the source term. We assume that atmospheric dispersion along the $x$-axis (stream-wise diffusion) is negligible in comparison to the transport term:

$$\left|U\frac{\partial\overline{\varphi}}{\partial x}\right| >> \left|\frac{\partial}{\partial x}\left(K_{xx}\frac{\partial\overline{\varphi}}{\partial x}\right)\right| \tag{24}$$

This assumption has been challenged recently by a few researchers. For example, Du and Venkatram (1998) have studied the effect of stream-wise diffusion on ground-level concentration. They found that the neglected term increases the dispersion rate to produce concentration decrease with distance following –2 power law (i.e., $\sigma_y^2 \propto x^2$) instead of –3/2 (i.e., $\sigma_y^2 \propto x^{3/2}$), which is predicted by the one-dimensional formula for the unstable boundary layer. Results from the wind tunnel experiment by Raupach and Legg (1983) also support the –2 power law. However, for the purpose of deriving analytical solutions, the assumption in Eq. (24) is used here. For convenience, the crosswind-integrated concentration is defined as

$$\langle\overline{\varphi}\rangle_y(x,z) = \int_{-\infty}^{\infty}\overline{\varphi}(x,y,z)dy \tag{25}$$

With the power-law expressions of wind and eddy diffusivity of Eqs. (21) and (22), but without the strict conjugate assumption, Yeh and Huang (1975) obtained a ground level crosswind integrated concentration for the case $h \to \infty$:

$$\left(\overline{\phi}\right)_y(x,0) = \frac{Q_{\varphi}}{\lambda^{\eta}}\frac{1}{\Gamma(\gamma)}\frac{h^{\eta}}{U_r^{\nu}(xK_{zo})^{\gamma}}\exp\left[-\frac{U_r z_r^{\omega} h_e^{\lambda}}{\lambda^2 K_{zr} x}\right] \tag{26}$$

where

$$\lambda = \alpha - \beta + 2 \tag{27a}$$

$$\nu = (1-\beta)/\lambda \tag{27b}$$

$$\gamma = (\alpha + 1)/\lambda \tag{27c}$$

$$\eta = (\alpha + \beta)/\lambda \tag{27d}$$

$$\omega = \beta - \alpha \tag{27e}$$

and $\Gamma$ denotes the Gamma function.

With a finite mixing height (i.e., $h < \infty$) and for a plume within the PBL (i.e., $h_e < h$), the steady state solution is (Demuth, 1978)

$$\left(\bar{\phi}\right)_y(x,0) = \frac{Q_\varphi \lambda z_r^\alpha}{U_r h^{\alpha+1}} \cdot$$

$$\left\{\gamma + R^p \sum_{i=1}^{\infty}\left[\frac{J_{\gamma-1}(\sigma_{\gamma(i)}R^{\lambda/2})\sigma_{\gamma(i)}^{\gamma-1}}{\Gamma(\gamma)J_{\gamma-1}^2(\sigma_{\gamma(i)})2^{\gamma-1}} \cdot \exp\left(-\frac{\sigma_{\gamma(i)}^2\lambda^2 K_{zr}x}{4U_r z_r^\omega h^\lambda}\right)\right]\right\} \tag{28}$$

where

$$R = h_e/h \tag{29a}$$

$$p = (1-\beta)/2 \tag{29b}$$

In Eq.(28), $J_\gamma$ represents the Bessel function of the first kind of order $\gamma$, and $\sigma_{\gamma(i)}$ ($i$=1,2,…) are its roots, i.e., $J_\gamma(\sigma_{\gamma(i)}) = 0$. The solutions given by Eqs. (26) and (28) represent the ground-level concentrations (i.e., $z$ = 0). The elevated crosswind integrated concentrations $\langle\bar{\varphi}\rangle_y(x,z)$ for the case $h \to \infty$ is derived by Huang (1979):

$$\left(\bar{\phi}\right)_y(x,z) = \frac{Q_\varphi (zh_e)^p z_r^\beta}{\lambda K_{zr} x}\exp\left(-\frac{U_r z_r^\omega (z^\lambda + h_e^\lambda)}{\lambda^2 K_{zr} x}\right) I_{-\nu}\left(\frac{2U_r z_r^\omega (zh_e)^{\lambda/2}}{\lambda^2 K_{zr} x}\right) \tag{30}$$

where $I_{-\nu}$ is the modified Bessel function of the first kind of order $-\nu$.

For a finite mixing height ($h < \infty$), the crosswind-integrated concentration is obtained from Demuth (1978), giving

$$\left(\bar{\phi}\right)_y(x,z) = \frac{Q_\varphi \lambda z_r^\alpha}{U_r h^{\alpha+1}}$$

$$\left\{\gamma+\left(\frac{zR}{h}\right)^{p}\sum_{i=1}^{\infty}\left[\frac{J_{\gamma-1}(\sigma_{\gamma(i)}R^{\lambda/2})J_{\gamma-1}(\sigma_{\gamma(i)}(z/h)^{\lambda/2})}{J^{2}_{\gamma-1}(\sigma_{\gamma(i)})}\cdot\exp\left(-\frac{\sigma^{2}_{\gamma(i)}\lambda^{2}K_{zr}x}{4U_{r}z_{r}^{\omega}h^{\lambda}}\right)\right]\right\} \quad (31)$$

Tirabassi et al. (1986) verified, analytically and numerically, that as $z\to 0$, the limit of Eq.(30) and (31) converges to Eq.(26) and (28), respectively; and that as $h\to\infty$, the limit of Eqs.(28) and (31) gives Eqs. (26) and (30), respectively.

These formulae, Eqs. (30) and (31), deal with the crosswind integrated concentration $\langle\overline{\varphi}\rangle_{y}$. To calculate the three-dimensional concentration, $\overline{\varphi}(x,y,z)$, horizontal diffusion needs to be included. Let's assume that the crosswind diffusivity is of the form

$$K_{y}=U(z)f(x)=\frac{U(z)}{2}\frac{d\sigma_{y}^{2}}{dx} \quad (32)$$

where $\sigma_{y}$ is the standard deviation of lateral dispersion. Eq. (32) can be obtained by relating the Fickian diffusion coefficient with the Gaussian dispersion (e.g., Arya, 1999) with the help of Taylor's Hypothesis. Then the solution is

$$\overline{\varphi}(x,y,z)=\langle\overline{\varphi}\rangle_{y}(x,z)\frac{1}{\sqrt{2\pi}\sigma_{y}}\exp\left(-\frac{y^{2}}{2\sigma_{y}^{2}}\right) \quad (33)$$

The formulae above have been incorporated into an organized computer package KAPPA-G (Tirbassi et al., 1986), which allows computation of three-dimensional steady-state simulations as proposed by Huang (1979).

Table 1 provides a few other analytical solutions of the Eulerian dispersion equation for simplified meteorological and boundary conditions. They can be used to study characteristics of simplified advection and diffusion equations and to verify numerical implementation of Eulerian dispersion models.

**Table 1. Analytical solutions of advection-diffusion equation in the incompressible atmosphere**

| Classification | Equations and Boundary Conditions (B/C) | Solution | References |
|---|---|---|---|
| 1-D, time-dependent, constant $K$, no wind, instantaneous area source | $\frac{\partial \varphi}{\partial t} = K\frac{\partial^2 \varphi}{\partial x^2}$, with $K = K_o$ (constant).<br>B/C: $\varphi \to 0$ as $t \to \infty \ \forall x$<br>$\varphi \to 0$ as $t \to 0$ all except $x$=0.<br>$\int_{-\infty}^{\infty} \varphi \, dx = Q_{ia}$, instantaneous area source (over y-z plane) | $\varphi = \frac{Q_{ia}}{(4\pi K_o t)^{1/2}} \exp[-\frac{x^2}{4K_o t}]$ | Hanna et al. (1982) |
| 3-D, time-dependent, constant $K$, no wind, instantaneous point source | $\frac{\partial \varphi}{\partial t} = K_{xo}\frac{\partial^2 \varphi}{\partial x^2} + K_{yo}\frac{\partial^2 \varphi}{\partial y^2} + K_{zo}\frac{\partial^2 \varphi}{\partial z^2}$, with constant $K$.<br>B/C: $\varphi \to 0$ as $t \to \infty \ \forall (x,y,z)$<br>$\varphi \to 0$ as $t \to 0$ all except $(x,y,z) = (0,0,0)$.<br>$\int_{-\infty}^{\infty}\int_{-\infty}^{\infty}\int_{-\infty}^{\infty} \varphi \, dxdydz = Q_{ip}$, instantaneous point source | $\varphi = \frac{Q_{ip}}{(4\pi K_o t)^{3/2}} \exp[-\frac{1}{4t}(\frac{x^2}{K_o} + \frac{y^2}{K_o} + \frac{z^2}{K_o})]$ | Hanna et al. (1982) |
| 2-D, time-independent, variable $U$ and $K$, continuous ground-level line source | $U\frac{\partial \varphi}{\partial x} = \frac{\partial}{\partial z}(K_z \frac{\partial \varphi}{\partial z})$<br>B/C: $\varphi \to 0$ as $x, z \to \infty$ and $\varphi \to \infty$ as $x, z \to 0$<br>$K_z \frac{\partial \varphi}{\partial z} \to 0$ as $z \to 0$ and $x > 0$<br>$\int_0^{\infty} U\varphi \, dz = Q_{cl}$, $\forall x > 0$ instantaneous line source, given<br>$K_z = K_1(z/z_1)^n$ and $U = U_1(z/z_1)^m$ | $\varphi(x,z) = \frac{(m-n+2)Q_{cl}z_1^m}{2U_1\Gamma(s)}\left[\frac{U_1}{(m-n+2)^2 z_1^{m-n}K_1 x}\right]^s$<br>$\times \exp[\frac{U_1 z^{m-n+2}}{(m-n+2)^2 z_1^{m-n}K_1 x}]$<br>where $s = (m+1)/(m-n+2)$ and $\Gamma$ is the gamma function | Roberts (1923), Hanna et al. (1982) |
| 3-D, time-independent, constant $U$, variable $K$, continuous-point source at height $z$=$h_e$ | $U\frac{\partial \varphi}{\partial x} = \frac{\partial}{\partial x}(K_x \frac{\partial \varphi}{\partial x}) + \frac{\partial}{\partial y}(K_y \frac{\partial \varphi}{\partial y}) + \frac{\partial}{\partial z}(K_z \frac{\partial \varphi}{\partial z})$<br>$K_x = \alpha Ux$, $K_y = \beta Ux$, and $K_z = \gamma Ux$<br>B/C: $\varphi \to 0$ as $x, \lvert y \rvert, z \to \infty$ and $\varphi \to \infty$ as $x, y, z \to 0$<br>$K_z \frac{\partial \varphi}{\partial z} \to 0$ as $z \to 0$; and $U\varphi = Q_{cp}\delta(z-h_e)\delta(y)$,<br>continuous-point source at $(x,y,z) = (0,0,h_e)$ | $\varphi(x,z) = \frac{Q_{cp}}{2\pi x^2 U\sqrt{\beta\gamma}}\left[F_{z+h_e} + F_{z-h_e}\right]$, where<br>$F_{z+h_e} = \left[1 + \frac{\alpha}{x^2}\left(\frac{y^2}{\beta} + \frac{(z+h_e)^2}{\gamma}\right)\right]^{-(1+1/2\alpha)}$<br>$F_{z-h_e} = \left[1 + \frac{\alpha}{x^2}\left(\frac{y^2}{\beta} + \frac{(z-h_e)^2}{\gamma}\right)\right]^{-(1+1/2\alpha)}$ | Sharan and Yadav (1998) |

# 4 Numerical Solution Methods

Numerical methods allow the computation of approximate solutions using an integration technique such as the operator splitting (fractional time steps) or a global implicit method with a spatial approximation method such as finite difference or finite element method. Other discretization methods such as spectral methods, boundary element methods, and particle methods are occasionally applied in computational fluid dynamics, but are not frequently used in mesoscale Eulerian dispersion models and thus will not be discussed.

## 4.1 Grid-Volume Averaged Atmospheric Diffusion Equation

A control volume approach is commonly used in atmospheric modeling. Using a control volume approach, the physical law governing the problem (i.e., the conservation principle) is examined. This principle is, then, applied to a control volume around the node. For example, in air quality modeling, the atmospheric continuity equation is written for each control volume by establishing a mass balance. It is important to note that, in this approach, the discrete nature of the finite difference method is recognized at the outset. Finally, a mathematical statement of the physical conservation principle is obtained in a way somewhat similar to the procedures used to derive the partial differential equations. The control volume approach is relatively simple when regular grids are used. In this case, the choice for the control volume is simply the grid cell itself. However, if nodes are to be placed at the boundaries of the domain, then the boundary cells must be a certain fraction of the interior cells (e.g., 1/2 or 1/4 for an equal spacing of the nodes). In the case of unequal spacing nodes the situation is more complicated, and therefore it is customary to write special finite difference equations at the boundary of domain. However, no limit is taken for shrinking the control volume to a point.

We apply volume averaging represented in Eq. (10) to the diffusion equation for trace species, Eq. (19), to obtain

$$\frac{\partial \left\langle \bar{\phi}_i \right\rangle}{\partial t} + \frac{\partial \left\langle \bar{\phi}_i \bar{u} \right\rangle}{\partial x} + \frac{\partial \left\langle \bar{\phi}_i \bar{v} \right\rangle}{\partial y} + \frac{\partial \left\langle \bar{\phi}_i \bar{w} \right\rangle}{\partial z}$$

$$- \frac{\partial}{\partial x}\left\langle \bar{\rho} K_{xx} \frac{\partial \bar{q}_i}{\partial x} \right\rangle - \frac{\partial}{\partial y}\left\langle \bar{\rho} K_{yy} \frac{\partial \bar{q}_i}{\partial y} \right\rangle - \frac{\partial}{\partial z}\left\langle \bar{\rho} K_{zz} \frac{\partial \bar{q}_i}{\partial z} \right\rangle = \left\langle Q_{\varphi_i} \right\rangle \qquad (34)$$

where the off-diagonal terms were neglected for simplicity. For example, a derivative of the volume average can be approximated by the finite difference scheme as

$$\frac{\partial \langle \overline{\varphi}_i \overline{u} \rangle}{\partial x} = \frac{1}{\Delta V} \frac{\partial}{\partial x} \left[ \int_{z-\Delta z/2}^{z+\Delta z/2} \int_{y-\Delta y/2}^{y+\Delta y/2} \int_{x-\Delta x/2}^{x+\Delta x/2} \overline{\varphi}_i \overline{u} \, dx dy dz \right] \cong \frac{1}{\Delta x} \left[ \langle \overline{\varphi}_i \overline{u} \rangle^{x+\Delta x/2} - \langle \overline{\varphi}_i \overline{u} \rangle^{x-\Delta x/2} \right] \tag{35}$$

The volume averaged pollutant flux is further approximated by

$$\langle \overline{\varphi}_i \overline{u} \rangle^{x+\Delta x/2} \cong \langle \overline{u} \rangle^{x+\Delta x/2} \left[ \frac{\langle \overline{\varphi}_i \rangle^{x} + \langle \overline{\varphi}_i \rangle^{x+\Delta x}}{2} \right] \tag{36}$$

where the wind components are defined at the cell interfaces. This type of two-dimensional staggered distribution of scalar and vector components is referred to as the Arakawa-*C* grid (Mesinger and Arakawa, 1976) and is often used in Eulerian modeling for solving the flux-form transport equations like Eq. (34).

## 4.2 Numerical Solution Techniques

The operators in Eq. (34) resulting from the discretization of the atmospheric diffusion equation are three-dimensional. Incorporating the approximations like Eqs. (35) and (36) in the spatial derivatives and applying temporal derivative like the Crank-Nicholson method (e.g., Pielke, 1984), Eq. (34) is reduced to a nonlinear algebraic equation involving a sparse matrix as an operand. Usually it is extremely expensive to solve the nonlinear algebraic equation with very large rank (for typical atmospheric diffusion problem, when the three dimensional problem is solved simultaneously, the rank is of order of $10^6$). Furthermore, the characteristic time scales associated with the chemical production and the turbulent diffusion rates in the atmosphere are very small (usually a few seconds). Thus, very small time steps are required to get accurate solutions. On the other hand, multi-day simulations are typically performed in many applications of atmospheric models. Inversion of the large matrix thousands of times, at every time step, is costly despite of the rapid development of computer capability now and in near future. The required computational resources for comprehensive air quality models that include various other atmospheric processes in addition to the transport and diffusion usually dictates the use of operator splitting techniques.

### 4.2.1 Operator and Time Splitting

The various physical processes in the Eulerian dispersion equation have different mathematical properties. Because they impose different restrictions in the numerical solutions, it is difficult to evaluate if a suite of numerical schemes for the physical processes is accurate and stable. When a time splitting technique is applied, the system is split into a number of simpler subsystems, which can be solved consecutively one at a time. When applying the splitting method, equal time steps are not required for each of the subsystems. A relatively long time step may be used for the subsystem governing a slow process, while many smaller

steps calculate faster processes. In Eulerian dispersion modeling, the advection and diffusion and chemistry processes, for example, are separated, and they can be further split into one-dimensional operators using local approximations. The three-dimensional problem is thus reduced to a sequence of one-dimensional problems, which Yanenko (1971) called the method of fractional steps. The time-splitting method is also often called as the operator-splitting method (Otey and Dwyer, 1978). Furthermore, each component can be solved using different numerical techniques suitable to the characteristics of the described physical problem.

Operator splitting methods have been used in most air quality models, primarily due to different time steps allowed for physical processes representing atmospheric transport and chemistry (McRae et al., 1982). However, to best maintain numerical accuracy, the time splitting method requires detailed understanding of the temporal scales of individual physical processes to determine proper sequence of operator calls.

### 4.2.2 Global Implicit/Explicit Method

An alternative to the splitting methods is a global implicit method. With this method, all the physical processes are parameterized and discretized over the entire three-dimensional grid simultaneously. Because all the processes are being simulated at the same time and has to meet the Courant number requirement of the fastest process, the global implicit method requires large computational resources. Also, it is difficult to know if the solution converged due to the numerical damping associated with the numerical algorithms. The method is difficult to implement because of the weak modularity. The fact that the time step splitting demands more thought and effort for arranging the computational sequence of the operators is counterbalanced by the fact that the resulting simulations are generally faster than those using global-implicit methods.

To overcome this limitation, an implicit-explicit (IMEX) method has been suggested (Ascher, et al., 1995; Knoth and Wolke, 1998a, b). In the IMEX approach the (horizontal) advection is handled explicitly with a large time step and act as an artificial source in the coupled implicit integration of all the vertical transport processes (Knoth and Wolke, 1998b). For the implicit part of solution, either semi-implicit Runge-Kutta methods or a second order explicit-implicit backward differentiation formula (BDF) can be applied. The resulting numerical scheme can be very efficient while removing the arbitrary determination of the sequence of operators associated with a time-splitting method. A thorough review on the numerical time integration methods for photochemical air quality models with a large number of chemical species in three space dimensions is provided by Verwer et al. (1998).

## 4.3 Spatial Approximation and Discretization Methods

The equations governing atmospheric dynamics and chemistry are nonlinear partial differential equations that must be solved numerically. On a computer with a limited amount of memory, the values of the solutions cannot be represented everywhere, but only at a limited number of sample points in the modeling domain. The collection of sample points makes up a grid, while the individual locations at which the field variables are to be determined are called grid points or nodes. The process of representing a continuum by a finite number of points in space and time is known as discretization.

In this section, two common methods for spatial discretization are discussed—the finite difference method and the Galerkin method. The way in which the discretization is done is fundamentally different in each method. These discretization methods are fundamentally different and have major differences in their formulations.

### 4.3.1 Finite Difference Method

The most common numerical integration procedure for atmospheric modeling has been the finite difference method. In the finite difference method, the region being modeled is divided into a finite number of grid cells. Each of these cells is assumed to have a uniform (well-mixed) value for the pertinent dependent variable. For this reason, it seems natural that the node should be associated with the centroid (geometric center) of the cell. Note that this is different than the finite element method (discussed later), where the nodes are placed at the corners of the cell. With the finite difference method, the derivatives in the governing differential equations are replaced by finite difference approximations (for example, using a Taylor series expansion) to establish algebraic equations at the discrete set of points (usually of order of hundred thousands for atmospheric simulations) in space and time. The computers today can solve such large algebraic equations in a relatively short time. Many Eulerian transport models, in particular those with regular grid system, rely on the finite difference for their basic discretization method.

### 4.3.2 Galerkin Method

In the Galerkin method the spatial structure of each dependent variable is represented by basis functions. Suppose that a partial differential equation with appropriate boundary conditions is to be solved in a certain domain. When the approximation to the dependent variable(s), which is a sum of the products of the time dependent coefficients with the basis functions, is substituted into the partial differential equation, it yields a residual (i.e., an error). The Galerkin method requires that the residual be orthogonal to each basis function. Since the orthogonality requirement is expressed as a weighted integral of the residual, the Galerkin method is alternately known as the *weighted residual method*. In the

classical Galerkin method, the weighting functions (i.e., the weights of the residual) are chosen from the same space as the basis functions used to approximate the dependent variable. This procedure known as the Bubnov-Galerkin method is very effective in solving elliptic partial differential equations. For hyperbolic problems, more stable solutions are obtained when the weighting functions are selected from a space different than the basis functions. Such methods are usually associated with the name of Petrov-Galerkin (Brooks and Hughes, 1982). Recently, other methods have been introduced that may be very useful in atmospheric modeling, such as the Taylor-Galerkin method (Donea, 1984) and the Characteristic Galerkin method (Childs and Morton, 1990).

The two most useful Galerkin algorithms are finite element and spectral methods. The finite element method employs simple polynomials that are local (i.e., equal to zero except in a limited region), while the spectral method utilizes global basis orthogonal functions. The spectral method is often used in meteorological and global modeling. The introduction of the finite element method into atmospheric modeling is more recent. The finite element method should not always be viewed as a weighted residual method. The latter always leads to equations of integral form, which can be obtained by summation of contributions from various sub-domains. Similar integral forms can be obtained from the variational method when the problem is governed by a variational principle.

In the finite element method the region can be divided into triangular as well as rectangular elements. The nodes are placed at the corners of the elements. This is quite different from the way in which discretization is done in the finite difference method. The dependent variable (e.g., pollutant concentration in air quality models) is generally not constant over an element but varies in some prescribed manner, depending on the interpolation polynomial (i.e., the basis function) being used. There are several advantages of the finite element method. The approach is readily adapted to the boundaries, especially in the case of irregular grids. Flux type boundary conditions are automatically included in the finite element formulation. The advantage of the weighted residual approach over the mass balance approach used in finite differences becomes evident in the presence of unstructured irregular grids. In fact, one of the main advantages of the finite element method over other spatial approximation techniques is that the finite element method can handle irregular grids routinely. Often models that use Galerkin methods solve the advection-diffusion equation with a global implicit method, instead of using the time splitting, to reduce the computational burden of minimization of the residual errors repeatedly.

## 4.4 Grid Structure of Eulerian Models

The accuracy of numerical solution of the atmospheric diffusion equation depends heavily on the discretization method. As discussed earlier, it is customary to treat the vertical and horizontal coordinates separately in meteorological models. Almost all the atmospheric models use a structured vertical grid system

discretized along the vertical coordinate. Except for models intended to study atmospheric phenomena near surface with limited vertical extent, a non-uniform vertical grid is usually used. In general, the grid spacing increases logarithmically with height to account for the variation in the air density. The grid spacing can be further modified based on the need for accurate descriptions of important dynamics and physics, such as cloud mixing and PBL structure.

In principle, simulations with higher horizontal grid resolutions provide more accurate solutions unless there are scale dependencies among physical parameterizations used in the model. However, as will be shown later, decreasing the grid spacing increases the number of cells and requires a reduced time step size to achieve stable computational results. Practical limitations in computer size and speed prohibit the use of uniformly high spatial resolution appropriate for the smallest scales of interest. Two such methods of increasing resolution are nested approaches with a structured uniform grid and an unstructured grid. In the following, we describe issues associated with these two contrasting approaches.

### 4.4.1 Structured Grid and Nesting

Most atmospheric models rely on regular (structured and uniform) horizontal grid systems for simplicity. To obtain accuracy of simulations for a desired area, a grid nesting technique can be used. Grid nesting involves the sequential placement of multiple finer-scale meshes in desired regions of the domain so as to provide increased spatial resolution locally. Nesting can be divided into static and dynamic nesting. In the static nesting, the resolution and size of each grid are determined *a priori* and remain fixed throughout the model simulation. In the dynamic nesting, grids may be changed following changes in the control parameters during the simulation to obtain efficient yet accurate solutions. The static nesting approach is illustrated in Figure 4. The spatial resolution of the coarse grid is usually an integer multiple of that of the fine grid. First, the coarse grid solution is marched forward one time step. This solution provides initial and lateral boundary conditions (both concentration and flux) to the fine grid solution that is advanced at a smaller time step (usually an integer fraction of the time step of coarse grid). It is customary to set the time step ratio between the coarse and fine grids to equal the grid size ratio between the same two grids in order to retain the numerical accuracy at the same order of approximation. After multiple steps of the fine grid computations are completed to catches up with the coarse grid solution, the former may or may not be used to update the latter (i.e., two-way vs. one-way nesting). Although dynamic nesting with a structured grid is used in some atmospheric models, it may not be efficient for dynamic grid adaptation because the fine nest grid generation requires a high degree of user interaction and user expertise.

There are a few shortcomings of using grid nesting. One is the tendency for propagating dispersive waves to discontinuously change their speeds upon passing from a mesh to the next and to reflect off the boundaries of each nest due

to an impedance mismatch across the mesh boundaries. In addition, when dealing with chemical reactions, there is a problem of species mass conservation across the grid interface because the chemical production and loss of trace species are nonlinearly related with the ratios of mixtures, which in turn depend on the grid size. The mass of certain species (e.g., radicals) may no longer be conserved because, when advancing the fine grid solution, the non-linear chemical reactions happen in addition to transport. However, the mass of the basic chemical elements such as sulfur, nitrogen, and carbon must be conserved. This requirement is often handled by re-normalization of the concentration of each species based on the assumption that the ratio of the species mass to element mass will remain the same before and after the correction.

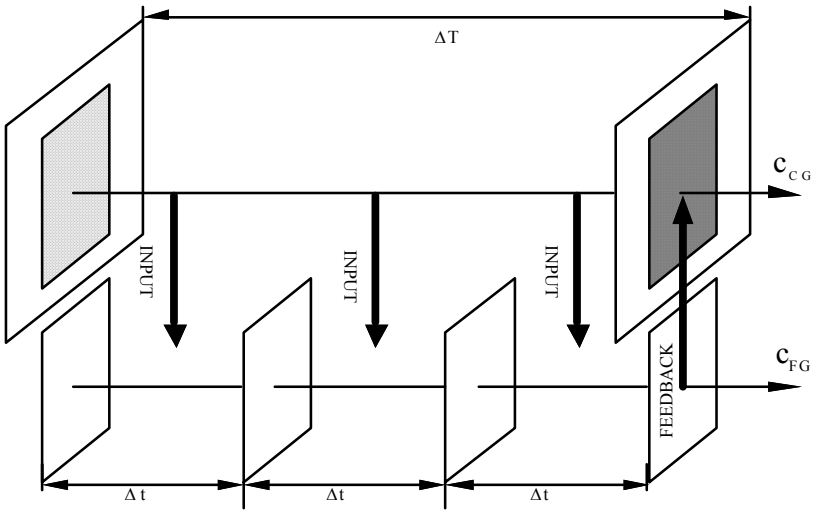


**Figure 4. Static grid nesting example. Multi-level nesting is capable through a natural extension of the single static grid nesting. $\Delta T$ and $\Delta t$ represent computational time steps of coarse and fine nest runs, respectively. In two-way nesting, the concentration from the fine nest grid simulation ($C_{FG}$) is used to update the coarse grid concentration ($C_{CG}$).**

### 4.4.2 Unstructured Grid

A few atmospheric models with unstructured horizontal grids have been developed recently. For example, a dynamically adapting weather and dispersion model, the Operational Multiscale Environmental Model with Grid Adaptivity (OMEGA) (Bacon et al., 2000) utilizes an adaptive unstructured grid technique that allows continuously varying horizontal grid resolutions ranging from 100 km down to 1 km. OMEGA can adapt its grid both statically to topographical features and dynamically to different adaptivity criteria such as fronts, clouds, hurricanes, and plumes. Also, Ghorai et al. (2000) solve the three-dimensional atmospheric dispersion equation using a time dependent adaptive grid technique based on tetrahedral elements. The unstructured grid technique is rather new to the atmospheric science community. In many fields of engineering applications, the unstructured grid method has been in use for more than a decade due to its

efficiency in the modeling of irregular domains. The flexibility of unstructured grids and their ability to adapt to transient physical phenomena are the features that give unstructured grid algorithms for partial differential equations their great power.

Grid refinement techniques can be subdivided into two basic categories. The first includes methods in which grid points are added locally to the computational domain as the calculation proceeds, or finite elements are subdivided locally, to provide increased spatial resolution based on predetermined physical criteria. The second category of refinement technique involves methods that redistribute a fixed number of grid points so as to provide locally increased resolution and thus an improved solution in certain regions of the domain. The static grid adaptability of an unstructured grid allows reduction of the total number of cells necessary to correctly simulate underlying physics, such as caused by the topography and land use. Further, a dynamic grid technique allows refinement of grids to resolve important physical events and features as the simulation is in progress. Bacon et al. (2000) summarize the dynamic grid adaptation process with four major steps: 1) at a predetermined time step specific variables or their gradients are evaluated to see if they meet the adaptivity criteria, 2) the mesh is refined where these criteria are satisfied, 3) the physical variables are interpolated to new cell centers, and finally 4) the mesh is coarsened where the criteria are not met. Setting the right criteria for adaptation is very important. There is a significant cost associated with a grid adaptation; hence, the ideal criteria are those that require minimum computational effort to evaluate yet indicate key regions requiring additional resolution.

## 5 Numerical Algorithms for Advection

In this section, we present advection separately from diffusion processes following the fractional time splitting concept. The algorithm discussions are mostly based on finite difference schemes on a structured grid system. In general, two transport processes are considered in atmospheric models: convection (or advection) and (turbulent) diffusion. Convection can only transport a disturbance in the direction of wind velocity. Turbulent diffusion, on the other hand, can spread a disturbance in every direction. The atmospheric continuity equation that governs pollutant transport and chemistry describes these transport mechanisms mathematically. Horizontal transport in the atmosphere is advection dominated. Numerical approximations to this equation have the *transportive* property, i.e., $d\langle q\rangle / dt = 0$. In Eulerian air quality models, the volume-integrated quantities for each cell are subject to following conservation equation:

$$\frac{\partial \langle \overline{\rho} \rangle}{\partial t} + \left[ \frac{\partial}{\partial x} \langle \overline{\rho} \overline{u} \rangle \right] + \left[ \frac{\partial}{\partial y} \langle \overline{\rho} \overline{v} \rangle \right] + \left[ \frac{\partial}{\partial z} \langle \overline{\rho} \overline{w} \rangle \right] = \langle \overline{Q}_{\rho} \rangle \tag{37}$$

The source term in the continuity equation $\langle \overline{Q}_\rho \rangle$ represents the error that might exist due to the mass-inconsistency in the input wind and density fields or deficiencies in the numerical scheme. Imposing the necessary condition $d(q)/dt = 0$ for the numerical transport under the possible mass consistency error, we obtain the following flux form conservation equation (Byun, 1999b).

$$\frac{\partial \langle \overline{\varphi}_i \rangle}{\partial t} + \left[ \frac{\partial}{\partial x} \langle \overline{\varphi}_i \overline{u} \rangle \right] + \left[ \frac{\partial}{\partial y} \langle \overline{\varphi}_i \overline{v} \rangle \right] + \left[ \frac{\partial}{\partial z} \langle \overline{\varphi}_i \overline{w} \rangle \right] = \langle \varphi_i \rangle \frac{\langle \overline{Q}_\rho \rangle}{\langle \overline{\rho} \rangle} \tag{38}$$

## 5.1 Numerical Advection Algorithms

There have been many studies on the numerical advection algorithms used in air quality models (e.g., Chock and Dunker, 1983; Chock, 1985, 1991; Rood, 1987) and the list is continuously growing. Numerical advection has attracted so much attention because it is the difficulty in obtaining a good numerical solution under variety of wind conditions and source distributions. Discretization of the hyperbolic equation generates only a finite number of Fourier modes that travel at different speeds and sometimes leads to destructive interference that causes interpretation of signals at different wavelengths. Various errors introduced by advection algorithms have historically been a major source of inaccuracy in air quality models. A classical problem in numerical analysis is to construct an advection scheme for a grid system that is not specially oriented to follow the characteristics of the solution. While it is essential to maintain conservative and transportive properties in the equations, the scheme must also satisfy stability and accuracy requirements. A signal being advected along the line of flow may also spread in a direction normal to the line of flow. This diffusion is referred to as artificial diffusion because it is inherent with the lack of numerical consistency in the numerical solutions.

The numerical algorithm is described with the one-dimensional version of the advection term with $\overline{u} = U$,

$$\frac{\partial \varphi}{\partial t} + \frac{\partial (U\varphi)}{\partial x} = 0 \tag{39}$$

where we replaced $\langle \overline{\varphi}_i \rangle$ with $\varphi$ for the simplicity in the expression. Eq. (39) is the flux (or conservation) form and the quantity $F_x = U\varphi$ is defined as the one-dimensional constituent flux. The flux form is a natural choice here because it is based on the continuity equation without any assumptions on the atmospheric dynamics. Discretization of the flux form of Eq. (39) results in

$$\varphi_j^{n+1} = \varphi_j^n - \frac{\Delta t}{\Delta x_j} \left( F_{j+1/2}^n - F_{j-1/2}^n \right) \tag{40}$$

where $F^n_{j+1/2}$ and $F^n_{j-1/2}$ denote the advective fluxes through the interfaces of cell $j$, $\Delta t$ is the time step, and $\Delta x_j$ is the cell length in the same metric space that the velocities are defined.

While it may appear that we have lost some coordinate system generality, multiplication of Eq.(40) by the cell's volume to yield cell mass, now leads us to a geometrical picture of the advection process that transcends the preceding mathematical complexity and leaves us with the simple algebraic equation:

$$M_j^{n+1} = M_j^n + (\Delta M^n_{j-1/2} - \Delta M^n_{j+1/2}) \tag{41}$$

where $M^n_j = \Delta x_j \varphi^n_j$ and $\Delta M^n_{j+1/2} = \Delta t_j F^n_{j+1/2}$. Basically, the mass in cell $j$ at the end of the time step is the mass at the beginning of the time step plus the mass increment entering the cell from its left-hand neighbor minus the mass increment passed along to the cell's right-hand neighbor (assuming all cell-face velocities are positive). The complexity is now buried in how we define the mass transfers, $\Delta M$, and the CFL numbers, $\beta$, at the cell faces. For a temporally-explicit (i.e., forward-in-time) scheme, and a positive value of $U_{j+1/2}$, we define the Courant-Fridlich-Lewy (CFL) as:

$$\beta_{j+1/2} = U_{j+1/2} \frac{\Delta t}{\Delta x_j} \tag{42}$$

Should $U_{j+1/2}$ be negative, the appropriate $\Delta x$ to be considered would be that of the upwind cell $\Delta x_{j+1}$. Similarly, the cell to be considered for the mass transfers is always the upwind cell, so for the case of the positive value of $U_{j+1/2}$, we define the current $\Delta M^n_{j+1/2}$ as: $\Delta M^n_{j+1/2} = -\beta_{j+1/2} M^{*n}_j$, where $M^{*n}_j$ can be a high-spatial-order definition of the mass distribution within the cell or reduces to the cell mass $M^n_j$ itself for the case of low-order, Donor-cell treatment or when $\beta_{j+1/2} = 1$. Thus, in the simple case of Donor-cell advection, the fraction of a cell's mass that is transferred across a face is just equal to the outgoing CFL number at that face. To maintain numerical stability and to accommodate other physical changes such as emissions input in a synchronized way, the time step of 1-D advection should satisfy the CFL condition for the whole domain:

$$\beta_{\max} = \max_j \frac{|U_{j+1/2}| \Delta t}{\Delta x_j} \le 1 \tag{43}$$

The only geometrical factor not considered in this view is the local spatial variation of the map factor within the particular cell being depleted. Though this

gradient term is present in the formulation of transport, these gradients are mostly discarded in finite difference implementations as being "higher-order" differentials. However, as they relate simply to the "shape" of the cell (i.e., to the cell being non-square), they may be easily included by a multiplicative "keystoning factor". Thus, in the two-dimensional transport example we now allow the cell to be trapezoidal in shape with differing transverse widths, $\Delta y_{j+1/2}$ and $\Delta y_{j-1/2}$, at the right and left faces and correct the CFL with the easily visualized and derived, multiplicative "keystoning factor", expressed as, for $\beta_{j+1/2} > 0$:

$$K_{j+1/2} = \beta_{j+1/2} + 2(1-\beta_{j+1/2})\frac{\Delta y_{j+1/2}}{\Delta y_{j+1/2} + \Delta y_{j-1/2}} \tag{44}$$

Using this corrected CFL, $K_{j+1/2} \cdot \beta_{j+1/2}$, means that advection will now transfer the correct fraction of cell area or mass destined to be transferred rather than the correct, *x*-directional fraction of cell length. It is interesting that by folding the length-scale parallel to the wind component into the face CFL and the aerial and vertical map factors into computation of the total cell mass, one is then able to proceed with the development of a sophisticated, mass-conservative, advection scheme for an arbitrary metric grid with simple arithmetic.

Although the Donor-cell advection scheme, which assumes a constant concentration distribution within each cell, has several necessary properties (i.e., it is mass-conservative, positive-definite, and transports material at the correct speed), it is extremely diffusive. The many dozens of pollutant advection schemes developed over the past decades attempt to minimize this numerical diffusion of material by employing a more accurate description of the concentration distribution within each cell. This is accomplished generally by describing the in-cell distribution with some higher-order polynomial and basing the coefficients of that polynomial on local or global variations of the gridded, average concentrations. For example, some schemes utilize a fairly local definition of a first-derivative, such as: $(\partial\varphi/\partial x)_j = (\varphi_{j+1} - \varphi_{j+1})/2\Delta x$, whereas other schemes would call upon more distant point pairs (e.g., (*j*+2,*j*-2), (*j*+3,*j*-3), and beyond) to compute this first derivative and/or higher derivatives, and are often referred to as higher-order-accurate or 'global' derivative definitions, those the term global is sometimes reserved for schemes where derivatives are computed based on implicit relationships rather than on an explicit, truncation-error-reducing series involving the more distant grid point information. The virtue of these higher-order polynomial schemes that involve various definitions of the spatial derivatives is that they can accurately capture realistic and dramatic spatial variations in $\varphi_j$ within in the cell *j*; however, such dramatic variations can also include undesired concentration overshoots and undershoots (e.g., Gibbs

ringing, negative concentrations, antidiffusive instability) that must be suitably blocked ahead of time or filtered out after the fact.

In Eulerian dispersion modeling, it is essential that an advection scheme be mass-conservative, but we have seen that this is guaranteed by the flux-formulation and not by the details of the advection scheme itself. If non-linear chemistry is to be modeled as well, then the scheme must be positive-definite (i.e., not permitting negative concentration solutions that would cause the chemical solver to add to this unphysical behavior) and should also avoid any excessive erosion of a uniform background concentration. Beyond these 'musts', the importance given to minimizing various uncertainty measures (e.g., root-mean-square error, maximum error, average error, sum of concentrations squared), or such measures applied to $\log(\varphi_j)$ or any measure as a function of the wavelength/shape of the test distribution, still remains rather subjective and, as a result, has inhibited converging on an algorithm that could reasonably be called the 'best'. For example, were it not for an abysmal response to single point-source emissions, few would contest the superiority of spectral methods in providing very high-fidelity response to longer wavelength distributions; however, computational expense is also a factor that weighs into this subjective judging, and this factor weighs against the spectral techniques. In addition, most advection tests are performed on uniform, constant thickness grids. An advection scheme should also yield smooth, accurate non-negative solutions over differently scaled portions of irregular grid systems. Similarly, sharp concentration gradients or horizontal variations in the vertical dimensions of grid cells should not lead to accelerations or decelerations of material in the horizontal direction (see Table 4 for the algorithms of several advection schemes often used in Eulerian dispersion modeling).

Performance characteristics of these advection schemes should also be studied for realistic atmospheric conditions rather than just for over-simplified flows and idealized distributions. The traditional long-wave propagation tests, such as the cosine-hill rotation test case (Crowley, 1968) tend to show an advection scheme at its best; however, adequate short wavelength performance is also extremely important in Eulerian dispersion models. One of the most stringent tests involves the two-dimensional transport and diffusion of emissions from a single-grid source (Yamartino, 1993). This situation often arises in air quality modeling despite the fact that the maximum resolution of transport algorithms is limited to two grid cell lengths (i.e., $\lambda = 2\Delta x$ waves are very rapidly diffused). Such test problems are often neglected in evaluating advection algorithms, but later become inevitable in actual simulations. Thus, identification of suitable evaluation cases is an issue just as important as developing advection schemes with *acceptable* characteristics.

## 5.2 Artificial Diffusion

It is well documented that numerical advection schemes are associated with the major sources of inaccuracy, particularly from artificial numerical diffusion and dispersion. Usually, low-order schemes display considerable diffusive dissipation. The amount of artificial diffusion introduced by low-order numerical algorithms can easily outweigh physical diffusion. On the other hand, higher-order schemes are dispersive and generate spurious oscillations that can even lead to instabilities. The more popular algorithms try to find the best compromise between these two sources of inaccuracy to arrive at an *acceptable* solution. What is meant by acceptable is still a major topic of discussion among atmospheric modelers.

The numerical dispersion can be easily understood by analyzing the one-dimensional version, Eq. (39). With a central first-order finite-difference scheme and for a constant wind speed $U$, we obtain

$$\frac{\varphi_j^{n+1} - \varphi_j^n}{\Delta t} = -U \frac{\varphi_{j+1}^n - \varphi_{j-1}^n}{2\Delta x} \tag{45}$$

where we used a central spatial differencing. Analysis of the truncation terms shows that the error $\varepsilon$ generated by the approximation of using Eq. (45) instead of Eq.(39) is

$$\varepsilon = \frac{U\Delta x}{2}(1 - U\frac{\Delta t}{\Delta x})\frac{\partial^2 \varphi}{\partial x^2} + H.O.T$$

$$= D_N \frac{\partial^2 \varphi}{\partial x^2} + H.O.T \tag{46}$$

which is a diffusion-type term with the associated diffusivity $D_N$ equal to

$$D_N = \frac{U\Delta x}{2}(1 - \beta) \tag{47}$$

where $\beta = U\Delta t/\Delta x$ represents the CFL number (signed) and *H.O.T.* denotes the higher-order terms. In general, the even-ordered derivatives in terms of $x$ represent the diffusion errors (i.e., loss of peak magnitude) while the odd-ordered derivatives represent the dispersion error (displacement of peak location in the signal, or phase-speed error). This analysis demonstrates that the numerical dispersion with the central difference scheme is proportional to the grid size $\Delta x$ and is dependent on the Courant number of the flow. Different advection algorithms exhibit different numerical diffusion characteristics.

## 5.3 Mass Correction after Numerical Advection

A fundamental requirement for the numerical transport algorithms is the conservation of trace species in the domain. A conservative numerical advection algorithm can conserve trace mass when driven by the mass consistent wind and density fields. However, the meteorological data used in trace transport are often mass inconsistent. Simulating meteorological conditions for a limited area like urban or regional scale, the total air mass in the modeling domain is subject to the inflow, outflow, top, and bottom boundary conditions imposed by large synoptic scale weather systems and surface exchanges of heat and moisture. Furthermore, the time splitting of the original three-dimensional transport into a sequence of one-dimensional solutions introduces cross-term errors that must be corrected. To take into account the residual (error) term as part of the numerical transport process, we must solve the following correction term as a part of the numerical transport.

$$\frac{\partial \langle \overline{\varphi}_i \rangle}{\partial t} = \langle \overline{\varphi}_i \rangle \frac{\langle \overline{Q}_\rho \rangle}{\langle \overline{\rho} \rangle} \tag{48}$$

Ideally, $\langle \overline{Q}_\rho \rangle$ must vanish everywhere in the computational cells. If not, an algorithm that theoretically conserves mass may fail to conserve trace species mass in the application. Byun (1999b) and others proposed to handle the mass inconsistency by forcing conservation of mixing ratio (instead of mass) during the advection process. The undesirable effects of the mass-inconsistent error can then be corrected with:

$$(\overline{\varphi}_i)^{cor} = (\overline{\varphi}_i)^T \exp[\int \frac{(\overline{Q}_\rho)}{(\overline{\rho})} dt] \tag{49}$$

where superscripts *T* and *cor* represent values after transport (advection) and after correction, respectively. An adequate correction scheme conserves the trace mixing ratio even if wind and density fields are not mass consistent. It is given as:

$$(\overline{\varphi}_i)^{cor} = \frac{(\overline{\varphi}_i)^T}{(\overline{\rho})^T} (\overline{\rho})^{\text{int}} \tag{50}$$

where $(\overline{\rho})^{\text{int}}$ is the volume-weighted density interpolated in time at the integration time step.

For a limited-area atmospheric model where air mass in the model domain is not conserved, the mixing-ratio conservation scheme is demonstrated to be useful for photochemical air quality simulations where chemical production and loss terms

are computed using molar mixing ratio. However, one should be reminded that the above approach only fulfills a necessary condition, but not sufficient condition, for mass conservation. Therefore, before applying this final correction step, the mass inconsistency in the meteorology data must be minimized such as using a variational wind field adjustment scheme. The correction scheme fixes mixing ratio conservation errors due to the time splitting, numerical algorithms, and the mass inconsistent meteorological data input altogether. It does not, however, improve the inherent properties of a numerical advection scheme such as monotonicity, or numerical diffusivity. It must be emphasized that time splitting of advection into horizontal direction and vertical direction is for the convenience of obtaining numerical solution. The three-dimensional advection and the mass adjustment are the necessary steps to simulate inseparable atmospheric advection process.

# 6 Horizontal Diffusion Algorithm

For atmospheric modeling the three-dimensional diffusion is often decomposed into horizontal and vertical directions because the two are subject to different distinctly different atmospheric processes. The horizontal mixing is influenced by the heterogeneous atmospheric conditions in a grid cell and is frequently parameterized with the eddy-diffusion theory. From Eq. (34) in which the off-diagonal terms are neglected, the horizontal diffusion equation is given as:

$$\frac{\partial(\overline{\varphi}_i)}{\partial t} = \frac{\partial}{\partial x}\left(\overline{\rho} K_{xx} \frac{\partial \overline{q}_i}{\partial x}\right) + \frac{\partial}{\partial y}\left(\overline{\rho} K_{yy} \frac{\partial \overline{q}_i}{\partial y}\right) \tag{51}$$

The horizontal diffusion is often solved with an explicit finite difference method to minimize memory requirements in Eulerian transport models with a sufficiently small time step to ensure the positivity of solution. In Eulerian air quality modeling, eddy diffusivities are usually not distinguished in two different horizontal directions (i.e., $K_{xx} = K_{yy} = K_H$). Then, the problem is reduced to parameterization of the eddy diffusivity to reflect the sub-grid scale diffusion.

## 6.1 Horizontal Diffusivity Estimated from the Lagrangian Dispersion Theory (from Section 6.3.2 of Zannetti, 1990)

Estimation of the horizontal diffusivity presents several intriguing aspects. It is often (and perhaps, improperly) assumed that $K_H \approx K_y$, where $K_y$ is the crosswind eddy diffusivity (i.e., with wind blowing along the positive *x*-axis). $K_y$ is not necessarily equivalent to $K_{yy}$ used for the Eulerian modeling exactly. For a plume originated at $x = 0$ and carried by the wind along the *x*-axis, $K_y$ is related through Eq. (32) to the standard deviation of $\sigma_y$ of the crosswind plume concentration spread. For a short travel time ($t = x/U(z) < T_L$)

$$K_y = c\left(\frac{U}{\Delta x}\right)^2 T_L \sigma_y{}^2 \tag{52}$$

where $c$ is a constant that depends on the distance from the source and $T_L$ is the Lagrangian turbulence time scale, which is the characteristic time scale determined by the auto-spectral correlation function following the movement of plume (with typical value of 100 sec for convective PBL). For a travel time much larger than the Lagrangian time scale (i.e., $t >> T_L$), the Lagrangian dispersion theory predicts that:

$$K_y = \frac{1}{2}\left(\frac{U}{\Delta x}\right)\sigma_y{}^2 \tag{53}$$

To estimate the horizontal eddy diffusivity $\sigma_y$ must be estimated from meteorological measurements. For example, the horizontal diffusion in a grid model is related to the long-range transport and diffusion of a plume from a point source at the ground surface (Pasquill, 1976):

$$\sigma_y = \sigma_\theta \Delta x f(\Delta x) \tag{54}$$

in which $\sigma_\theta$ is the standard deviation of the horizontal wind direction expressed in radians. The empirical function $f(\Delta x)$ is specified following Hanna et al. (1977); Irwin (1979); and Arya (1999):

$$f(\Delta x) = \begin{cases} \left[1 + 0.308\Delta x^{0.455}\right]^{-1}, & for\ \Delta x \le 10^4\, m \\ 33.3\Delta x^{-1/2}, & for\ \Delta x > 10^4\, m \end{cases} \tag{55}$$

Eq. (55) represents a curve fit to Table 2.

**Table 2. Pasquill's (1976) empirical function $f(\Delta x)$**

| $\Delta x$ (m) | 0 | 100 | 200 | 400 | 1000 | 2000 | 4000 | 10000 | >10000 |
|---|---|---|---|---|---|---|---|---|---|
| $f(\Delta x)$ | 1.0 | 0.8 | 0.7 | 0.65 | 0.6 | 0.4 | 0.4 | 0.33 | $33.3(\Delta x)^{1/2}$ |

The horizontal eddy diffusivity is:

$$K_y = \begin{cases} c\left(U\sigma_\theta\right)^2 \dfrac{T_L}{\left[1 + 0.308\Delta x^{0.455}\right]^2}, \text{ for } \Delta x \le 10^4 \text{ m} \\ 0.5 \times 10^3 U\sigma_\theta{}^2, \qquad \text{for } \Delta x > 10^4 \text{ m} \end{cases} \tag{56}$$

As expected, $K_y$ is independent of the grid size for large downwind distance (which corresponds to the grid size in Eulerian models).

For $\Delta x > 10^4$ m, given typical values of $\sigma_\theta < 0.5$ radian and $U < 10$ ms$^{-1}$, Eq. (56) gives $K_y$ values one to two orders of magnitude lower than the bottom range of $K_H = 10^4$ to $10^7$ m$^2$ s$^{-1}$ currently used in most long-range models and considered to be the best values to fit actual measurements. This inconsistency can be traced back to the implicit assumption of the Lagrangian transport that the plume trajectory is known exactly and that $\sigma_y$ and $K_H$ characterizes only the horizontal growth of plume and not the uncertainty in the plume location. There are serious limitations estimating the Eulerian eddy diffusivity ($K_H$) at a certain location ($x,y,z$), for example at the boundary of a grid cell, with the Lagrangian dispersion theory. Different values of $K_y$ would be required for the pollutant plumes traveling from different sources, and therefore, having different travel times. An Eulerian model cannot handle this, because, after pollutants are injected into the grid cells, the memory of their different origins is lost. Actual modeling simulations, however, use meteorological wind fields, which contain a large degree of uncertainty when used for trajectory computations. Therefore, it is not surprising that actual model calibration tests suggest large values of $K_H$. This indicates that horizontal diffusion needs to be artificially enhanced for the model to incorporate the uncertainties in the wind fields.

To visualize the above considerations, consider a simple example shown in Figure 5, in which the contributions of three air pollution sources ($S_1$, $S_2$, and $S_3$) at the receptor $R$ are evaluated through dispersion modeling with large $K_H$ values. Although the model largely overestimates horizontal diffusion, it provides a total concentration value at $R$ (the sum of three dashed curves) that is quite similar to the measured value (on the solid curve) due to compensation of errors in diffusion and wind fields. The model is, in a way, "validated", but its use for evaluating emission reduction strategies will provide incorrect results; specifically in the case of emission reductions in $S_1$, $S_3$ with insufficient control of $S_2$. It is true that regular fluctuations in wind direction cause the solid plumes in Figure 5 to sweep around the azimuth in such a way that they all may envelope the receptor $R$. This variation of the short-term average wind can sometimes be correctly simulated, for long-term averages, by the dashed plumes, which are computed with an enhanced horizontal diffusion. However, wind direction fluctuations often do not show regular behavior and therefore, do not support the approximation. In complex terrain, especially, preferred directional patterns play important roles in determining plume trajectories, and the artificial enhancement of horizontal diffusion for long-term averages may provide incorrect results. Moreover, if nonlinear chemical reactions are used, the formation of secondary pollutants is incorrectly computed when the plume is diffused with artificially high dispersion rate, since the centerline plume concentration is consistently underestimated.

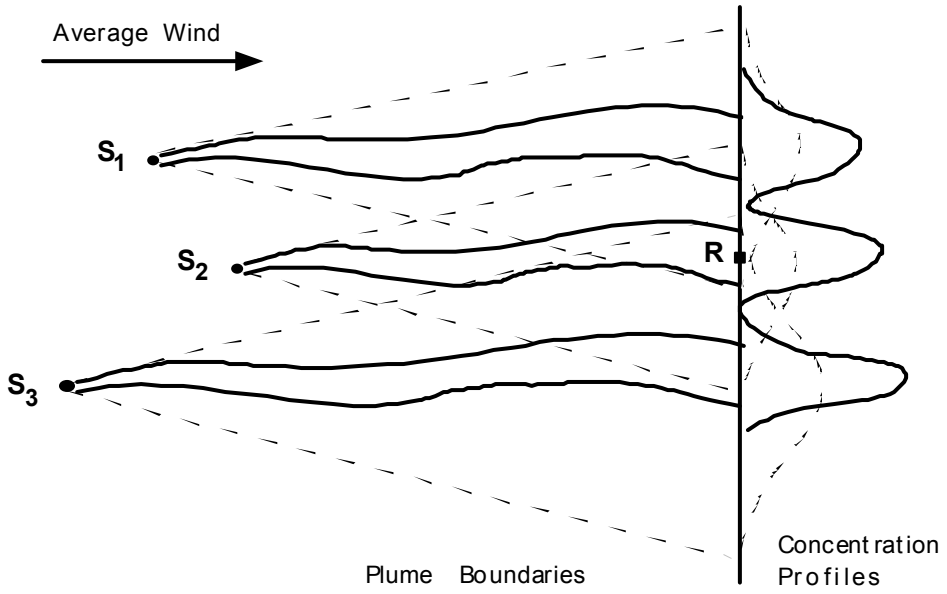


**Figure 5. An example of the consequence of overestimating horizontal diffusion on the concentration at the receptor R. Solid lines show the actual average plume, while dotted lines show the plumes as simulated by the model.**

## 6.2 Other Approaches for Estimating Horizontal Eddy Diffusivity

In an ideal case, the process must represent the effects of physical diffusion on pollutant dispersion. Although our understanding of horizontal turbulence is rather limited, appropriate accounting of physically based horizontal diffusion is necessary. We can identify certain types of nonphysical horizontal diffusion such as numerical diffusion resulting from the inconsistency (i.e., errors in higher-order expansion terms) in the advection scheme and artificial diffusion resulting from the instantaneous dilution of emissions and concentrations by the finite volume of the Eulerian grid cells. In the past, the horizontal diffusion process was often omitted because the numerical diffusion associated with the advection algorithm was large. It is also important to realize that the Eulrian simulation takes into account for the genuinely advective characteristics of pollutants.

For example, Smargorinsky's (1963) horizontal diffusivity algorithm accounts for the transport (stretching and shearing deformation) characteristics of wind flows:

$$K_{HT} = 2\alpha_o{}^2 (S_\Gamma{}^2 + S_\Lambda{}^2)^{1/2} (\Delta x)^2 \tag{57}$$

where $\alpha_o \cong 0.28$ and stretching strength ($S_\Gamma$) and shearing ($S_\Lambda$) strength are defined by

$$S_{\Gamma} = \frac{1}{2}\left(\frac{\partial U}{\partial x} - \frac{\partial V}{\partial y}\right) \tag{58a}$$

$$S_{\Lambda} = \frac{1}{2}\left(\frac{\partial V}{\partial x} + \frac{\partial U}{\partial y}\right) \tag{58b}$$

Because Eq. (57) relies on the grid-scale wind components, it is not suitable for estimating the sub-grid scale diffusion not resolved by the provided wind fields. Furthermore, for coarse resolution where numerical diffusion is already large, use of this formula seems inadequate. Draxler and Hess (1997) used similar formula in the HYSPLIT, a Lagrangian modeling system where numerical dispersion is not much an issue.

Yamartino and Machiraju (2000) suggest a method to determine appropriate horizontal diffusion coefficients by subtracting the numerical diffusivity already accompanying the advection scheme (see above). Artificial diffusion refers to the instantaneous dilution of emissions and concentrations by the finite volume of the grid cells. This instantaneous diffusion has traditionally been accepted as a penalty for using Eulerian grid models. If a few sources contributing to a cell are deemed important enough to avoid the instantaneous diffusion, they must be treated by either a finer nested mesh to cover the sub-domain of interest, or with a plume-in-grid module (see section 1.4) to describe the early dispersion/chemistry evolution of pollutants emitted. The specified horizontal diffusion term in Eulerian dispersion models, when combined with the effects of the input wind fields, the numerical diffusion of the advection scheme and the instantaneous dilution in the grid cell, should best simulate diffusion that is observed in the atmosphere. To achieve this goal, the artificial diffusion and numerical diffusion terms must be quantified for each of the advection algorithms. This is difficult, though not impossible, to accomplish because the numerical diffusion characteristics of a specific advection algorithm are not only dependent on the wave number of the signal but also the CFL number of the transport flow (Odman, 1998).

If numerical diffusion dominates, to compensate for the effectively larger instantaneous dilution in a larger grid size, eddy diffusivity component accounting for the grid size difference, $K_{HN}$, may be parameterized to counter act the numerical diffusivity $D_N$ to give (e.g., Byun et al., 1999):

$$K_{HN}(\Delta x) = K_{Hf}(\Delta x_f)\left(\frac{\Delta x_f}{\Delta x}\right)^2 \tag{59}$$

where $K_{Hf}(\Delta x_f)$ is a uniform eddy diffusivity at a fixed resolution $\Delta x_f$. In Eulerian dispersion models, $K_{Hf}(\Delta x_f)$ of order of 50-2000 $m^2s^{-1}$ is used,

depending on the magnitude of $\Delta x_f$. The formula, however, is inadequate for a very fine grid size where the physical dispersion dominates over the numerical diffusion. The difference between the grid size dependencies represented in Eqs. (57) and (59), respectively, is striking. A heuristic method combining the two formulae is suggested here with an analogy to the resistance law concept used for the estimation of deposition velocity:

$$\frac{1}{K_H} = \frac{1}{K_{HT}} + \frac{1}{K_{HN}} \tag{60}$$

This formula, which has yet to be evaluated with realistic Eulerian dispersion simulations, attempts to resolve the dichotomy existing between the contrasting dependencies on grid resolution in the components of horizontal diffusivity. For a large grid size, the effect of the transportive dispersion is minimized while for a small grid size the impact of the numerical diffusion term is reduced.

In the literature, there are a few horizontal-diffusivity formulations that depend on the atmospheric stability and/or height from the surface. In the Fifth-Generation Penn State/NCAR Mesoscale Model (MM5) (Grell et al., 1994), both the second-order diffusion similar to Eq. (51) and a more scale-selective fourth-order diffusion are used. The second-order diffusion is applied only for the coarsest MM5 simulation domain and the fourth-order form is used in the interior of the coarsest domain as well as in the entire domain of any refinement mesh. The horizontal diffusion coefficient $K_H$ consists of a background value $K_{H0}$ and a term proportional to the deformation $D = 2(S_\Gamma{}^2 + S_\Lambda{}^2)^{1/2}$:

$$K_H = K_{H0} + 0.5k^2 \Delta x^2 D \tag{61}$$

where $K_{H0} = 3.0 \times 10^{-3} \Delta x^2 / \Delta t$. In RAMS, the eddy mixing coefficient is a function determined by the deformation ($D$), Brunt-Vaisala frequency ($N_B$), and the Richardson number ($Ri$)

$$K_{hi} \sim (c_x \Delta x)(c_z \Delta z) \;\; f(D, N_B, Ri) \tag{62}$$

where $c_x$ and $c_z$ are dimensionless coefficients multiplying the horizontal and vertical spacings $\Delta x$ and $\Delta z$ to obtain characteristic horizontal and vertical mixing length scales, respectively. There are a few formulations that depend on the boundary layer height $h$. For example, for unstable conditions, $K_H$ is parameterized by (Seinfeld, 1986)

$$K_H = 0.1 w_* h = 0.1 h^{3/4} (-k/L)^{-1/3} u_* \tag{63}$$

which was derived from the measurements of Willis and Deardorff (1976). Eppel et al. (1995) parameterized horizontal diffusivity as a simple factor of the vertical

eddy diffusivity, such as $K_H = 2.3\ K_{zz}$, in which $K_{zz}$ is in turn dependent on the mixing length scale. Considering the size of eddies grow with height, and assuming the continuity of eddy motion, the dependency of $K_H$ on altitude is plausible. However, in Eulerian models, $K_H$ must represent the effects of horizontal wind variability, which in fact is reduced with height as the air moves away from the surface roughness elements.

Hanna (1994) stated that the procedure for estimating horizontal diffusion at the sub-grid scale has not yet been resolved in a consistent manner in three-dimensional Eulerian models. He concluded that the Eulerian models must employ wind fields that include the full spectrum of mesoscale and regional fluctuations in space and time. Overly smooth wind fields provided by the diagnostic wind field modeling or mesoscale meteorological models cannot yield sufficient horizontal diffusion in the model. McNider et al. (1996) stated that in current meteorological models the energy spectrum corresponding to 120 km (or four times the horizontal grid spacing used) to 1 km (below which boundary layer turbulence is parameterized) is not well represented. Furthermore, the parameterizations of sub-grid scale horizontal diffusivities incorporated in commonly used regional models produce $K_H$ values that range over several orders of magnitude.

Once the value of eddy diffusivity is defined, we can use an explicit solution method for Eq. (51):

$$(\rho)_{l,m}^{n+1} q_{l,m}^{n+1} = (\rho)_{l,m}^{n} q_{l,m}^{n} + \frac{\Delta t}{(\Delta x)^2}\left[(\rho)_{l+1,m}^{n} \overline{K_{l+1,m}^{11}}(q_{l+1,m}^{n} - q_{l,m}^{n}) - (\rho)_{l,m}^{n} \overline{K_{l,m}^{11}}(q_{l,m}^{n} - q_{l-1,m}^{n})\right]$$

$$+ \frac{\Delta t}{(\Delta y)^2}\left[(\rho)_{l,m+1}^{n} \overline{K_{l,m+1}^{22}}(q_{l,m+1}^{n} - q_{l,m}^{n}) - (\rho)_{l,m}^{n} \overline{K_{l,m}^{22}}(q_{l,m}^{n} - q_{l,m-1}^{n})\right] \qquad (64)$$

where $\overline{K_{l,m}^{11}} = (K_{l,m+1}^{11} + K_{l,m}^{11})/2$ and $\overline{K_{l,m}^{22}} = (K_{l+1,m}^{22} + K_{l,m}^{22})/2$. At the boundary cells, a zero-gradient Neumann boundary condition can be applied. The implicit scheme is not used here to minimize the computer memory requirement for handling large horizontal grid in the subroutine. Because Eq. (61) is an explicit scheme, the time-step should be chosen to prevent numerical instability and to maintain positivity. With an appropriate CFL number for horizontal diffusion $\beta_{hdiff}$, when $\Delta x = \Delta y$, the time-step can be determined with:

$$\Delta t\big|_{hdiff} = \beta_{hdiff} \frac{(\Delta x)^2}{\max\limits_{\forall(l,m)} (K_{l,m}^{11}, K_{l,m}^{22})} \qquad (65)$$

A range of $\beta_{hdiff}$ value 0.5-0.75 is often used in air quality modeling.

As discussed above, specification of horizontal eddy diffusivity is one of critical problems associated with the *K*-theory grid models. In order to compensate for uncertainties in wind direction and speed information, these models always overestimate horizontal diffusion in a process that smears concentration peaks. With more or less uniformly distributed emission sources and with wind spectrum following a normal Gaussian distribution, this assumption is quite acceptable. But, in many cases, this smoothing process creates a loss of deterministic information related to the source-receptor relationship. This loss becomes particularly critical when selective emission reduction strategies are inferred from modeling outputs in order to meet air quality goals.

# 7 Vertical Diffusion Algorithm

Sub-grid-scale vertical diffusion of trace pollutants in the atmospheric boundary layer is an important physical process that must be addressed in Eulerian dispersion models. It needs to be modeled to allow realistic mixing under various meteorological conditions. Two different turbulence closure schemes, *local* closure and *nonlocal* closure, have been used for the parameterization of vertical diffusion. Local closure assumes that turbulence is analogous to molecular diffusion, i.e., the flux at any point in space is parameterized by known mean values at the same point (Stull, 1988). Most models use either a first order *K*-theory or simplified second order closure for the local approach. In a nonlocal closure the turbulent flux at one point is parameterized by mean quantities at many vertical layers thus allowing exchange of mass between nonadjacent layers. The nonlocal closure usually is intended for convectively unstable conditions, while the first and second order closures can be applied to both stable and unstable conditions.

## 7.1 First-Order Local Closure Techniques

First-order closure retains the prognostic equations for only the mean variables such as wind, temperature, humidity, and trace-gas concentrations while the second-order moments (Reynolds fluxes) are modeled. The Reynolds flux term is approximated with a gradient transport theory (*K*-theory), or mixing length theory. These methods are widely used in both meteorological and air quality modeling studies because of their simplicity. These methods frequently fail however when eddies larger than the grid size are present in the flow. For example, in the presence of convective conditions, *K*-theory is not recommended. With the *K*-theory, the vertical diffusion equation is given in the Cartesian coordinate system as

$$\left.\frac{\partial \overline{\varphi}_i}{\partial t}\right|_{vdiff} = \frac{\partial}{\partial z}\left(\overline{\rho} K_{zz} \frac{\partial \overline{q}_i}{\partial z}\right) \tag{66}$$

One of the problems with first-order closure is finding a rational basis for parameterizing the eddy diffusivity. Only routinely measured or model-resolvable meteorological variables are used to explicitly specify a *K*-profile.

### 7.1.1 Vertical Eddy Diffusivity Parameterizations

While models with constant *K* values are easily solved analytically, they do not represent the turbulent exchange characteristics of the planetary boundary layer very well. Therefore, a more physically realistic *K*-profile that varies with height is often used. $K_{zz}$ is allowed to vary depending on height, thermal stability, local gradients of potential temperature. There is a drawback in that the parameterizations sometimes cannot characterize the total turbulent flow adequately. A slightly different approach uses $K_{zz}$ parameterization in terms of a mixing length $l$ so that one must directly determine $l$ instead of $K_{zz}$. Blackadar (1962) extended Prandtl's mixing length hypothesis to determine the length at which an eddy loses it identity and mixes completely with the environment. Lacser and Arya (1986) summarized many related works and provided a review of mixing length parameterizations in the stable stratified nocturnal boundary layer.

Hanna (1994) expressed some concerns about the proper formulation of $K_{zz}$ in Eulerian dispersion models. In particular, the accurate specification of vertical diffusivity is highly important during stable conditions near the ground and aloft throughout a day. Observations often show layers of pollutants persisting at elevations of a few hundred meters during most of the night. If a value is specified for $K_{zz}$ that is too large, these layers are diffused away. The problem with specifying $K_{zz}$ is that very little is known about the stable boundary layer near the ground and aloft. Turbulence is chaotic, intermittent and unpredictable. Gravity waves are often present and the layer structure depends on factors outside the influence of local space and time constraints.

We assume that eddy diffusivity for trace species have non-dimensional profile characteristics similar to potential temperature, $\Theta$, i.e., $K_{zz} = K_h$. Numerous authors including O'Brien (1970), Businger and Arya (1974), Brost and Wyngaard (1978), and Bodin (1980) have considered this approach to study a variety of atmospheric conditions. Pielke and Mahrer (1975) combined O'Brien's (1970) formulation with Deardorff's (1974) prognostic equation for mixed layer height to better resolve boundary layer growth.

Most of modern Eulerian models employ the eddy diffusivity concepts described by Louis (1979). He proposed the use of Monin-Obukhov similarity theory to parameterize surface fluxes and vertical profiles. The Monin-Obukhov similarity is well described in references such as Businger et al. (1971), Panofsky and Dutton (1984), Pielke (1984), Stull (1988) and Arya (1988; 1999). The stability regime is defined with a nondimensional number $z/L$, where $z$ is the height above

the ground and $L$ is the Monin-Obukhov length. For the surface layer, the non-dimensional profile functions of the vertical gradient of $\Theta$ are expressed as:

$$\phi_h = \mathrm{Pr}_o(1+\beta_h \frac{z}{L}) \qquad \text{for moderately stable conditions } (1 \geq z/L \geq 0) \tag{67}$$

$$\phi_h = \mathrm{Pr}_o(1-\gamma_h \frac{z}{L})^{-1/2} \quad \text{for unstable conditions } (z/L < 0) \tag{68}$$

where $\mathrm{Pr}_o$ is the Prandtl number for neutral stability and $\beta_h$ and $\gamma_h$ are coefficients of the profile functions determined through field experiments. In addition, following Holtslag et al. (1990) we add a function for the very stable condition ($z/L \geq 1$) to extend the applicability of the surface layer similarity:

$$\phi_h = \mathrm{Pr}_o(\beta_h + \frac{z}{L}) \tag{69}$$

Parameterizations for eddy diffusivity for the surface layer can be represented as:

$$K_h = \frac{k u_* z}{\phi_h(z/L)} \tag{70}$$

where $u_*$ is the surface friction velocity.

Previous studies (Chang et al., 1987; Hass et al., 1991) indicated that this type of formulation can represent turbulent mixing in air quality models adequately. For the PBL (above the surface layer), eddy diffusivity is parameterized with:

$$K_h = \frac{k u_* z(1-z/h)^{3/2}}{\phi_h(z/L)} \qquad \text{for } \frac{z}{L} > 0 \text{ (stable)} \tag{71}$$

$$K_h = k w_* z(1-z/h) \qquad \text{for } \frac{z}{L} < 0 \text{ (unstable).} \tag{72}$$

In the above expressions, $h$ is the depth of the boundary layer, $k$ the von Karman constant, and $w_*$ the convective velocity.

In the free atmosphere above the mixed layer, the eddy diffusivity can be represented as a function of the bulk Richardson number and vertical wind shear:

$$K_h = K_o + S\frac{Ri_c - Ri_B}{Ri_c} l^2 \tag{73}$$

where $K_o$ is the background value set at 1 $m^2$ $s^{-1}$, $S$ is the vertical wind shear, $S = \sqrt{(\Delta U)^2 + (\Delta V)^2} / \Delta z$, the Richardson number is defined as

$$Ri_B = \frac{g}{\Theta_o S^2} \frac{\Delta \Theta}{\Delta z} \tag{74}$$

and its critical value is assumed to be $Ri_c$=0.25, and $l$ is the mixing length. Usually a constant value around 40 m is used for the mixing length for the free-tropospheric exchange. For different $K_h$ formulations in the literature, refer to Appendix A.

### 7.1.2 Numerical Solver

When the temporal change in air density during computational time step can be ignored, Eq. (66) is given in a generic form as,

$$\frac{\partial q}{\partial t} = \frac{\partial}{\partial z}\left( K \frac{\partial q}{\partial z} \right) \tag{75}$$

To account for the loss process due to deposition in the lowest model layer, dry deposition flux is considered as the flux boundary condition at the surface, i.e.,

$$\left. \frac{\partial q_1}{\partial t} \right|_{dep} = -\frac{v_d}{h_{dep}} q_1 \tag{76}$$

where the geometric thickness of the lowest model layer is used for $h_{dep}$ and $v_d$ is the deposition velocity. The diffusion equation can be discretized and solved with explicit, semi-explicit or fully implicit algorithms (see Table 3 in Appendix B). The tridiagonal system can be solved with a Thomas algorithm (Gaussian elimination without pivoting) followed by back substitution.

## 7.2 Higher-Order Local Closure Techniques

Improvements to the simplicity of first order closure are closure schemes in which more of the physics of the atmosphere is taken into account in the formulation of the eddy diffusivity coefficient. They are the turbulent kinetic energy (TKE) closure and second-order closure schemes. Higher-order closure is accomplished by parameterizing high-order terms in terms of mean variables and lower-order terms.

### 7.2.1 Second-Order Closure Techniques

Several basic closure ideas such as down-gradient diffusion, return to isotropy, and turbulent dissipation in the inertial sub range are used in the

parameterizations of the third moment terms. These parameterizations must be especially applicable to the scales of the energy containing eddies which are very sensitive to atmospheric stability. Measurements of high-order moments in the real atmosphere are very difficult because there is a large amount of scattering in the direct flux measurements and a long averaging time is required to estimate higher-order moments using the eddy-correlation methods. For air quality applications, especially for a complicated reactive system, the technique requires several ad hoc assumptions that cannot be supported by observations or other theoretical reasoning.

The set of second-order turbulence equations includes the prognostic equations of the mean variables and the equations of their variances. Instead of parameterizing these fluxes, conservation equations are written for each flux term. This leads to the presence of third moment fluxes on the right side of the conservation equations for the second moment fluxes. To close the system, we must parameterize the third-moments in these equations with known parameters. Thus, second-order closure involves increased complexity and computation. In closing the set of equations, higher order terms are parameterized and these assumptions may not be valid for all types and scales of atmospheric motions. In the third-order closure scheme, conservation equations for third moments are considered and closure is achieved by parameterizing the fourth moments. This involves further increased complexity and computation. Literature indicates that only slight improvements are found over the TKE closure method (see next section) at the expense of huge computation and added complexity with the higher-order schemes. Very limited studies are available on the performance of the second-order methods applied to air quality modeling.

### 7.2.2 TKE Closure Technique

TKE closure is a simplification of the second-order closure technique. Instead of using the velocity component variance equations, the turbulent kinetic energy equation is used. Other equations can be used, together with the TKE, like the equations for the turbulent variances of temperature and humidity (e. g., Mellor and Yamada, 1974) or the turbulent kinetic energy dissipation rate ($\varepsilon$) equation (e. g., Alapaty et. al., 1996). The eddy diffusivity can be represented as,

$$K_{zz} = cTKE^2 / \varepsilon \tag{77}$$

where $c$ is an experimental constant.

This type of closure is also more economical as compared to higher-order closure schemes. The TKE scheme requires additional equations relative to the first order closure thus providing more physically realistic solutions to the closure problem than first order. Thus, TKE closure is often termed as 1.5-order closure (Mellor and Yamada, 1974). Literature indicates that numerical simulations are far better with the TKE closure method than with the first order closure K-theory techniques without a large jump in computational expense.

## 7.3 Non-Local Closure Techniques

Non-local methods have been used mostly with first-order closure. Generally, the higher-order local closures and the nonlocal closures yield more accurate solutions than lower order, but they do so at added expense and complexity. Nonlocal closure recognizes that larger-size eddies can transport fluids across finite distances before the smaller eddies have a chance to cause mixing. This advective-like concept is supported by observations of thermals rising with undiluted cores, finite size swirls of leaves or snow, and the organized circulation patterns sometimes visible from cloud photographs.

Two main approaches to nonlocal closure methods are transilient turbulence theory and spectral diffusivity theory. Both allow a range of eddy sizes to contribute to the turbulent mixing process. A variety of physical processes can be modeled with a transilient scheme depending on the form of the transilient matrix. Examples include complete mixing, top-down/bottom-up mixing, asymmetric convective mixing, small-eddy mixing, cloud top entrainment, a detraining updraft core, patchy turbulence, no turbulence, or eddies triggered by the surface layer. Some closure schemes that have strong applicability to air quality modeling are described in the following subsections. Nonlocal closure schemes are the most suitable for describing the vertical turbulence mixing process, which should represent turbulent diffusion and atmospheric transport by eddies simultaneously.

In the non-local closure method, larger-size eddies can transport fluid across finite distances before the smaller eddies have a chance to cause mixing. In the literature mostly first-order nonlocal closure models can be found, except the study of Stull and Driedonks, (1987) where TKE (one-and-a-half-order closure) is used. In the nonlocal closure method mixing is done from the surface layer to the top of the convective boundary layer. The vertical diffusion of trace gases is accomplished by determining a matrix containing the fraction of mass entering or leaving each particular layer. This matrix containing information about the rate of mass fractional mixing from one level to another level is often called the

transilient matrix. There are several ways to specify this matrix (Stull and Driedonks, 1987; Chatfield and Crutzen, 1984; Fiedler and Moeng, 1985). The Blackadar scheme (Zhang and Anthes, 1982) uses the conservation of heat flux in a vertical column to determine the matrix.

Recent studies using a nonlocal closure technique (Pleim and Chang, 1992) for vertical diffusion during convective conditions indicated that it was able to simulate rapid transport upward from the surface layer to all levels in the convective boundary layer. Also, the study results indicate that air quality model simulations are better with this nonlocal closure technique compared to that with the simple *K*-theory (local closure) technique. Some of the disadvantages of this technique are that during nonconvective conditions the model has to rely on other closure methods, and that turbulence generated by vertical wind shear is neglected.

Transilient turbulence representation (Stull and Driedonks, 1987; Zhang and Stull, 1992; Stull, 1993) provides a general paradigm for the description of the nonlocal diffusion algorithms. However, it has high computational cost and there are some difficulties in determining the exchange coefficients among the model layers. Instead, there are a few simple nonlocal models that can be applied to Eulerian dispersion modeling, as described below.

### 7.3.1 Blackadar Convective Scheme

It is the simplest form of nonlocal scheme used in atmospheric modeling. This scheme, first introduced by Blackadar (1978), has long been used as one of the PBL schemes in MM5 and its predecessors. The concept of the Blackadar convective mixing scheme is that during conditions of free convection air in the surface layer is heated, to a superadiabatic potential temperature by the sensible heat flux from the surface. Thermal plumes rise from the surface layer due to their buoyancy until encountering air with higher potential temperature at the top of the convective boundary layer. Mixing occurs at all heights through plume detrainment while the plume core maintains the characteristics of the surface layer. Upward mixing and downward mixing are symmetric as in the case of Blackadar convection as shown in Figure 6a. Penetration into the capping inversion can be included by allowing a small amount of over-shooting into a region of negative buoyancy. This scheme is used only in the convective boundary layer and must be coupled with another scheme for non-convective conditions and above the boundary layer, such as *K*-theory. The Blackadar model does not take the effect of asymmetric vertical velocity spectra into account.

The convective mixing is assumed to be dominated by eddies of varying sizes but all having roots in the surface layer, with each eddy exchanging a certain amount of its mass with the air around it as it ascends. The rate of change of mean potential temperature caused by the mass exchange in the mixed layer can be expressed as

$$\frac{\partial \overline{\theta}}{\partial t} = M_u \omega(z)(\overline{\theta}_{sfc} - \overline{\theta}) \tag{78}$$

where $\omega(z)$ is a weight function that accounts for the variation of exchange rate with height. The mass exchange rate, $M_u$, can be estimated from conservation of energy, which requires the heat flux at any level to satisfy the equation

$$H = H_{sfc} - M_u \int_{z_{sfc}}^{z} c_p \rho(\overline{\theta}_{sfc} - \overline{\theta}) \omega(\xi) d\xi \tag{79}$$

where $H_{sfc}$ is the sensible heat flux leaving the surface layer and $c_p$ is the specific heat at constant pressure. When the integration limit is extended to the top of the boundary layer, where $H$ is assumed to be zero, we can estimate $M_u$ with

$$M_u = H_{sfc} / \int_{z_{sfc}}^{z_h} c_p \rho(\overline{\theta}_{sfc} - \overline{\theta}) \omega(\xi) d\xi \tag{80}$$

Usually the weight function $w$ is approximated to be unity in the mixed layer. With this information, one can solve Eq. (75) with the deposition flux as the bottom boundary condition, Eq. (76). With the Blackadar scheme, the mixing algorithm is represented with,

$$\frac{\partial q_1}{\partial t} = -\frac{v_d}{h_{dep}} q_1 - \sum_{k=1}^{L_p} M_u \frac{\Delta z_k}{\Delta z_1} [q_1(t) - q_k(t)] \tag{81}$$

for the lowest model layer, where $L_p$ is the index for the PBL top, and

$$\frac{\partial q_j}{\partial t} = -M_u \frac{\Delta z_1}{\Delta z_j} [q_j(t) - q_1(t)] \qquad \text{for } 2 \le j \le L_p \tag{82}$$

The system can be solved with the numerical scheme described in Table 3 (Appendix B).

### 7.3.2 Asymmetric Convective Model (ACM)

The Asymmetric Convective Model (ACM) (Pleim and Chang, 1992) is based on Blackadar's nonlocal closure scheme (Blackadar, 1978) but has a different scheme for downward mixing in the convective boundary layer (CBL). Observational evidence and large-eddy simulation modeling studies indicate that mixing processes in a convective boundary layer are essentially asymmetric (i.e., turbulence is anisotropic; Schumann, 1989) with fast upward buoyant plumes and slow broad compensatory subsidence. Therefore the direct, non-local downward

transport of the Blackadar scheme is replaced with layer by layer subsidence which increases in mass flux as it descends, like a cascading waterfall (see Figure 6b).

Because the mass influx to the lowest model layer is from the second layer only in ACM, we can write

$$\frac{\partial q_1}{\partial t} = -\frac{v_d}{h_{dep}} q_1 - \frac{1}{\Delta z_1}[M_u(z_h - z_1)q_1(t) - M_{d2}\Delta z_2 q_2(t)] \tag{83}$$

For $2 \le j \le L_p$, we have

$$\frac{\partial q_j}{\partial t} = M_u q_1 - M_{dj} q_j + M_{dj+1}\frac{\Delta z_{j+1}}{\Delta z_j} q_{j+1} \tag{84}$$

where $M_u$ represents upward mixing rate, Eq. (80), and $M_{dj}$ represents downward mixing rate at layer $j$. It is determined by

$$M_{dj} = M_u \frac{z_h - z_{j-1}}{\Delta z_j} \tag{85}$$

Then the system can be solved with the algorithm described in Table 3 (Appendix B). As with the Blackadar model, the ACM can only be used during convective conditions in the PBL. For other stability regimes, one needs to rely on other schemes such as *K*-theory.

### 7.3.3 Ertel Non-Local Scheme

The local diffusion approach described earlier can be extended to include the nonlocal mixing under convective boundary layer. Ertel (1942) first proposed that the potential temperature ($\theta$) flux could be expressed with two terms, the eddy diffusion term and the nonlocal Ertel flux ($N$) to account for the counter-gradient flux:

$$\overline{w'\theta'} = -K_{zz}\frac{\partial \overline{\theta}}{\partial z} + N \tag{86}$$

Similarly, Deardorff (1966) suggested the vertical turbulent mixing for the unstable boundary layer could be parameterized by

$$\frac{\partial q}{\partial t} = \frac{\partial}{\partial z}\left[K_{zz}\left(\frac{\partial q}{\partial z} - \gamma_q\right)\right] \tag{87}$$

where $\gamma_q$ is a correction to the local gradient that incorporates the contribution of the large-scale eddies to the total flux. This formulation was initially introduced to handle vertical mixing of potential temperature (i.e., when $q = \theta$) under strong convective conditions where the stability $\partial\overline{\theta}/\partial z$ can change sign above the surface layer and remain slightly positive over most of the mixed layer (Wyngaard, 1982). This implies negative eddy diffusivity values.

One obvious difficulty of this method is how to determine the magnitude of $\gamma_q$, nonlocal transport correction factor. Several authors have suggested similar methods to estimate $\gamma_q$:

Troen and Mahrt (1986): $$\gamma_q = C' \frac{\overline{w' q'_s}}{w_* h}, \; C' \approx 10 \qquad (88a)$$

Holtslag et al. (1995): $$\gamma_q = a w_* \frac{\overline{w' q'_s}}{w_m^{\,2} h}, \; a \approx 7.2 \qquad (88b)$$

Hong and Pan (1996): $$\gamma_q = b \frac{\overline{w' q'_s}}{w_s h}, \; b \approx 7.8 \qquad (88c)$$

Siebesma and Teixeira (2000): $$\gamma_q = a w_* \frac{\overline{w' q'_s}}{\sigma_w^{\,2} h}, \; a \approx 2 \qquad (88d)$$

where $w_*$ is the convective velocity scale, $w_m$ is the velocity scale combining the influence of shear and convection (with free convection limit $w_m \sim 0.85\, w_*$), $w_s$ is the mixed-layer velocity scale represented as $w_s = u_* \phi_m^{\,-1}$, and $\sigma_w$ is the standard deviation of vertical wind fluctuation.

For potential temperature, $\gamma_q$ can be estimated by relating the counter-gradient term with the flux-profile formulation at the top of the surface layer (Troen and Mahrt, 1986; Hong and Pan, 1996) to give $\gamma_q = \gamma_\theta \sim 0.7 \times 10^{-3}$ m$^{-1}$ K. As shown by Stevens (2000), the Ertel nonlocal scheme approaches to the well-mixed boundary layer asymptotically. The nonlocal scheme transports scalar quantities away from the surface more rapidly than the local scheme (Holtslag and Boville, 1993; Holtslag et al., 1995). Although the Ertel nonlocal scheme is used in some meteorological models, it has not been used in Eulerian transport models because of the uncertainties in determining the nonlocal flux correction factors for different air pollutants.

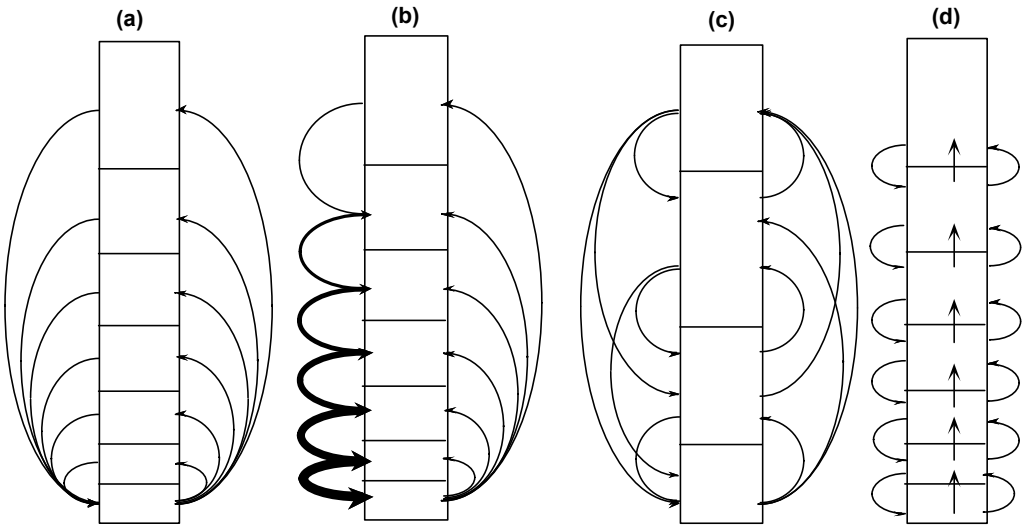


**Figure 6. Schematics of nonlocal schemes: (a) the Blackadar scheme (b) the asymmetric convective model, (c) the transilient turbulence model, and (d) eddy diffusion with nonlocal Ertel flux. The arrows point directions of mass fluxes, the relative sizes of boxes represent the volume of air in vertical cells and the line thickness is related with the relative magnitudes of fluxes.**

# 8 Simplified Eulerian Models

Although most modern operational Eulerian air quality models are based on numerical methods described above, simplified models can provide useful insights of the atmospheric dispersion processes. We describe these models from a historic perspective.

## 8.1 Single Box Models

The single box model (Lettau, 1970) is the simplest air pollution model and is based on the mass conservation of pollutant inside a Eulerian box, which generally represents a large area such as a city. The physical concept underlying the box model approach is depicted in Figure 7. Mass conservation gives

$$\frac{\partial}{\partial t}(\overline{\varphi}h) = -\overline{\varphi}h\frac{U}{L_x} + \overline{\varphi}_b h\frac{U}{L_x} + \overline{\varphi}_a\frac{\partial h}{\partial t} + Q_a \tag{89}$$

in which $\overline{\varphi}_a$ is the (average) concentration aloft ($z>h$) over the city, for example, and $\overline{\varphi}_b$ is the background concentration at the upwind location. The term $\overline{\varphi}_a\frac{\partial h}{\partial t}$ represents entrainment effects of pollutants due to the growth of the boundary layer. For simple conditions with negligible background concentrations (i.e.,

$\overline{\varphi}_a = 0$ and $\overline{\varphi}_b = 0$) one can find the solution to Eq. (89) readily (Venkatram, 1978)

$$\overline{\varphi}(t)h(t) = \overline{\varphi}_o h_o \exp(-t/T_f) + Q_a T_f \left[1 - \exp(-t/T_f)\right] \tag{90}$$

where $\overline{\varphi}_o$ and $h_o$ are initial concentration and boundary layer height, at $t = t_o$ respectively, and $T_f = L_x / U$ is the "flushing time" required for the air to pass completely over the urban area. If the diurnal evolution of the boundary layer are known, Eq. (90) allows the computation of pollutant concentrations at a given time *t*. In a theoretical stationary condition (i.e., $t = \infty$), $\varphi$ tends to the limit $\varphi_e$:

$$\overline{\varphi}_e = \overline{\varphi}\big|_{t=\infty} = Q_a T_f / h \tag{91}$$

which is sometimes a reasonable quasi-stationary approximation in the urban areas.

The single box modeling approach, which is a simplest form of the Eulerian model, provides a basis for regional scale Lagrangian models in which a volume of air is assumed to move along with the prevailing wind without losing its integrity. The single box model has been applied for both inert and reactive pollutants. The model for the latter case is called the Photochemical Box Model (PBM) and Eq. (89) is modified to incorporate effects of photochemical reactions in the mass balance expression (Schere and Diemrjian, 1984):

$$\frac{\partial \overline{\varphi}_i}{\partial t} = -U\frac{\partial \overline{\varphi}_i}{\partial x} + \frac{\partial h}{\partial t}\frac{\partial \overline{\varphi}_i}{\partial z} + \frac{Q_a}{h} + R_i(\overline{\varphi}_i, ...., \overline{\varphi}_n) \tag{92}$$

where $\overline{\varphi}_i$ is mean concentration of species *i* within the PBM, and $R_i$ is rate of production and/or destruction of species *i* by chemical reactions. Refer to Figure 7 for the schematic illustration of processes simulated in PBM. Diemrjian and Schere (1979) used such a model to predict ozone concentrations over a city. The vertical entrainment is important for the ozone predictions because ozone is often trapped above the boundary layer at night and is mixed down to the surface by the convective mixing in the following morning. Meszaros et al. (1978) used a box model to compute anthropogenic emissions and dry/wet deposition processes. Jensen and Petersen (1979), who used an acoustic sounder for evaluating the boundary layer height, found a very good agreement between the single box model output and urban concentration measurements. One variant of the photochemical box model that has been widely used for estimating ozone concentration in urban areas is EKMA (empirical kinetic modeling approach) technique (Dodge, 1977).

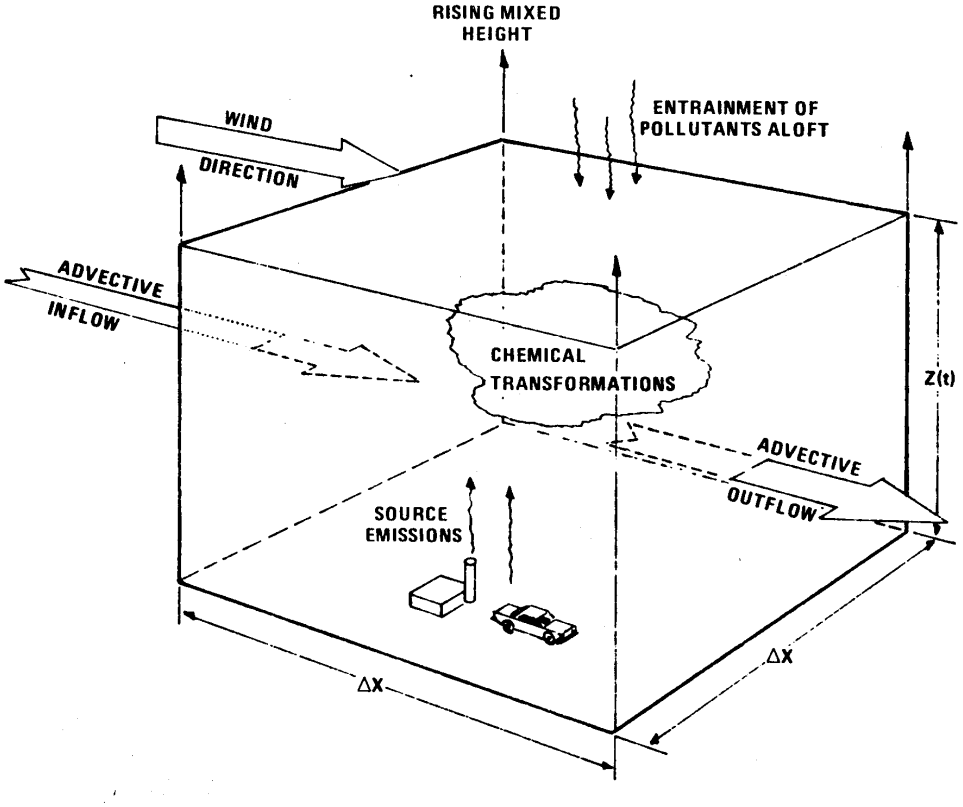


**Figure 7. Schematic illustration of the photochemical box model (PBM) domain. [from Schere and Diemrjian,1984]**

## 8.2 The Slug Model

Venkatram (1978) showed that the box model has unrealistic inertia and cannot properly handle rapid temporal changes in either $Q$ or $U$. He proposed the slug model as an improvement to the box model, especially during stagnation episodes (Figure 8). The slug model allows a concentration $\varphi$ to vary in the along-wind direction $x$ and in the vertical direction $z$, but assumes that the concentration does not vary in the crosswind direction $y$. This allows us to write the mass conservation equation within the single box in terms of two distances ($x$, $z$) as

$$\frac{\partial \varphi}{\partial t} + U\frac{\partial \varphi}{\partial x} = Q_l \tag{93}$$

where $x$ is the downwind distance inside the box and $U$ is assumed to be independent of height. We can avoid making assumptions about the vertical concentration distribution by integrating Eq. (93) in vertical direction:

$$\frac{\partial \Phi}{\partial t} + U\frac{\partial \Phi}{\partial x} = \int_o^{h(x)} Q_l dz \tag{94}$$

where $\Phi(x) = \int_o^{h(x)} \varphi(x,z)dz$ and $h$ is either the mixing height or the vertical height of the box (may be dependent on the distance $x$) that encompasses the plume generated by the emission $Q_l$.

The steady state solution of Eq. (94) is

$$\Phi(x)\big|_\infty = \frac{1}{U}\int_o^x \int_o^{h(x)} Q_l dz dx' \tag{95}$$

The solution at time $t$ after the emission is shut off (i.e., $Q_l$ becomes zero),

$$\Phi(x,t) = \Phi(x - Ut)\big|_\infty = \frac{1}{U}\int_o^{x-Uth(x)} \int_o^{} Q_l dz dx' \; ; \; t \le T_f \tag{96a}$$

$$\Phi(t) = 0 \; ; \; t > T_f \tag{96b}$$

As before, $T_f = L_x / U$ is the flushing time. For a special case that the vertically integrated source strength does not change with distance $x$, (i.e., $\int_o^{h(x)} Q_l dz$ = constant), we have

$$\Phi(t) = \frac{x - Ut}{U}\int_o^{h(x)} Q_l dz \; ; \; t \le L_x / U \tag{97}$$

One of advantage of the slug model over the box model is that the volume is completely flushed out after the flushing time, where as the single box solution of Eq. (89) is not able to reproduce this complete flushing.

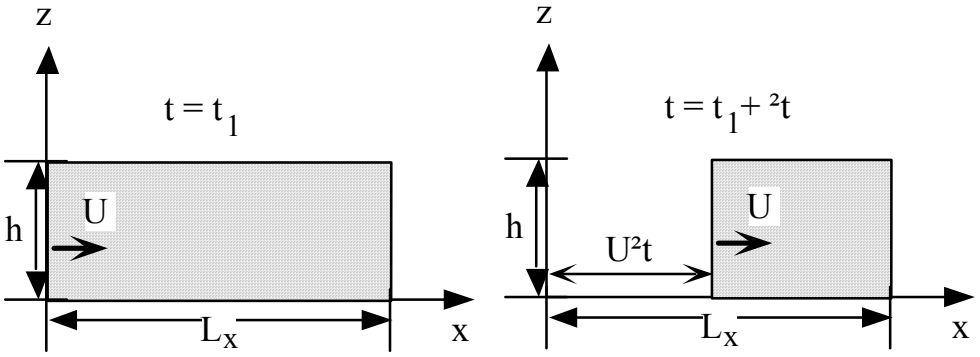


**Figure 8. A schematic illustration of flushing of pollutants through a city. (After Venkatram, 1978)**

# Appendix A

## $K_{zz}$ Formulations in the Literature

Following Yamartino et al. (1992), Nikomo et. al. (1999) divided the PBL into several atmospheric turbulence regimes (see Figure A-1) and for each regime they proposed $K_{zz}$ parameterization:

For surface layer, $K_{zz} = ku_* z / \phi_h(z/L)$

near neutral upper layer $K_{zz} = ku_* z / \phi_h(z_{SL}/L)$

free convection $K_{zz} = 1.22 w_f z$, with $w_f = (zg\,\overline{w'\theta'}/\Theta_o)^{1/3}$

mixed layer $K_{zz} = 0.57 w_* z$ ,with $w_* = (hg\,\overline{w'\theta'_s}/\Theta_o)^{1/3}$

local scaling layer $K_{zz} = ku_l z / \phi_h(z/\Lambda)$

z – less scaling $K_{zz} = 0.17 ku_l \Lambda$

intermittent layer $K_{zz}$ = 10% of the layer below,

where $k$ is the Von Karman constant, $u_*$ friction velocity, $L$ is the Monin-Obukhov length, and $\phi$ is the similarity function for heat, $h$ is the boundary layer height, $z_{SL}$ is the surface layer height, approximated by $0.1h$, $u_l$ is the local friction velocity, $\Lambda$ is the local Monin-Obukhov length.

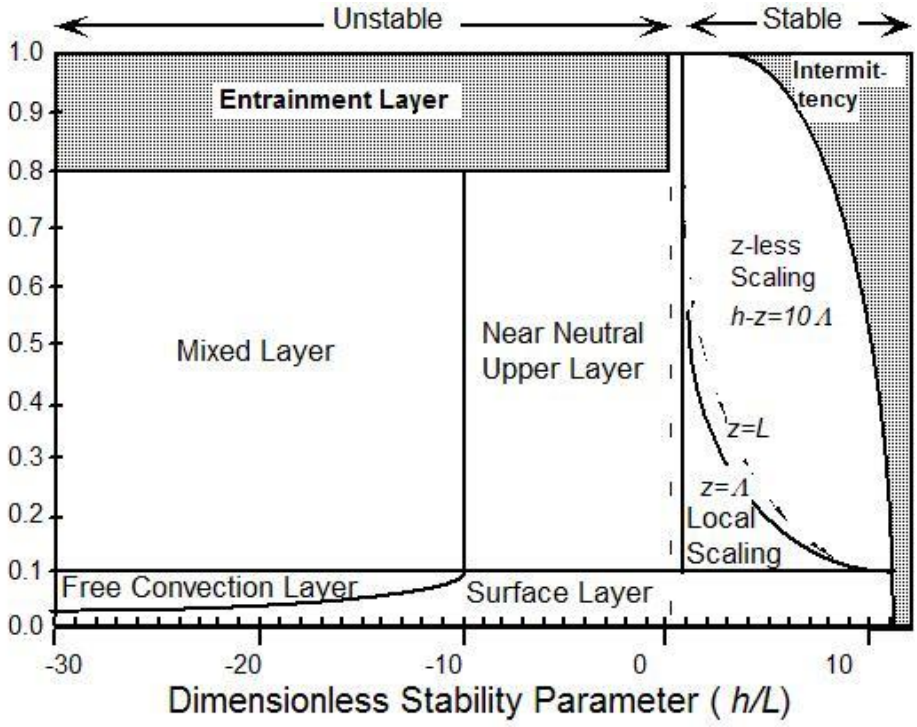


**Figure A-1. Stability regimes of the atmospheric boundary layer (From Nikomo et al., 1999)**

Yamartino et al. (1992) used similar approach:

For unstable case (L < 0)

surface layer where $z/h < 0.1$ and $-z/L < 1$

$$K_{zz} = ku_* z / \phi_h(z/L), \text{ with } \phi_h(z/L) = 0.74(1 - 9z/L)^{-1/2}$$

free convection where $z/h < 0.1$ $-z/L > 1$

$$K_{zz} = w_* z$$

near neutral upper layer where $0.1 < z/h < 1$ and $-h/L < 10$

$$K_{zz} = 0.1ku_* h / \phi_h(0.1h/L)$$

mixed layer where $0.1 < z/h < 1$ and $-h/L > 10$

$$K_{zz} = 0.1w_* h$$

and where $z/h > 1$, $K_{zz}$ = 10% of the value below

For the stable cases (L > 0),

surface layer where $z/h < 0.1$, $(h-z)/\Lambda < 10$

$$K_{zz} = ku_* z / \phi_h(z/L), \text{ with } \phi_h(z/L) = 0.74(1 + 5z/L)$$

in the boundary layer where $0.1 < z/h < 1$ and $h/L < 1$

$$K_{zz} = 0.1ku_* h / \phi_h(0.1h/L)$$

where $z$/h > 0.1 and $h/L > 1$

$$K_{zz} = ku_* (1 - z/h)^{3/4} z / \phi_h(z/\Lambda)$$

where $z/h > 0.1$, $h/L > 1$, and $1 < z/\Lambda < (h/\Lambda - 10)$,

$$K_{zz} = ku_* (1 - z/h)^{3/4} \Lambda$$

outer layer where $z/h > 1$ and $z/\Lambda > (h/\Lambda - 10)$

$K_{zz}$ = 10% of the value below

Some other formulations, which appear in the literature, are mentioned below:

For unstable conditions:

Yokoyama et al. (1979)

$$K_{zz} = cw_* h(z/h)^{1/3}(1 - z/h)^{1/3}, \text{ with c} = 0.06 \sim 0.13,$$

Sorbjan (1986b), above z/h=0.77 the flux is negative,

$$K_{zz} = 1.54 w_* h(z/h)^{4/3}(1 - 1.3z/h)^{1/3}$$

Troen and Mahrt (1986), for $z/h$>0.1,

$$K_{zz} = kh(u_*^3 + 0.7kw_*^3)^{1/3}(z/h)(1 - z/h)^2,$$

Lange (1989)

$$K_{zz} = ku_* z / \phi_h(z/L)\exp(-V_g h / u_* z), \text{ where } V_g \text{ is geostrophic wind}$$

Pleim and Chang (1992)

$$K_{zz} = ku_* z / \phi_h(z/L) \text{ for surface layer}$$

$$K_{zz} = kw_* z(1 - z/h) \text{ for mixed layer}$$

Holtslag and Boville (1993)

$$K_{zz} = l_c^2 SF_c(Ri), \text{ where } S \text{ is local vector wind shear,}$$

$Ri$ is the Richardson number

$$F_c(Ri) = (1 - 18Ri)^{1/2}$$

$$1/l_c = 1/kz + 1/\lambda,\ \lambda = 30 + 270\exp(1 - z/1000)$$

Liu and Caroll (1996)

$$K_{zz} = l_c^2 S(1 - 87Ri)^2$$

λ=80 in the boundary layer

λ= 60% of grid size in the free atmosphere

Tirabassi and Rizza (1997)

$K_{zz} = kw_* z(1 - z/h)$ for $h/L$ <-10

Degrazia et al. (1997)

$$K_{zz} = 0.15 w_* h[(1 - \frac{z}{h})^2 (\frac{-z}{L})^{-2/3} + 0.75]^{1/2} F(\frac{z}{h})$$

or, $$K_{zz} = 0.22(\frac{z}{h})^{1/3}(1 - \frac{z}{h})^{1/3} F(\frac{z}{h}),$$

where $F(\frac{z}{h}) = [1 - \exp(-4\frac{z}{h}) - 0.0003\exp(8\frac{z}{h})]^{4/3}$

Prabha et al. (1999)

$$K_{zz} = 2.5 w_* h(\frac{kz}{h})^{4/3}(1 - 15\frac{z}{L})^{1/4},\ 0<z/h<0.05$$

$$K_{zz} = w_* h\ f(\frac{z}{h}),$$

where $f(\eta) = 0.021 + 0.408\eta + 1.351\eta^2 - 4.096\eta^3 + 2.56\eta^4$,

for $0.05<\eta=z/h<0.6$

$f(\eta) = 0.2\exp(6 - 10\eta)$, for $0.6<\eta=z/h<1.1$

$f(\eta) = 0.0013$, for $\eta=z/h<>1.1$

Ulke (2000)

$$K_{zz} = ku_* h(\frac{z}{h})(1 - \frac{z}{h})[1 - 22(\frac{h}{L})(\frac{z}{h})]^{1/4}$$

Degrazia et. al. (2000)

$$K_{zz} = 0.16 w_* h[0.01(-\frac{h}{L})]^{1/2}[1 - \exp(-4\frac{z}{h}) - 0.003\exp(8\frac{z}{h})]^{4/3}$$

Siebesma and Teixeiro (2000)

$$K_{zz} = ku_* z(1 - \frac{z}{h})^2/(1 - 39\frac{z}{L})^{-1/3}$$

For stable conditions, we have:

Brost and Wyngaard (1978)

$$K_{zz} = 1.25ku_* z(1 - \frac{z}{h})^{3/2}/(1 + 4.7\frac{z}{L})$$

Yokoyama et al. (1979)

$$K_{zz} = cu_* z(1 - \frac{z}{h})/(1 + 6\frac{z}{L}),\ c=0.06\sim0.13$$

Sorbjan (1986a)

$$K_{zz} = ku_* z(1 - \frac{z}{h})/(0.74 + 4.7\frac{z}{L})$$

Sorbjan (1986b)

$$K_{zz} = ku_*z(1-\frac{z}{h})^{(2\alpha_1-\alpha_2)}/(1+5.2\frac{z}{L}),\ \alpha_1=2;\ \alpha_2=3$$

Lange (1989)

$$K_{zz} = \frac{ku_*z}{\phi_h(z/L)}\exp(-\frac{V_g z}{u_* h})$$

Pleim and Chang (1992)

$$K_{zz} = \frac{ku_*z}{\phi_h(z/L)}, \text{ for } z/h<0.1,$$

where $\phi_h(z/L) = 0.74 + 4.7z/L$, $0<z/L<1$

$$\phi_h(z/L) = 4.7 + 0.74z/L,\ z/L>1$$

$$K_{zz} = \frac{ku_*z(1-z/h)^2}{\phi_h(z/L)}, \text{ for } 1>z/h>0.1$$

Holtslag and Boville(1993)

$$K_{zz} = l_c^2 SF_c(Ri), \text{ where } F_c(Ri) = [1+10Ri(1+8Ri)]^{-1}$$

Liu and Carroll (1996)

$$K_{zz} = l_c^2 S(1-Ri/Ri_c)^2$$

Degrazia et. al. (2000)

$$K_{zz} = ku_*z(1+3.7z/\Lambda)^{1/3}/(1+15f_c z/u_* + 3.7z/\Lambda)^{4/3},$$ in stable shear layer

where $f_c \sim 10^{-4}s^{-1}$ is the Coriolis factor

$$\Lambda = L(1-\frac{z}{h})^{(1.5\alpha_1-\alpha_2)},\ \alpha_1=1.5;\ \alpha_2=1$$

$$K_{zz} = \frac{ku_*z(1-z/h)^{4/3}}{[1+3.7(z/L)(1-z/h)^{5/4}]}, \text{ for highly stable case } (z/L\to\infty)$$

$$K_{zz} = 0.11u_*L(1-z/h)^2, \text{ when eddy sizes are limited by stability}$$

Ulke (2000)

$$K_{zz} = \frac{ku_*z(1-z/h)}{(1+6.9z/L)}$$

Ha and Mahrt (2000)

$$K_{zz} = l^2\left|\frac{dV_h}{dz}\right|, \text{ where } l = l_o[\exp(-c_1Ri) + c_2/(Ri+c_3)],$$

$c_1$=8.5, $c_2$=0.15, $c_3$=3, $l_o$=8.5.

This is applied at all levels subject to $l_o < kz$.

Within the PBL, they use the larger value between the formula above and

$$K_{zz} = ku_*z(1-\frac{z}{h})^2/\Pr\phi_m(\frac{z}{L}),$$

where $\Pr = 1.5 + 3.08Ri$, and $\phi_m(\frac{z}{L}) = 1 + 4.7(z/L)$.

For $z/L>1$, $z/L$ in above formula is replaced by 1.

# Appendix B

**Table 3. Vertical diffusion algorithms (Byun and Ching, 1999)**

| Classification | Algorithm | Solver |
|---|---|---|
| Semi-implicit eddy diffusion solver | For j=1 (layer 1):<br>$q_1^{n+1} = q_1^n - \Delta t \frac{v_d}{h_{dep}}\left[\vartheta q_1^{n+1} + (1-\vartheta) q_1^n\right]$<br>$+\frac{\Delta t}{\Delta \xi_1}\left[\frac{K_{1+\frac{1}{2}}}{\Delta \xi_{1+\frac{1}{2}}}\left(\vartheta(q_2^{n+1} - q_1^{n+1}) + (1-\vartheta)(q_2^n - q_1^n)\right)\right]$<br>For $2 \le j \le L-1$:<br>$q_j^{n+1} = q_j^n + \frac{\Delta t}{\Delta \xi_j} \bullet$<br>$\left[\frac{K_{j+1/2}}{\Delta \xi_{j+1/2}}\left(\vartheta(q_{j+1}^{n+1} - q_j^{n+1}) + (1-\vartheta)(q_{j+1}^n - q_j^n)\right)\right.$<br>$\left. - \frac{K_{j-1/2}}{\Delta \xi_{j-1/2}}\left(\vartheta(q_j^{n+1} - q_{j-1}^{n+1}) + (1-\vartheta)(q_j^n - q_{j-1}^n)\right)\right]$<br>At the top of layer<br>$q_N^{n+1} = q_N^n -$<br>$\frac{\Delta t}{\Delta \xi_N}\frac{K_{N-1/2}}{\Delta \xi_{N-1/2}}\left(\vartheta(q_N^{n+1} - q_{N-1}^{n+1}) + (1-\vartheta)(q_N^n - q_{N-1}^n)\right)$ | $\begin{pmatrix} d_1 & c_1 & \cdots & 0 & \cdots & 0 \\ a_2 & d_2 & c_2 & 0 & \cdots & 0 \\ \vdots & a_3 & \ddots & \cdots & \cdots & 0 \\ 0 & \vdots & \vdots & d_j & \vdots & \vdots \\ \vdots & 0 & 0 & 0 & \ddots & c_{L-1} \\ 0 & \cdots & 0 & 0 & a_L & d_L \end{pmatrix}\begin{pmatrix} q_1^{n+1} \\ q_2^{n+1} \\ \vdots \\ q_j^{n+1} \\ \vdots \\ q_L^{n+1} \end{pmatrix} = \begin{pmatrix} b_1 \\ b_2 \\ \vdots \\ b_j \\ \vdots \\ b_L \end{pmatrix}$<br>$d_1 = 1 + \frac{\vartheta \Delta t}{\Delta \xi_1}\frac{K_{1\frac{1}{2}}}{\Delta \xi_{1\frac{1}{2}}} + \vartheta \Delta t \frac{v_d}{h_{dep}}$; $c_1 = -\frac{\vartheta \Delta t}{\Delta \xi_1}\frac{K_{1\frac{1}{2}}}{\Delta \xi_{1\frac{1}{2}}}$; $a_N = -\frac{\vartheta \Delta t}{\Delta \xi_N}\frac{K_{N-\frac{1}{2}}}{\Delta \xi_{N-\frac{1}{2}}}$; $d_N = 1 + \frac{\vartheta \Delta t}{\Delta \xi_N}\frac{K_{N-\frac{1}{2}}}{\Delta \xi_{N-\frac{1}{2}}}$<br>$b_1 = \left(1 - \frac{(1-\vartheta)\Delta t}{\Delta \xi_1}\frac{K_{1\frac{1}{2}}}{\Delta \xi_{1\frac{1}{2}}} - (1-\vartheta)\Delta t \frac{v_d}{h_{dep}}\right) q_1^n + \frac{(1-\vartheta)\Delta t}{\Delta \xi_1}\frac{K_{1\frac{1}{2}}}{\Delta \xi_{1\frac{1}{2}}} q_2^n$<br>$b_N = \left(1 - \frac{(1-\vartheta)\Delta t}{\Delta \xi_N}\frac{K_{N-\frac{1}{2}}}{\Delta \xi_{N-\frac{1}{2}}}\right) q_N^n + \frac{(1-\vartheta)\Delta t}{\Delta \xi_N}\frac{K_{N-\frac{1}{2}}}{\Delta \xi_{N-\frac{1}{2}}} q_{N-1}^n$<br>for $2 \le j \le L-1$: $a_j = -\frac{\vartheta \Delta t}{\Delta \xi_j}\frac{K_{j-\frac{1}{2}}}{\Delta \xi_{j-\frac{1}{2}}}$; $d_j = 1 + \frac{\vartheta \Delta t}{\Delta \xi_j}\left(\frac{K_{j+\frac{1}{2}}}{\Delta \xi_{j+\frac{1}{2}}} + \frac{K_{j-\frac{1}{2}}}{\Delta \xi_{j-\frac{1}{2}}}\right)$; $c_j = -\frac{\vartheta \Delta t}{\Delta \xi_j}\frac{K_{j+\frac{1}{2}}}{\Delta \xi_{j+\frac{1}{2}}}$<br>$b_j = \left(1 - \frac{(1-\vartheta)\Delta t}{\Delta \xi_j}\left[\frac{K_{j+\frac{1}{2}}}{\Delta \xi_{j+\frac{1}{2}}} + \frac{K_{j-\frac{1}{2}}}{\Delta \xi_{j-\frac{1}{2}}}\right]\right) q_j^n + \frac{(1-\vartheta)\Delta t}{\Delta \xi_j}\frac{K_{j+\frac{1}{2}}}{\Delta \xi_{j+\frac{1}{2}}} q_{j+1}^n + \frac{(1-\vartheta)\Delta t}{\Delta \xi_j}\frac{K_{j-\frac{1}{2}}}{\Delta \xi_{j-\frac{1}{2}}} q_{j-1}^n$ |

$\theta$=a time-step weighting factor (0.5 for Crank-Nicholson method) and $\xi_{j+1/2} = (\xi_j + \xi_{j+1})/2$; $\Delta \xi_{j+1/2} = \xi_{j+1/2} - \xi_{j-1/2}$; $\Delta \xi_{j+1} = \xi_{j+1} - \xi_j$.

**Table 3. (continued)**

| Classification | Algorithm | Solver |
|---|---|---|
| Blackadar symmetric eddy; Blackadar (1978) | For j=1 (layer 1): $\frac{\partial q_1}{\partial t} = -\frac{v_d}{h_{dep}} q_1 - \sum_{k=1}^{L_p} m_{1k}(t)[q_1(t) - q_k(t)$ , for $2 \le j \le L_p$: $\frac{\partial q_j}{\partial t} = -\sum_{k=1}^{L_p} m_{jk}(t)[q_j(t) - q_k(t)]$ where $m_{jk}$ = rate of mass exchange between two layers $m_{1k} = M_u \frac{\Delta\xi_k}{\Delta\xi_1}$; $m_{j1} = M_u \frac{\Delta\xi_1}{\Delta\xi_j}$ and the upward flux is obtained from $M_u = H_{sfc} / \int_{\xi_{sfc}}^{\xi_h} C_{pd}\rho(\Theta_{sfc} - \Theta)w(\xi)J_\xi d\xi$ | Crank-Nicholson time differencing $\begin{pmatrix} d_1 & f_2 & \cdots & f_j & \cdots & f_{L_p} \\ e_2 & d_2 & 0 & 0 & \cdots & 0 \\ \vdots & 0 & \ddots & \cdots & \cdots & 0 \\ e_j & \vdots & \vdots & d_j & \vdots & \vdots \\ \vdots & 0 & 0 & 0 & \ddots & 0 \\ e_{L_p} & \cdots & 0 & 0 & 0 & d_{L_p} \end{pmatrix} \begin{pmatrix} q_1^{n+1} \\ q_2^{n+1} \\ \vdots \\ q_j^{n+1} \\ \vdots \\ q_{L_p}^{n+1} \end{pmatrix} = \begin{pmatrix} b_1 \\ b_2 \\ \vdots \\ b_j \\ \vdots \\ b_{L_p} \end{pmatrix}$ $d_1 = 1 + \vartheta\frac{v_d\Delta t}{h_{dep}} + \vartheta\frac{\Delta t M_u}{\Delta\xi_1}(\xi_h - \Delta\xi_1)$ $b_1 = \left[1 - (1-\vartheta)\frac{v_d\Delta t}{h_{dep}} - (1-\vartheta)\frac{\Delta t M_u}{\Delta\xi_1}(\xi_h - \Delta\xi_1)\right] q_1^n + (1-\vartheta)\frac{\Delta t M_u}{\Delta\xi_1}\sum_{k=2}^{L_p}\Delta\xi_k q_k^n$ for $2 \le j \le L_p$: $f_j = -\vartheta\left(\frac{\Delta t M_u}{\Delta\xi_j}\right)\Delta\xi_1$; $e_j = -\vartheta\left(\frac{\Delta t M_u}{\Delta\xi_1}\right)\Delta\xi_j$; $d_j = 1 + \vartheta\left(\frac{\Delta t M_u}{\Delta\xi_j}\right)\Delta\xi_1$; $b_j = \left[1 - (1-\vartheta)\left(\frac{\Delta t M_u}{\Delta\xi_j}\right)\Delta\xi_1\right] q_j^n + (1-\vartheta)\left(\frac{\Delta t M_u}{\Delta\xi_j}\right)\Delta\xi_1 q_1^n$ |

**Table 3. (continued)**

| Classification | Algorithm | Solver |
|---|---|---|
| Asymmetric Convective Model (Pleim and Chang, 1992) | For j=1 (layer 1):<br>$\frac{\partial q_1}{\partial t} = -M_u \frac{\xi_h - \xi_1}{\Delta\xi_1}(q_1 - q_2) - \frac{v_d}{h_{dep}} q_1$<br>for $2 \le j \le L_p$:<br>$\frac{\partial q_j}{\partial t} = M_u \left[ q_1 - \left( \frac{\xi_h - \xi_{j-1}}{\Delta\xi_j} \right) q_j + \left( \frac{\xi_h - \xi_j}{\Delta\xi_{j+1}} \right) q_{j+1} \right]$<br>where $M_u$ represents upward mixing rate. $M_{dj}$ represents downward mixing rate at layer $j$ and is defined as:<br>$M_{dj} = M_u \frac{\xi_h - \xi_{j-1}}{\Delta\xi_j}$<br>and the upward flux is obtained from<br>$M_u = H_{sfc} / \left[ c_p \rho (\bar{\theta}_{sfc} - \theta_2) J_\xi (\xi_1 - \xi_h) \right]$<br>$M_{dj-1} = M_u + M_{dj} \frac{\Delta\xi_{j+1}}{\Delta\xi_j}$ | $\begin{pmatrix} d_1 & c_1 & \cdots & 0 & \cdots & 0 \\ e_2 & d_2 & c_2 & 0 & \cdots & 0 \\ \vdots & 0 & \ddots & \ddots & \cdots & 0 \\ e_j & \vdots & \vdots & d_j & c_j & \vdots \\ \vdots & 0 & 0 & 0 & \ddots & c_{L_p-1} \\ e_{L_p} & \cdots & 0 & 0 & 0 & d_{L_p} \end{pmatrix} \begin{pmatrix} q_1^{n+1} \\ q_2^{n+1} \\ \vdots \\ q_j^{n+1} \\ \vdots \\ q_{L_p}^{n+1} \end{pmatrix} = \begin{pmatrix} b_1 \\ b_2 \\ \vdots \\ b_j \\ \vdots \\ b_{L_p} \end{pmatrix}$<br>$d_1 = 1 + (\frac{v_d}{h_{dep}} + M_u \frac{\xi_h - \xi_1}{\Delta\xi_1}) \vartheta \Delta t$ ; $c_1 = -M_u \frac{\xi_h - \xi_1}{\Delta\xi_1} \vartheta \Delta t$<br>$b_1 = [1 - (\frac{v_d}{h_{dep}} + M_u \frac{\xi_h - \xi_1}{\Delta\xi_1})(1 - \vartheta)\Delta t] q_1^n + M_u \frac{\xi_h - \xi_1}{\Delta\xi_1} (1 - \vartheta) \Delta t q_2^n$<br>for $2 \le j \le L_p$:<br>$e_j = -M_u \vartheta \Delta t$; $d_j = 1 + M_u (\frac{\xi_h - \xi_j}{\Delta\xi_{j+1}}) \vartheta \Delta t$ ; $c_j = -M_u (\frac{\xi_h - \xi_j}{\Delta\xi_j}) \vartheta \Delta t$ ;<br>$b_j = [1 - M_u \frac{\xi_h - \xi_{j-1}}{\Delta\xi_j})(1 - \vartheta)\Delta t] q_j^n + M_u \frac{\xi_h - \xi_j}{\Delta\xi_{j+1}} (1 - \vartheta) \Delta t q_{j+1}^n + M_u (1 - \vartheta) \Delta t q_1^n$ |

# Appendix C

**Table 4. Numerical algorithms with two-level time differencing for constant grid spacing (Sources: Pielke, 1984; Long and Pepper, 1981; Odman, 1998; Chock and Dunker, 1983, Chock, 1985; Chock, 1991)**

| Classification | Scheme | Algorithm | Characteristics | References |
|---|---|---|---|---|
| Flux form finite Difference | Donor Cell (upwind difference) Scheme, forward in time | $\varphi_j^{n+1} = \varphi_j^n - [F(\varphi_j^n, \varphi_{j+1}^n, u_{j+1/2}) - F(\varphi_{j-1}^n, \varphi_j^n, u_{j-1/2})]$, where $F(\varphi_j, \varphi_{j+1}, u) = [(u + \lvert u\rvert)\varphi_j + (u - \lvert u\rvert)\varphi_{j+1}]\frac{\Delta t}{2\Delta x}$ | Very diffusive, Positive definite, monotonic, linear, fast | Roache (1972) |
| Flux form, iterative finite Difference | Smolarkiewcz Scheme | $\varphi_j^* = \varphi_j^n - [F(\varphi_j^n, \varphi_{j+1}^n, u_{j+1/2}) - F(\varphi_{j-1}^n, \varphi_j^n, u_{j-1/2})]$, $\varphi_j^{n+1} = \varphi_j^* - [F(\varphi_j^*, \varphi_{j+1}^*, \tilde{u}_{j+1/2}) - F(\varphi_{j-1}^*, \varphi_j^*, \tilde{u}_{j-1/2})]$, where $F(\varphi_j, \varphi_{j+1}, u) = [(u + \lvert u\rvert)\varphi_j + (u - \lvert u\rvert)\varphi_{j+1}]\frac{\Delta t}{2\Delta x}$ $\tilde{u}_{j+1/2} = \frac{(\lvert u_{j+1/2}\rvert \Delta x - \Delta t u_{j+1/2}^2)(\varphi_{j+1}^* - \varphi_j^*)}{(\varphi_{j+1}^* + \varphi_j^* + \varepsilon)\Delta x}$, $\varepsilon$ = a small value ($10^{-15}$) | Moderately diffusive, Positive definite, nonlinear, relatively fast | Smolarkiewicz (1983) |
| Advective form, upstream interpolation | Upstream Cubic-spline Scheme, forward in time | $\varphi_j^{n+1} = \begin{cases} S(x_j - \lvert\beta_j\rvert\Delta x), & for\ \ u_j \geq 0 \\ S(x_j + \lvert\beta_j\rvert\Delta x), & for\ \ u_j < 0 \end{cases}$, where $S(x_j - \lvert\beta_j\rvert\Delta x) = \varphi_j^n - \lvert\beta_j\rvert\Delta x N_j + \beta_j^2[\Delta x N_{j-1} + 2\Delta x N_j + 3(\varphi_{j-1}^n - \varphi_j^n)]$ $-\lvert\beta_j\rvert^3[\Delta x N_{j-1} + \Delta x N_j + 2(\varphi_{j-1}^n - \varphi_j^n)]$ $S(x_j + \lvert\beta_j\rvert\Delta x) = \varphi_j^n + \lvert\beta_j\rvert\Delta x N_j - \beta_j^2[\Delta x N_{j+1} + 2\Delta x N_j + 3(\varphi_j^n - \varphi_{j+1}^n)]$ $+\lvert\beta_j\rvert^3[\Delta x N_j + \Delta x N_{j+1} + 2(\varphi_j^n - \varphi_{j+1}^n)]$, and $S'(x_j) = N_j$ satisfies $3(\varphi_{j+1}^n - \varphi_{j-1}^n)/\Delta x = N_{j-1} + 4N_j + N_{j+1}$. | Diffusive, Produces negative conc. | |

$\beta_j = u_j \Delta t / \Delta x$ and $\beta_{\max} = \max(\lvert\beta_j\rvert)$, the maximum Courant-Fridlich-Lewy (CFL) number for the grid domain.

**Table 4. (continued)**

| Classification | Scheme | Algorithm | Characteristics | References |
|---|---|---|---|---|
| Flux form, Galerkin Finite element | Chapeau Function Scheme, implicit (Crank-Nicholson) | $[2-(2\beta_{j-1}+\beta_j)]\varphi_{j-1}^{n+1}+[8+(\beta_{j+1}-\beta_{j-1})]\varphi_j^{n+1}+[2+(\beta_j+2\beta_{j+1})]\varphi_{j+1}^{n+1}$ $=[2+(2\beta_{j-1}+\beta_j)]\varphi_{j-1}^{n}+[8-(\beta_{j+1}-\beta_{j-1})]\varphi_j^{n}+[2-(\beta_j+2\beta_{j+1})]\varphi_{j+1}^{n}$ | Less diffusive. Spurious oscillations. Produces negative conc. Often needs a smoothing filter | McRae et al. (1982), Odman and Russell (1993) |
| Flux form, Pseudo-spectral technique | Accurate Space Derivative Method | Expand the flux form advection as a truncated Taylor series in time. $\varphi^{n+1}=\varphi^n+\left(\frac{\partial\varphi}{\partial t}\right)^n\Delta t+\left(\frac{\partial^2\varphi}{\partial t^2}\right)^n\frac{\Delta t^2}{2!}+\left(\frac{\partial^3\varphi}{\partial t^3}\right)^n\frac{\Delta t^3}{3!}+\cdots$ Assuming the velocity is not a function of time, the spatial equivalents of time derivatives are computed in chain rule form with the fast Fourier transform: $\frac{\partial\varphi}{\partial t}=-\varphi\frac{\partial u}{\partial x}-u\frac{\partial\varphi}{\partial x}$, $\frac{\partial^2\varphi}{\partial t^2}=\frac{\partial}{\partial x}\left[u\frac{\partial u\varphi}{\partial x}\right]=\varphi\left[u\frac{\partial^2 u}{\partial x^2}+(\frac{\partial u}{\partial x})^2\right]+3u\frac{\partial\varphi}{\partial x}\frac{\partial u}{\partial x}+u^2\frac{\partial^2\varphi}{\partial x^2}$, $\frac{\partial^3\varphi}{\partial t^3}=-\varphi\left[4u\frac{\partial u}{\partial x}\frac{\partial^2 u}{\partial x^2}+u^2\frac{\partial^3 u}{\partial x^3}+(\frac{\partial u}{\partial x})^3\right]$ $-\frac{\partial\varphi}{\partial x}\left[4u^2\frac{\partial^2 u}{\partial x^2}+7u(\frac{\partial u}{\partial x})^2\right]-6u^2\frac{\partial^2\varphi}{\partial x^2}\frac{\partial u}{\partial x}-u^3\frac{\partial^3\varphi}{\partial x^3}\cdot$ Due to the dispersive quality, it produces high-frequency noise. Often used in combination with a filter (e.g., Forest filter) | Very accurate, Produces negative conc. High computational cost Needs a smoothing filter | Gazdag (1973) Dabdub and Seinfeld (1994) |

**Table 4. (continued)**

| Classification | Scheme | Algorithm | Characteristics | References |
|---|---|---|---|---|
| Flux form, finite volume scheme | Piecewise Parabolic Method (PPM) | Concentration distribution is assumed to be parabolic in any given grid cell. $\varphi_j^{n+1}(\eta) = \varphi_{L,j} + \eta\left[(\varphi_{R,j} - \varphi_{L,j}) + 6\left(\varphi_j^n - \frac{\varphi_{L,j} + \varphi_{R,j}}{2}\right)(1-\eta)\right]$, Where $\eta$ is the nondimensional coordinate and left and right boundary values are defined as $\varphi_{L,J+1} = \varphi_{R,J} = \varphi^*_{j+1/2}$ with initial guess, $\varphi^*_{j+1/2} = \frac{7}{12}(\varphi_j^n + \varphi_{j+1}^n) - \frac{1}{12}(\varphi_{j+2}^n + \varphi_{j-1}^n)$. Edge values are modified such that the results are monotonic: (1) if $\varphi_j$ is a local extremum, then the distribution is assumed to be constant, (2) when $\varphi_j$ is between $\varphi_{L,j}$ and $\varphi_{R,j}$, but sufficiently close to one of the values, one of the edge values is reset so that the derivative of $\varphi(\eta)$ is zero at the opposite edge | Moderately diffusive, Positive definite, monotonic | Colella and Woodward, (1984) Carpenter et al., (1990) |
| Flux form, finite volume scheme | Bott's Scheme | The distribution of the concentration within the cell is represented by a polynomial of order *l:* $\varphi_j(\eta) = \sum_{k=0}^{l} a_{j,k}\eta^k$. The polynomial can be made to preserve area by requiring: $\varphi_{j+i} = \int_i^{i+1} \sum_{k=0}^{l} a_{j,k}\eta^k d\eta$, $i = 0,\pm1,\pm2,...,\pm\frac{l}{2}$ over a stencil of $l$+1 grid cells by varying the value of $i$. The solution to this linear system yields the coefficients $a_{j,k}$. For example, coefficients for a quadratic ($l$=2) scheme are; $a_0 = -\frac{1}{24}\left(\varphi_{j+1} - 26\varphi_j - \varphi_{j-1}\right)$, $a_1 = \frac{1}{2}\left(\varphi_{j+1} - \varphi_{j-1}\right)$, and $a_2 = \frac{1}{2}\left(\varphi_{j+1} - \varphi_j + \varphi_{j-1}\right)$ | Mildly diffusive, Positive definite*, nonlinear, relatively fast, non-monotonic | Smolarkiewicz (1983) |

Non-dimensional local coordinate is defined as $\eta = (x - x_{j-1/2})/\Delta x$.

*Small negative numbers can result for a signal with large gradients due to machine precision problems

**Table 4. (continued)**

| Classification | Scheme | Algorithm | Characteristics | References |
|---|---|---|---|---|
| Flux form, finite volume scheme | Yamatino-Blackman Cubic scheme | Interpolating cubic spline: $\varphi_j(\eta) = a_0 + a_1\eta + a_2\eta^2 + a_3\eta^3$, with $a_0 = \varphi_j$, $a_1 = d_j\,\Delta x$, $a_2 = -\frac{1}{4}\left(\varphi_{j+1} - 2\varphi_j + \varphi_{j-1}\right) + \frac{3\Delta x}{8}\left(d_{j+1} - d_{j-1}\right)$, $a_3 = \left(\varphi_{j+1} - \varphi_{j-1}\right) - \frac{\Delta x}{6}\left(d_{j+1} + 10d_j + d_{j-1}\right)$ The spline derivatives, $d_j$, are obtained from the tridiagonal system: $\alpha\, d_{j-1} + (1-2\alpha)\, d_j + \alpha\, d_{j+1} = \frac{\varphi_{j+1} - \varphi_{j-1}}{2\Delta x}$. ($\alpha$=0.22826). Positivity is maintained by (1) when $\varphi_j$ is a local minimum, a donor-cell scheme is used instead of the cubic spline; (2) the spline is spectrally limited by the relation: $\left\|a_k / a_0\right\| \le \pi^k / k!, \quad k = 1,2,3.$ (3) a mass conservative flux renormalization is applied, and finally (4), a mildly diffusive filter is applied in an attempt to block the depletion of donor cells. | A little diffusive, Positive definite, non-monotonic | Yamatino (1993) |
| Advective form, Semi-Lagrangian Transport (SLT) scheme | SLT with cubic spline interpolation | The Lagrangian solution to this equation determines the departure point $(x_D,\, y_D)$ of a particle at $(x_A,\, y_A)$ as $(x_D, y_D) = (x_A - \Delta t\, u, y_A - \Delta t\, v)$. This scheme first determines the midpoint of the trajectory iteratively as $(x_M^{k+1}, y_M^{k+1}) = (x_A - \frac{\Delta t}{2} u(x_M^k, y_M^k), y_A - \frac{\Delta t}{2} v(x_M^k, y_M^k))$ Four iterations are used for the very first time step which starts with the arrival points as a first guess (for the midpoints) and one iteration thereafter where the midpoints from the previous time step are used as a first guess. The velocities at the midpoints are calculated using Lagrange cubic interpolation. Monotonicity is maintained by limiting the interpolated value. | Diffusive, Positive definite Monotonic. | Williamson and Rasch (1989) |

## References

Alapaty, K., R. Mathur, and D.W. Byun, 1996: A modeling study of vertical diffusion of passive and reactive tracers using local- and nonlocal-closure boundary layer schemes. Air Pollution Modeling and Its Application XI, ed. S.E. Gryning and F. Schiermeier. 433-442.

Alapaty, K.A., J.E. Pleim, S. Raman, D.S. Niyogi, and D.W. Byun. 1997: Simulation of atmospheric boundary layer processes using local- and nonlocal-closure schemes. *J. Applied Meteor*. Vol. **36**. 214-233.

Arya. S. P. , 1988. *Introduction to Micrometeorolgy*. Academic Press, San Diego, CA. 307 pp.

Arya. S. P. , 1999. *Air Pollution Meteorology and Dispersion*. Oxford University Press, New York, NY. 310 pp.

Ascher, U.M., S.J. Ruuth, and B.T.R. Wetton, 1995: Implicit-explicit methods for time-dependent PDE's, *SIAM J. Numer. Anal*., **32**, 797-823.

Bacon, D.P., N.N. Ahmad, Z. Boybeyi, T.J. Dunn, M.S. Hall, P.C.S. Lee, R. A. Sarma, and M.D. Turner, 2000: A dynamically adapting weather and dispersion model: The Operational Multiscale Environment Model with Grid Adaptivity (OMEGA). *Mon. Wea. Rev.* **121**. 2637-2641.

Batchelor, G.K., 1967: *An Introduction to Fluid Mechanics*. Cambridge University Press, London.

Blackadar, A. K., 1962: The vertical distribution of wind and turbulent exchange in neutral atmosphere. *J. of Geophys. Res.*, **67**, 3095-3103.

Blackadar, A. K., 1978: Modeling pollutant transfer during daytime convection, *Preprints, Fourth Symposium on Atmospheric Turbulence, Diffusion, and Air Quality*, Reno, Am. Meteor. Soc., 443-447.

Bodin, S., 1980: Applied numerical modeling of the atmospheric boundary layer, Atmos. Plan. Bou. Lay. Phy., A. Longhetto, Ed., Elsevier Scientific Publ. Co., Amsterdam, 1-76.

Bott, A., 1989: A positive definite advection scheme obtained by nonlinear renormalization of the advective fluxes. *Mon. Wea. Rev.* **117**, 1006-1015.

Bott, A., 1992: Monotone flux limitation in the area-preserving flux-form advection algorithm. *Mon. Wea. Rev.* **120**, 2592-2602.

Bott, A., 1993: The monotone area-preserving flux-form advection algorithm: reducing the time-splitting error in two-dimensional flow fields. *Mon. Wea. Rev.* **121**. 2637-2641.

Briggs, G. A., 1973: Diffusion estimates for small emissions. ATDL Contribution No. 79 [Available from Atmospheric Turbulence and Diffusion Laboratory, Oak Ridge, Tenn.]

Brooks, A. N., and T. J. R. Hughes, 1982: Streamline upwind/Petrov-Galerkin formulations for convection dominated flows with particular emphasis on the incompressible Navier-Stokes equations. *Comp. Meth. Appl. Mech. Eng.* **32**, 199-259.

Brost R. A. and J. C. Wyngaard, 1978: A model study of the stably stratified planetary boundary layer. *J. Atmos. Sci.*, **35**, 1427-1440.

Burk, S.D., and W.T. Thompson, 1989: A vertically nested regional numerical weather prediction model with second-order physics. *Mon. Wea. Rev.* **117**, 2305-2324.

Businger, J.A., and Arya, S.P.S., 1974: Height of the mixed layer in the stably stratified planetary boundary layer. *Advan. Geophys.,* **18A**, 73-92.

Businger J. A., J. C. Wyngaard, Y. Izumi, and E. F. Bradley, 1971: Flux profile relationships in the atmospheric surface layer, *J. Atmos. Sci.*, **28**, 181-189.

Byun, D. W., 1999a: Dynamically consistent formulations in meteorological and air quality models for multi-scale atmospheric applications: I. Governing equations in a generalized coordinate system. *J. Atmos. Sci*., **56**, 3789-3807.

Byun, D. W., 1999b: Dynamically consistent formulations in meteorological and air quality models for multi-scale atmospheric applications: II. Mass conservation issues. *J. Atmos. Sci*., 56, 3808-3820.

Byun, D.W. and J.K.S. Ching, ed., 1999: *Science Algorithms of the EPA Models-3 Community Multiscale Air Quality (CMAQ) Modeling System.* EPA Report. EPA/600/R-99/030. [Available from National Exposure Research Laboratory, U.S. Environmental Protection Agency, Research Triangle Park, NC 27711]

Byun, D. W., and R. L. Dennis, 1995: Design artifacts in Eulerian air quality models: Evaluation of the effects of layer thickness and vertical profile correction on surface ozone concentrations. *Atmos. Environ*., **29**, 105-126.

Byun, D.W., J. Young., J. Pleim, M.T. Odman, and K. Alapaty, 1999: Numerical transport algorithms for the community multiscale air quality (CMAQ) chemical transport model in generalized coordinates. pp 58, Chapter 7 in *Science Algorithms of the EPA Models-3 Community Multiscale Air Quality (CMAQ) Modeling System*. Byun, D.W. and J.K.S. Ching, ed., National Exposure Research Laboratory, U.S. Environmental Protection Agency, Research Triangle Park, NC.

Calder, K.L, 1949: Eddy diffusion and evaporation in flow over aerodynamically smooth and rough surfaces: A treatment based on laboratory laws of turbulent flow with special reference to conditions in the lower atmosphere. *Quart. J. Mech. Math.*, **2**, 153.

Carpenter, R. L., K. K. Droegemeier, P. R. Woodward, and , C. E., Hane, 1990: Application of the piecewise parabolic method (PPM) to meteorological modeling. *Mon. Wea. Rev.* **118**, 586-612.

Chang, J.S., P.B. Middleton, W.R. Stockwell, C.J. Walcek, J.E. Pleim, H.H. Lansford, S. Madronich, F.S. Binkowski, N.L. Seaman, and D.R. Stauffer, 1990: The Regional Acid Deposition Model and Engineering Model, NAPAP SOS/T Report 4, in: National Acid Precipitation Assessment Program: State of Science and Technology, Volume 1, National Acid Precipitation Assessment Program, 722 Jackson Place, N.W., Washington, D.C.

Chang, J.S., R.A. Brost, I.S.A. Isaksen, S. Madronich, P. Middleton, W.R. Stockwell, and C.J. Walcek, 1987: A three-dimensional Eulerian acid deposition model: Physical concepts and formulation, *J. of Geophys. Res.*, **92**, 14,681-700.

Chang J. S., S. Jin, Y. Li, M. Beauharnois, C.-H. Lu, H.-C. Huang, S. Tanrikulu, and J. DaMassa, 1997: *The SARMAP air quality model. Final Report*, SJVAQS/AUSPEX Regional Modeling Adaptation Project, 53 pp. [Available from California Air Resources Board, 2020 L Street, Sacramento, California 95814.]

Chatfield, R.B. and P.J. Crutzen, 1984: Sulfur dioxide in remote oceanic air: cloud transport of reactive precursors, J. Geophys. Res., 89, 7111-7132.

Childs, P. N., and K. W. Morton, 1990: Characteristic Galerkin methods for scalar conservation laws in one dimension. *SIAM J. Numer. Anal.* **27**, 553-594.

Chock, D. P., and A. M. Dunker, 1983: A comparison of numerical methods for solving the advection equation. *Atmos. Environ.* **17**(1), 11-24.

Chock, D. P., 1985: A comparison of numerical methods for solving the advection equation - II. *Atmos. Environ.* **19**(4), 571-586.

Chock, D. P., 1991: A comparison of numerical methods for solving the advection equation-III. *Atmos. Environ.* **25A**(5/6), 853-871.

Colella, P., and , P. R. Woodward, 1984: The piecewise parabolic method (PPM) for gas-dynamical simulations. *J. Comp. Phys* **54**, 174-201.

Cotton, W.R. and R.A. Anthes, 1989: *Storm and Cloud Dynamics*, Academic Press, San Diego, CA.

Crowley, W.P., 1968: Numerical advection experiments, *Mon. Weather Rev*., **96**, 1-11.

Dabdub, D., and Seinfeld, J. H., 1994: Numerical advective schemes used in air quality models - sequential and parallel implementation. *Atmos. Environ.* **28**(20), 3369-3385.

Deardorff, J.W., 1966: The counter-gradient heat flux in the lower atmosphere and in the laboratory. *J. Atmos. Sci*., **23**, 503-506.

Deardorff, J.W., 1972: Theoretical expression for the counter gradient vertical heat flux. *J. Geophys. Res*., **77**, 5900-5904.

Deardorff, J.W., 1974: Three-dimensional numerical study of the height and mean structure of a heated planetary boundary layer. *Bound.-Layer Meteor.,* **7**, 81-106.

Degrazia, G.A., U. Rizza, C. Mangia, and T. Tirabassi, 1997: Valication of a new turbulent parameterization for dispersion models in convective conditions. *Bound.-Layer Meteor.,* **85**, 243-254.

Degrazia, G.A., D. Anfossi, J.C. Carvalho, C. Mangia, T. Tirabassi, and H.F. Campos Velho, 2000: Turbulence parameterizations for PBL dispersion models in all stability conditions. *Atmos. Environ.* **34**, 3575-3583.

Demuth,C., 1978: A contribution to the analytical steady solution of the diffusion equation for line sources. *Atmos. Environ.* **12**, 1255-1258.

Dennis, R.L., D.W. Byun, J.H. Novak, K.J. Galluppi, C.J. Coats, and M.A. Vouk, 1996: The next generation of integrated air quality modeling: EPA's Models-3. *Atmos. Environ.* **30**, 1925-1938.

Detering, H.W., and D. Etling, 1985: Application of E-$\varepsilon$ turbulence model to the atmospheric boundary layer. *Bound.-Layer Meteor.,* **33**, 113-133.

Diemrjian, K.L. and K.L. Schere, 1979: Applications of a photochemical box model for ozone air quality in Houston, Texas. Proceedings, *Ozone/Oxidants: Interactions with the Total Environment II*, Houston, TX, 14-17 Oct. 1979, APCA, Pittsburgh, PA, 329-352.

Dodge, M.C.,1977: Combined Use of Modeling Techniques and Smog Chamber Data to Derive Ozone Precursor Relationships, Rep. EPA-600/3-77-001a, pp 881-889.

Donea, J., 1984: A Taylor-Galerkin method for convective transport problems. *Int. J. Num. Meth. Engng* **20**, 109-119.

Draxler, R.R. and G.D. Hess, 1997: Description of the HYSPLIT 4 modeling system.*NOAA Technical Memo* ERL, ARL-224, Dec., 24pp.

Du, S. and A. Venkatram,1998: The effect of streamwise diffusion on ground-level concentrations. *Atmos. Environ.* **32**(11), 1955-1961.

Ebert, E.E., U. Schumann, and R. B. Stull, 1989: Nonlocal turbulence mixing in the convective boundary layer evaluated from large-eddy simulation. *J. Atmos. Sci.*, **46**, 2178-2207.

Eppel, D.P., H. Kapitza, M. Claussen, D. Jacob, W. Koch, L. Levkov, H.-T. Mengelkamp, and N. Werrmann, 1995: The nonhydrostatic mesoscale model GESIMA. Part II: Parameterizations and applications. *Beitr. Phys. Atmosph.*, **68**, 15-41.

Ertel, H., 1942: Der vertikale Turbulenz-Wärmestrom in der Atmosphäre. *Metreor. Z.*, **59**, 250-253.

Fiedler, B.H. and C.H. Moeng, 1985: A practical integral closure model for mean vertical transport of a scalar in a convective boundary layer, J. Atmos. Sci., 42, 359-363.

Flatoy, F., 1993: Balanced wind in advanced advection schemes when species with long lifetimes are transported. *Atmos. Environ.* **27A**(12), 1809-1819.

Ghorai, S., A.S. Tomlin, and M. Berzins, 2000: Resolution of pollutant concentrations in the boundary layer using a fully 3D adaptive gridding technique. *Atmos. Environ.* **34**, 2851-2863.

Grell, G. A., J. Dudhia, and D. R. Stauffer, 1994: A description of the fifth-generation Penn State/NCAR mesoscale model (MM5). NCAR Tech. Note NCAR/TN 398+STR, 117 pp. [Available from the National Center for Atmospheric Research, P. O. Box 3000, Boulder, CO 80307.]

Ha, K.J. and L. Mahrt, 2000: A new nocturnal boundary layer model. Proceedings. *14th Symposium on Boundary Layers and Turbulence*. Aspen, CO, AMS, pp. 581-584.

Hanna, S.R., G.A. Briggs, J. Deardorff, B.A. Egan, F.A. Gifford, and F. Pasquill, 1977: AMS Workshop on Stability Classification Schemes and Sigma Curves–summary of recommendations. *Bull. Amer. Meteorol. Soc*., **58**, 1305-1309.

Hanna, S.R., G.A. Briggs, and R.P. Hosker, 1982: *Handboook on Atmospheric Diffusion*. U.S. Department of Energy, Technical Information Center, Oak Ridge, TB.

Hanna, S.R., 1994: Random variability in mesoscale wind observations and implications for diffusion models. Preprints. *Eigth Joint Conference on Applications of Air Pollution Meteorology with A&WMA*. Nashville, Tennessee, AMS, pp. 1-5.

Hass, H., H.J. Jacobs, M. Memmescheimer, A. Ebel, and J.S. Change, 1991: Simulation of a wet deposition case in Europe using the European Acid Deposition Model (EURAD). *Air Pollution Modelling and Its Applications*, Vol. VIII (edited by van Dop H. and D.G. Steyn), Plenum Press, 205-213.

Holtslag, A. A. M., E. I. F. de Bruin, and H.-L. Pan, 1990: A high resolution air mass transformation model for short-range weather forecasting. *Mon. Wea. Rev.*, **118**, 1561-1575.

Holtslag, A. A. M., and C.-H. Moeng, 1991: Eddy diffusivity and countergradient transport in the convective atmospheric boundary layer. *J. Atmos. Sci.*, **48**, 1690-1698.

Holtslag, A. A. M., and B. A. Boville, 1993: Local versus nonlocal boundary-layer diffusion in a global climate model. *J. Climate.*, **6**, 1825-1842.

Holtslag, A. A. M., E. van Meijgaard, and W.C. de Rooy, 1995: A comparison of boundary layer diffusion schemes in unstable conditions over land. *Bound.-Layer Meteor.*, **76**, 69-95.

Hong, S.-Y., and H.-L. Pan, 1996: Nonlocal boundary layer vertical diffusion in a medium-range forecast model. *Mon. Wea. Rev.*, **124**, 2322-2339.

Huang, C.H., 1979: A theory of dispersion in turbulent shear flow. *Atmos. Environ.* **13**, 453-463.

Irwin, J.S., 1979: Estimating plume dispersion–A recommended generalized scheme. Presented at 4th Symposium on Turbulence and Diffusion, American Met. Soc., Reno, Nevada.

Jensen, N.O., and E. L.. Petersen, 1979: The box model and the acoustic sounder, a case study. *Atmos. Environ.* **13**, 717-720.

Klemp J.B., and R. Wilhelmson, 1978: The simulation of three dimensional convective storm dynamics. *J. Atmos. Sci.*, **35**, 1070-1096.

Knoth, O. and R. Wolke, 1998a: An explicit-implicit numerical approach for atmospheric chemistry–transport modeling. *Atmos. Environ.* **32**, 1785-1797.

Knoth, O. and R. Wolke, 1998b: Implicit-explicit Runge-Kutta methods for computing atmospheric reactive flows. *Appl. Nemer. Math.* **28**, 327-341.

Lacser, A. and S.P.S. Arya, 1986: A comparative assessment of mixing-length parameterizations in the stably stratified nocturnal boundary layer*, Bound. Layer Meteor.*, 36, 53-70.

Lange,.R., 1989: Transferability of a 3-D air quality model between two different sites in complex terrain. *J. Appl. Meteo*., **28**, 665-679.

Lettau, H. H., 1970: Physical and meteorological basis for mathematical model of urban diffusion processes. *Proceedings* , Symposium on Multiple-Source Urban Diffusion Models. U.S. EPA Publication No. AP-86.

Liu, M and J. J. Carroll,.1996: A high resolution air pollution model suitable for dispersion studies in complex terrain. *Mon. Wea. Rev.*, **124**, 2396-2409.

Löhner, R., K. Morgan, J. Peraire, and M. Vahdati, 1987: Finite element flux-corrected transport (FEM-FCT) for the Euler and Navier-Stokes Equations. *Finite Elements in Fluids. Vol. 7*. John Wiley & Sons. 105-121.

Long, P.E., and D.W. Pepper, 1981: An examination of some simple numerical schemes for calculating scalar advection, *J. Appl. Meteo*., **20**, 146-156.

Longhetto, A., ed., 1980: *Atmospheric Planetary Boundary Layer Physics*. New York, Elsevier.

Louis, J.F., 1979: A parametric model of vertical eddy fluxes in the atmosphere. *Bound.-Layer Meteor.*, **17**, 187-202.

McNider, R.T., M. P. Singh, and S. Gupta., 1996: Nocturnal wind structure and plume growth rates due to inertial oscillation. Preprints. *Ninth Joint Conference on Applications of Air Pollution Meteorology with A&WMA*. Atlanta, Georgia, AMS, pp. 455-458.

McRae, G.J., W.R. Goodin, and J.H. Seinfeld, 1982: Development of a second generation mathematical model for urban pollution: I. Model formulation. *Atmos. Environ.* **16**, 679-696.

Mellor, G.L. and T. Yamada, 1974: A hierarchy of turbulence closure models for planetary boundary layers, *J. Atmos. Sci.*, **31**, 1791-1806.

Mellor, G.L. and T. Yamada, 1982: Development of a turbulence closure model for geophysical fluid problems. *Reviews of Geophysical and Space Physics*, **20**, 851-875.

Mesinger, F. and A. Arakawa, 1976: *Numerical Methods Used in Atmospheric Models*. In: Global Atmospheric Research Programme (GARP), Joint Organization Committee, GARP Publication Series, No 17 [Available from WMO Secretariat, Geneva].

Meszaros, E., G. Varhelyi, and L. Haszpra, 1978: On the atmospheric sulfur budget over Europe. *Atmos. Environ.* **12**, 2273-2277.

Nikomo,.J., J.P. Tuovinen, J. Kukkonen and I. Valkama, 2000: A hybrid plume model for local scale atmospheric dispersion, *Atmos. Environ.* **33**, 4389-4399.

O'Brien, J., 1970: On the vertical structure of the eddy exchange coefficient in the planetary boundary layer, *J. Atmos. Sci.*, **27**, 1213-1215.

Odman, M. T., 1998: Research on Numerical Transport Algorithms for Air Quality Simulation Models. EPA Report. EPA/660/R-97/142. [Available from National Exposure Research Laboratory, U.S. Environmental Protection Agency, Research Triangle Park, NC 27711].

Odman, M. T., and Russell, A. G., 1993: A nonlinear filtering algorithm for multi-dimensional finite element pollutant advection schemes. *Atmos. Environ.* **27A**, 793-799.

Odman, M. T., A. Xiu, and D. W. Byun, 1993: Evaluating advection schemes for use in the next generation of air quality modeling systems, Paper OT7-I.5, International Specialty Conference on Regional Photochemical Measurement and Modeling Studies, Air & Waste Management Association, Pittsburgh, PA. 1386-1401.

Oran, E., and J. Boris, 1987: Numerical Solution of Reactive Flow, New York, Elsevier.

Otey, G. R. and H.A. Dwyer, 1978: Numerical study of the interaction of fast chemistry and diffusion. *AIAA J.* **17**, 606-613.

Otte, M.J. and J.C. Wyngaard, 1996: A general framework for an "unmixed layer" PBL model. *J. Atmos. Sci.*, **53**, 2652-2670.

Panofsky, H. A. and J. A. Dutton, 1984: *Atmospheric Turbulence*. Wiley-Interscience, New York.

Pasquill, F., 1976: Atmospheric dispersion parameters in Gaussian plume modeling. Part II. Possible requirements for change in the Turner Workbook values. Report No. EPA-600/4-76-030b, U.S. Environmental Protection Agency, Research Triangle Park, NC.

Pasquill, F. and F. B. Smith, 1983: *Atmospheric Diffusion*, 3rd ed. Ellis Horwood Ltd., Chichester, England.

Pielke, R.A., 1984: *Mesoscale Meteorological Modeling*, Academic Press, Orlando, FL.

Pielke, R.A. and Y. Mahrer, 1975: Technique to represent the heated planetary boundary layer in mesoscale models with coarse vertical resolution. *J. Atmos. Sci.*, **32**, 2288-2308.

Pleim, J.E. and J. Chang, 1992: A non-local closure model for vertical mixing in the convective boundary layer. *Atmos. Envi*., **26A**, 965-981.

Prabha, T.V. and E. Mursch-Radlgruber, 1999: Modeling of diffusion in a Wide Alpine Valley. *Theor. Appl. Climatol*., **64**, 93-103.

Raupach, M.R., and B.J. Legg, 1983: Turbulent dispersion from an elevated line source: Measurements of wind-concentration moments and budgets. *J. Fluid Mech*., **136**, 111-137.

Raymond, W.H. and R.B. Stull, 1990: Application of transilient turbulence theory to mesoscale numerical weather forecasting. *Mon. Weather Rev.*, **118**, 2471-2499.

Roache, P.J, 1972: *Computational Fluid Dynamics*, Hermosa Publishers, Albuquerque, New Mexico.

Rood, R. B., 1987: Numerical advection algorithms and their role in atmospheric transport and chemistry models. *Rev. Geophysics* **25**(1), 71-100.

Rounds, W., 1955: Solutions of the two-dimensional diffusion equation. *Trans. Am. Geophysics. Union* **36**, 395.

Russell, A, and R. Dennis, 2000: NARSTO critical review of photochemical models and modeling. *Atmos. Envi*., **34**, 2283-2324.

Schere, K. L. and K. L. Diemrjian, 1984: User's Guide for the Photochemical Box Model (PBM). U.S. EPA Report. EPA-600/8-84-022a, Research Triangle Park, NC.

Schumann, U., 1989: Large-eddy simulation of turbulent diffusion with chemical reactions in the convective boundary layer. *Atmos. Envi*., **26A**, 965-981.

Seinfeld, J.H., 1986: *Atmospheric Chemistry and Physics of Air Pollution*. John Wiley and Sons, New York.

Siebesma, A.P. and J. Teixeira, 2000: An advection-diffusion schema for the CBL: description and 1-D results. Proceedings. *14th Symposium on Boundary Layers and Turbulence*. Aspen, CO, AMS, pp. 133-136.

Smagorinsky, J., 1963: General circulation experiments with the primitive equations: 1. The basic experiment. *Mon. Wea. Rev.* **91**, 99-164.

Smith, F.B., 1957: The diffusion of smoke from a continuous elevated point source into a turbulent atmosphere. *J. Fluid Mech.,* **2**, 491-508.

Smolarkiewicz, P.K., 1983: A simple positive definite advection transport scheme with small implicit diffusion. *Mon. Wea. Rev.* **111**, 479-486.

Sorbjan Z., 1986a, On similarity in the atmospheric boundary layer, *Bound.-Layer Meteor* **34**, 377-397.

Sorbjan Z., 1986b, On the vertical distribution of passive species in the atmospheric boundary layer, *Bound.-Layer Meteor* , **35**, 73-81.

Stevens, B., 2000: Quasi-steady analysis of a PBL model with an eddy-diffusivity profile and nonlocal fluxes. *Mon. Wea. Rev.* **128**, 824-836.

Stull, R. B., 1988: *An Introduction to Boundary Layer Meteorology*. Kluwer Academic, 666 pp.

Stull, R. B., 1993: Review of non-local mixing in turbulent atmosphere: Transilient turbulence theory. *Bound.-Layer Meteor.,* **62**, 21-96.

Stull, R. B., and A.G.M. Driedonks, 1987: Applications of the transilient turbulence parameterization to atmospheric boundary layer simulations. *Bound.-Layer Meteor.,* **40**, 209-239.

Tirabassi, T., M. Tagliazucca, and P. Zannetti, 1986: KAPPA-G, a non-Gaussian plume dispersion model: Description and evaluation against tracer measurements. *JAPCA*, **36**, 196-211.

Tirabassi, T., and U. Rizza, 1997: Boundary layer parameterization for a non-Gaussian puff model. *J. Appl. Meteo*., **36**, 1031-1037.

Tremback, G. J., Powell, J., Cotton, W. R. and Pielke, R. A., 1987: The forward-in-time upstream advection scheme: extension to higher orders. *Mon. Wea. Rev,* **115**, 540-555.

Troen, I. B., and L. Mahrt, 1986: A simple model of the atmospheric boundary layer: Sensitivity to surface evaporation. *Bound.-Layer Meteor.,* **37**, 129-148.

Ulke, A. G., 2000: New turbulent parameterization for a dispersion model in the atmospheric boundary layer. *Atmos. Envi*., **34**, 1029-1042.

Venkatram, A., 1978: An examination of box models for air quality simulation. *Atmos. Envi*., **12**, 2243-2249.

Verwer, J.G., W.H. Hundsdorfer, and J.G. Blom, 1998: Numerical time integration for air pollution models. *Modeling, Analysis and Simulation (MAS), MAS-R9825,* 58pp.

Williamson, D.L., and P.J. Rasch, 1989: Two-dimensional semi-Lagrangian transport with shape-preserving interpolation. *Mon. Wea. Rev.* **117**, 102-117.

Willis, G.E., and J.W. Deardorff, 1976: A laboratory model of diffusion into the convective planetary boundary layer. *Quart. J. R. Met. Soc.*, **102**, 427-446.

Wyngaard, J.C., 1982: Boundary-layer modeling. In *Atmospheric Turbulence and Air Pollution Modelling* (F.T.M. Nieustadt and H. van Dop., eds.), pp. 69-106. D. Reidel Pub. Co., Dordrecht, Holland.

Yamartino, R. J., 1993: Nonnegative, conserved scalar transport using grid-cell-centered, spectrally constrained Blackman cubics for applications on a variable-thickness mesh. *Mon. Wea. Rev.* **121**, 753-763.

Yamartino, R.J., J.S. Scire, G.R. Carmichael, and Y.S. Chang, 1992: The CALGRID mesoscale photochemical grid model - Part I. Model formulation, *Atmos. Environ.* **26A**, 1493-1512.
Yamartino, R.J., 1998: Improvements to horizontal transport in grid models. *Preprints*, 23rd International Technical Meeting on Air Pollution Modelling and its Application, Varna, Bulgaria, NATO/CCMS, pp. 51-56.

Yamartino, R.J., and S. Machiraju, 2000: Determination of the Horizontal Diffusion Coefficient for Use in the SARMAP Air Quality Model. SCARB Report, State of California Air Resources Board, Sacramento, CA.

Yanenko, N.N., 1971: The method of fractional steps: The solution of problems of mathematical physics in several variables, (M. Holt, ed.) Springer-Verlog, New York.

Yeh, G.T., and C.H. Huang, 1975: Three-dimensional air pollutant modeling in the lower atmosphere. *Bound.-Layer Meteor.*, **9**, 381-390.

Yokoyama, O., Gamo M. and Yamamoto S., 1979, The vertical profiles of the turbulence quantities in the atmospheric boundary layer, J. Met. Soc. Japan, 57(3), 264-272.

Zannetti, P., 1990: *Theories, Computational Methods, and Available Software*, Computational Mechanics Publications, Southhampton and Van Nostrand Reonhold, New York.

Zhang, D., and R.A. Anthes, 1982: A high-resolution model of the planetary boundary layer - Sensitivity tests and comparisons with SESAME-79 data, *J. Appl. Meteo*., **21**, 1594-1609.

Zhang, Q., and R. B. Stull, 1992: Alternative nonlocal descriptions of boundary-layer evolution. *J. Atmos. Sci.*, **49**, 2267-2281.